AWARD NUMBER: W81XWH-14-1-0448

TITLE: Characterizing the Hypermutated Subtype of Advanced Prostate Cancer as a Predictive Biomarker for Precision Medicine

PRINCIPAL INVESTIGATOR: Pritchard, Colin

CONTRACTING ORGANIZATION: University of Washington
Seattle, WA 98195

REPORT DATE: October 2015

TYPE OF REPORT: Annual Report

PREPARED FOR: U.S. Army Medical Research and Materiel Command
Fort Detrick, Maryland 21702-5012

REPORT DOCUMENTATION PAGE

Form Approved
OMB No. 0704-0188

1. REPORT DATE	2. REPORT TYPE	3. DATES COVERED
October 2015	Annual Report	15 Sep 2014 - 14 Sep 2015

4. TITLE AND SUBTITLE

Characterizing the Hypermutated Subtype of Advanced Prostate Cancer as a Predictive Biomarker for Precision Medicine

5a. CONTRACT NUMBER

5b. GRANT NUMBER
W81XWH-14-1-0448

5c. PROGRAM ELEMENT NUMBER

6. AUTHOR(S)
Pritchard, Colin C.

E-Mail: cpritch@uw.edu

5d. PROJECT NUMBER

5e. TASK NUMBER

5f. WORK UNIT NUMBER

7. PERFORMING ORGANIZATION NAME(S) AND ADDRESS(ES)

University of Washington
4333 Brooklyn Ave NE
Seattle, WA 98195-0001

8. PERFORMING ORGANIZATION REPORT NUMBER

9. SPONSORING / MONITORING AGENCY NAME(S) AND ADDRESS(ES)

U.S. Army Medical Research and Materiel Command
Fort Detrick, Maryland 21702-5012

10. SPONSOR/MONITOR'S ACRONYM(S)

11. SPONSOR/MONITOR'S REPORT NUMBER(S)

12. DISTRIBUTION / AVAILABILITY STATEMENT

Approved for Public Release; Distribution Unlimited

13. SUPPLEMENTARY NOTES

14. ABSTRACT

The goal of this research is to characterize the mechanisms leading to hypermutated prostate cancer and to integrate tumor hypermutation status with clinical decision making and therapy to improve the care of men with advanced prostate cancer. We identified 7/60 patients (12% of men) with hypermutated advanced prostate cancers. Using a targeted deep sequencing assay that includes intronic and flanking regions we discovered DNA mismatch repair (MMR) gene mutations in all hypermutated tumors. Mutations were commonly complex genomic rearrangements in the *MSH2* and *MSH6* mismatch repair genes. There was loss of the corresponding MMR protein expression in tumor tissue and phenotypic microsatellite instability in every hypermutated tumor. Our results support that microsatellite instability resulting from loss of function mutations in DNA mismatch repair genes is the major mechanism leading to hypermutation in prostate cancer. During the next year we plan to focus work on aims 2 and 3, which will involve testing responsiveness of hypermutated prostate tumors to genotoxic therapies and developing clinical testing approaches to identify hypermutated prostate cancers.

15. SUBJECT TERMS

Prostate cancer, hypermutation, hyper-mutation, microsatellite instability, MSI, MLH1, MSH2, MSH6, PMS2, metastasis, precision medicine

16. SECURITY CLASSIFICATION OF:			17. LIMITATION OF ABSTRACT	18. NUMBER OF PAGES	19a. NAME OF RESPONSIBLE PERSON
a. REPORT	b. ABSTRACT	c. THIS PAGE			USAMRMC
U	U	U	UU	71 pages	19b. TELEPHONE NUMBER *(include area code)*

Table of Contents

Page

1. INTRODUCTION

The goal of this project is to characterize the mechanisms leading to hypermutated prostate cancer and to integrate tumor hypermutation status with clinical decision making and therapy to improve the care of men with advanced prostate cancer. Using Next-Gen sequencing approaches my colleagues at the University of Washington recently identified a hypermutated phenotype/genotype in 10-20% of advanced prostate cancers. This phenotype was subsequently observed in primary prostate cancer. Prostate cancer hypermutation is a promising target for precision therapy, but the mechanisms leading to hypermutation, optimal methods to measure hypermutation status in the clinic, and clinical implications for prostate cancer patients are not yet understood. Our hypothesis is that hypermutated advanced prostate cancer is caused by defects in genes regulating DNA repair pathways, which can be accurately identified using existing clinical diagnostics, and that hypermutation status can predict responses to therapy.

2. KEYWORDS

Prostate cancer, hypermutation, hyper-mutation, microsatellite instability, MSI, MLH1, MSH2, MSH6, PMS2, metastasis, precision medicine

3. ACCOMPLISHMENTS

Accomplishments in the first year for research-specific tasks are reported according to major goals of the project in the approved SOW, and organized by specific aim.

3.1 What were the major goals of the project?

Specific Aim 1: Identify mechanisms that drive the hypermutated phenotype in advanced prostate cancer.	**Months**	**Completed in Year 1?**
Major Task: Sequence DNA repair pathway genes in advanced prostate cancer tumor samples	**1-12**	**Yes**
Subtask 1: Examine hypermutated and non-hypermutated UW prostate cancer rapid autopsy samples using BROCA and UW-OncoPlex assays	1-6	**Yes**
Subtask 2: Assess for functional loss of DNA repair pathway gene expression by IHC, and MSI PCR	3-12	**Yes**
Milestone(s) Achieved: identification of specific mutated DNA repair pathway genes in hypermutated prostate cancer	12	**Yes**

Specific Aim 2: Determine unique vulnerabilities of hypermutated prostate cancer to therapy in xenograft models.	**Months**	**Completed in Year 1?**
Major Task: Assess differential responses to chemotherapy and targeted therapy in LuCaP tumor cell lines xenografted in mice	12-36	No
Subtask 1: Use xenograft LuCaP hypermutated prostate cancer cells lines 58, 73, and 147 and 3 non-hypermutated control cell lines. Assess xenograft tumor responses to chemotherapy and targeted therapy agents	12-36	Partially
Milestone(s) Achieved: Identification of differential efficacy of targeted therapies in hypermutated prostate cancer	24-36	No

Specific Aim 3: Develop and validate a clinical diagnostic approach to determine hypermutation status in advanced prostate cancer.	**Months**	**Completed in Year 1?**
Major Task: Establish a clinical assay(s) to detect tumor hypermutation	1-24	Partially
Subtask 1: Develop bioinformatics methods to accurately detect hypermutation and microsatellite instability using the UW-OncoPlex assay	1-12	Yes
Subtask 2: Establish the performance characteristics of MSI-PCR and IHC-based approaches to detect hypermutation compared to the UW-OncoPlex genomic sequencing	12-24	No
Milestone(s) Achieved: Clinically validated approach to detect the hypermutated subtype of advanced prostate cancer established	24	No
Milestone(s) Achieved: Original manuscript on bioinformatics method on detected MSI by next-generation sequencing	12-24	Yes

Specific Aim 4: Implement diagnostic testing for hypermutation status in the UW-OncoPlex program for precision cancer medicine.	**Months**	**Completed in Year 1?**
Major Task: Clinical trial of UW-OncoPlex testing in advanced prostate cancer that includes assessment of hypermutation status	24-36	No
Subtask 1: Establish a clinical trial that includes hypermutation testing by UW-OncoPlex with or without additional MSI-PCR/MSI-IHC tests depending on results of Aim 3	24-36	No
Subtask 2: Report hypermutation status results to medical oncologists in prostate cancer precision tumor board meetings and document treatment decisions and short-term outcomes.	24-36	No
Milestone(s) Achieved: Hypermutation status is used in clinical decision making for men with advanced prostate cancer with feedback on outcomes	36	No
Milestone(s) Achieved: Manuscript describing the clinical role of tumor hypermutation status as a predictive biomarker for advanced prostate cancer	36	No

3.12 What was accomplished under these goals?

Specific Aim 1: Identify mechanisms that drive the hypermutated phenotype in advanced prostate cancer

Work on Specific Aim 1 was largely completed in Year 1 and is summarized below. We published a manuscript in *Nature Communications* based on the work accomplished in Aim 1 (Pritchard et al. *Nat Commun.* 2014 5:4988, see Appendix 1).

Specific Aim 1, Subtask 1: *Examine hypermutated and non-hypermutated UW prostate cancer rapid autopsy samples using BROCA and UW-OncoPlex assays*

We hypothesized that mutations in key DNA repair pathway genes lead to the hypermutated subtype of advanced prostate cancer, most likely mutations in DNA mismatch repair genes. To test this hypothesis we performed targeted deep sequencing of DNA repair genes in hypermutated and non-hypermutated advanced prostate cancer samples from two sources: LuCaP xenograft lines and tumors from the UWMC rapid autopsy program. Both tumor sources consisted primarily of castration resistant prostate cancer (CRPC). Using exome sequencing we identified 3 hypermutated patient-derived xenograft (PDX) lines (LuCaP 58, LuCaP 73, and LuCaP 147) and 5 of 50 rapid autopsy patients with hypermutated tumors (05-165, 03-130, 06-134, 00-010, 05-123). There was partial overlap between the PDX and the autopsy cases because some LuCaP lines had been derived from the autopsy patients. There were a total of 7 out of 60 unique patients who had hypermutated tumors, for an overall prevalence of 11.6% in our cohort.

We performed the BROCA targeted DNA capture and massively parallel sequencing assay that assesses single nucleotide variants (SNVs), small insertions and deletions (indels), copy number variants (CNVs), and structural variants (SVs) in DNA repair genes simultaneously. Importantly, the BROCA assay includes capture of complete genes including introns and flanking sequences, which is in contract to exome sequencing which captures exons only. This detail proved to be crucial to our success in this research aim. We sequenced samples to an average of ~800x depth, multiplexing 24 samples per lane on a HiSeq2500. The BROCA assay uses the Agilent SureSelect enrichment system to capture the coding exons and flanking splice sites of genes listed in **Table 1**.

Table 1: BROCA genes (assay version 6)

DNA Repair Pathways	*ATM*	*ATR*	*BAP1*	*BARD1*	*BRCA1*	*BRCA2*	*BRCC3*	*BRIP1*
	CHEK1	*CHEK2*	*FAM175A*	***MLH1***	*MRE11A*	***MSH2***	***MSH6***	*NBN*
	PALB2	***PMS2***	*PRSS1*	*PTEN*	*RAD50*	*RAD51B*	*RAD51C*	*RAD51D*
	RBBP8	*TP53*	*TP53BP1*	*XRCC2*				
Additional Cancer-Related	*AKT1*	*APC*	*BMPR1A*	*CDH1*	*CDK4*	*CDKN2A*	*CTNNA1*	*GALNT12*
	GEN1	*GREM1*	*HOXB13*	*MEN1*	*MUTYH*	*PIK3CA*	***POLD1***	***POLE***
	PPM1D	*RET*	*SDHB*	*SDHC*	*SDHD*	*SMAD4*	*STK11*	*VHL*

To assess within-patient tumor mutation heterogeneity we tested up to 4 different metastatic sites in a subset of patients. For each patient we also tested matched normal (non-tumor) tissue to determine if mutations were inherited or somatic.

All three PDX hypermutated tumors had complex structural rearrangements in *MSH2*, *MSH6* or both genes (**Table 2**), while only 1 of 20 non-hypermutated xenografts had mutations in these genes (LuCaP 145, derived from a patient with neuroendocrine prostate cancer, Supplementary Fig. 4). A second loss-of-function mutation in *MSH2* or *MSH6* was detected in the three hypermutated PDX tumors, but not in LuCaP 145, supporting a requirement for bi-allelic gene inactivation underlying the hypermutated genome.

We performed the BROCA targeted DNA capture and massively parallel sequencing assays that assesses single nucleotide variants (SNVs), small insertions and deletions (indels), copy number variants (CNVs), and structural variants (SVs) in DNA repair genes simultaneously.

All three PDX hypermutated tumors had complex structural rearrangements in *MSH2*, *MSH6* or both genes (**Table 2**), while only 1 of 20 non-hypermutated xenografts had mutations in these genes (LuCaP 145, derived from a patient with neuroendocrine prostate cancer). A second loss-of-function mutation in *MSH2* or *MSH6* was detected in the three hypermutated PDX tumors, but not in LuCaP 145, supporting a requirement for bi-allelic gene inactivation underlying the hypermutated genome.

Table 2: Mismatch Repair (MMR) Gene Mutations Detected in All Hypermutated Prostate Cancers

Tumor	Source	Hyper-mutated	MSI	MMR Gene Mutation(s)*
LuCaP 58	PDX	Yes	Yes	1) *MSH6* del exon 8 to 3'UTR 2) *MSH6* frameshift (c.3799_3800del)
LuCaP 73	PDX	Yes	Yes	1) *MSH2* and *MSH6* copy loss (del 3Mb) 2) *MSH2-FBXO11* inversion
LuCaP 147**	PDX	Yes	Yes	1) *MSH2-KCNK12* 74kb inversion 2) *MSH2-KCNK12* 40kb inversion 3) *MSH2-C2orf61* inversion
05-165**	Autopsy	Yes	Yes	1) *MSH2-KCNK12* 74kb inversion 2) *MSH2-KCNK12* 40kb inversion 3) *MSH2-C2orf61* inversion
03-130	Autopsy	Yes	Yes	1) *MSH2* translocation splits the gene t(2;18) 2) *MSH2* copy loss 3) *MSH6* frameshift (c.2690del) 4) *MSH6* copy loss
06-134	Autopsy	Yes	Yes	*MLH1* homozygous copy loss
00-010	Autopsy	Yes	Yes	*MSH2* frameshift (c.2364_2365insTACA)
05-123	Autopsy	Yes	Yes	1) *MSH2* frameshift (c.1124_1125insG) 2) *MSH2* frameshift (c.1082del) 3) *MLH1* frameshift (c.1310del), lymph node only

*Mosaic *MSH6* frameshift mutations observed in a poly G tract in exon 5 (c.3261dup/del) and poly A tract in exon 7 (c.3573del) were detected in several hypermutated samples and are not included in the table because they are presumed to be due to MSI.
**LuCaP 147 is derived from patient 05-165

We detected mutations with predicted loss-of-function in *MSH2*, *MSH6*, or both genes in 4 of 5 rapid autopsy patients with hypermutated tumors. Mutations included complex structural rearrangements, copy losses, and frameshift mutations (**Table 2, Figure 1**). Two hypermutated patients had mutations in the MMR gene *MLH1*. In all patients hypermutation status and MMR mutations were concordant at different metastatic sites tested in the same patient. MMR mutations were also concordant between primary tumor and metastasis except for a single *MLH1* frameshift mutation in patient 05-123 not found in the primary (**Table 2**). No MMR mutations were detected in patient-matched non-tumor tumor tissue, indicating that that none of the MMR mutations were inherited in the germline.

A) *MSH2* Structural Rearrangement in Hypermutated Autopsy Tumor 05-165 and LuCaP 147

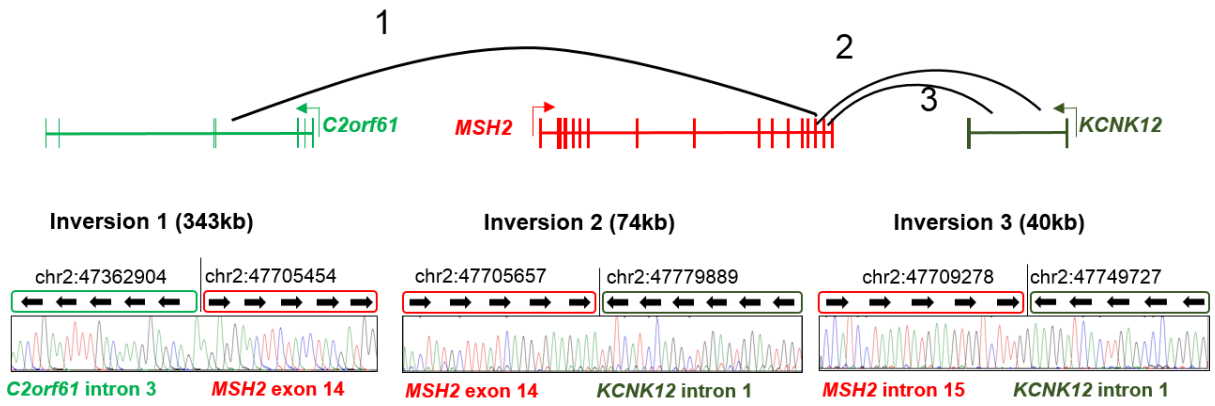

B) *MSH2* Structural Rearrangement in Hypermutated Autopsy Tumor 03-130

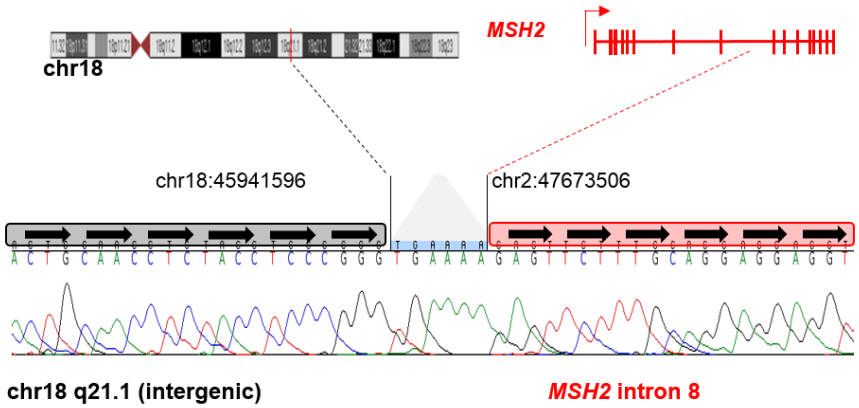

Figure 1: Examples of complex *MSH2* structural rearrangement detected in hypermutated prostate tumors. A) In autopsy sample 05-165 and patient-derived xenograft LuCaP 147 is a representative complex *MSH2* rearrangement (LuCaP 147 was derived from autopsy patient 05-165). B) *MSH2* structural rearrangement in hypermutated autopsy tumor 03-130. Breakpoints were confirmed by Sanger sequencing. Genomic coordinates are build hg19. A total of 4 or 7 hypermutated cases had complex rearrangements in *MSH2* and *MSH6* or both genes.

To cross-validate mutation calling for our UW-OncoPlex targeted sequencing platform that is the focus of clinical sequencing work for precision medicine we tested one hypermutated rapid autopsy prostate cancer case (00-010) and two non-hypermutated autopsy cases (00-029 and 00-090) using UW-OncoPlex. We also tested one LuCaP line (LuCaP 23.1). Among the genes that overlap the two panels there was 100% concordance of somatic coding mutation calls that were present at >5% variant allele fraction between the two platforms.

Specific Aim 1, Subtask 2: *Assess for functional loss of DNA repair pathway gene expression by IHC, and MSI PCR*

MSH2 and *MSH6* are mismatch DNA repair genes that act together as a heterodimer, and bi-allelic inactivating mutations of either gene are predicted to result in microsatellite instability (MSI). PCR of microsatellite loci revealed MSI in all hypermutated tumors, from both PDX and autopsy patients (**Figure 2**, **Table 2**). IHC for DNA mismatch repair proteins in hypermutated tumors demonstrated complete loss of MSH2 and/or MSH6 in a pattern consistent with the inactivating mutations detected by sequencing (**Figure 3**). Non-hypermutated tumors were microsatellite stable and had intact MSH2 and MSH6 protein.

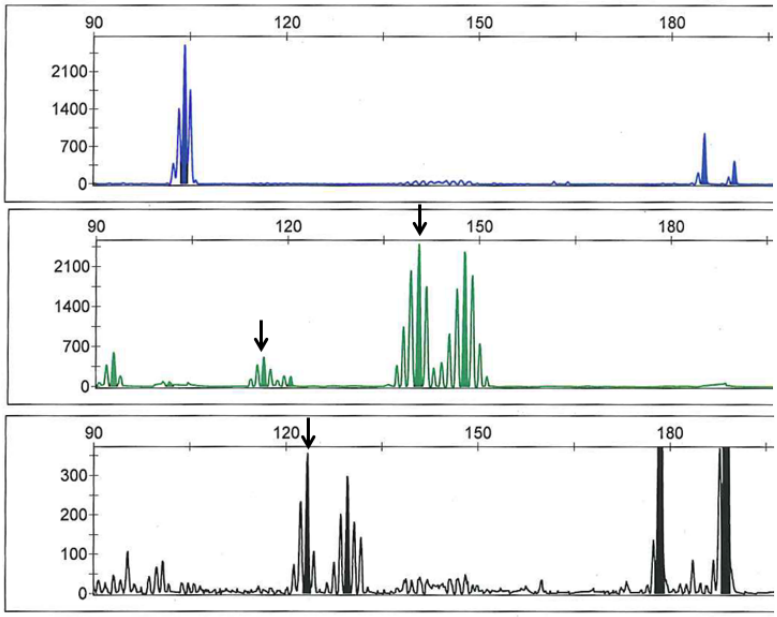

Figure 2: Hypermutated tumors are MSI-High. Hypermutated tumors exhibited microsatellite instability by PCR. Shown is representative data for LuCaP 58 which is positive for MSI in 3/5 mononucleotide marker systems (BAT25, MONO27, NR26, arrows). All hypermutated tumors were MSI-PCR positive in at least 2/5 loci.

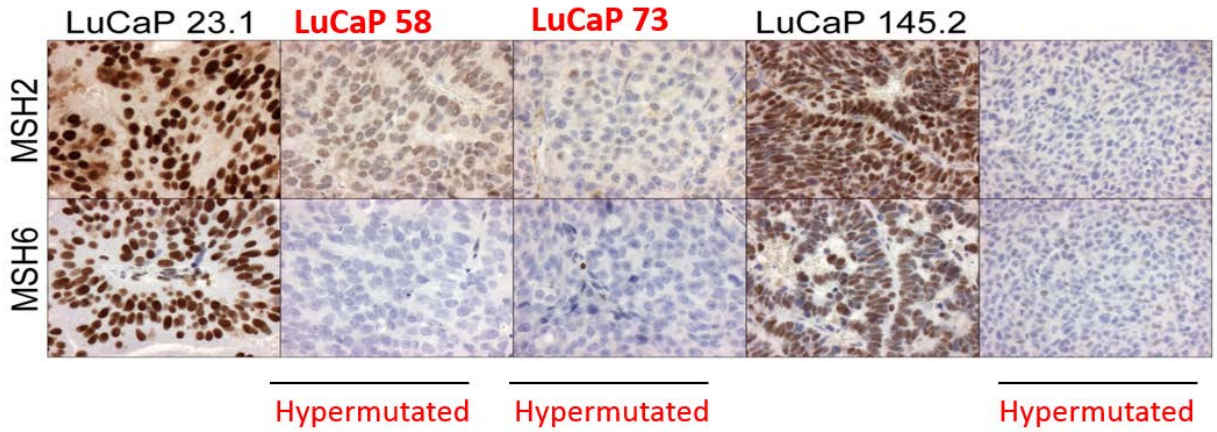

Figure 3: Hypermutated have loss of MSH2 and MSH6 protein by IHC. Similar results were observed in hypermutated tumors from rapid autopsy patients (see Appendix 1).

The findings support the conclusion that the hypermutated subtype of prostate cancer is chiefly due to loss-of-function mutations in *MSH2* and *MSH6* that result in MSI. Most interestingly, 4 of 7 hypermutated cases had complex structural rearrangements in *MSH2* and *MSH6* that were not detected by exome sequencing in the same samples, and would also not be expected to be detected by traditional exon-based Sanger sequencing methods. Previous studies have reported MMR protein loss and MSI in both primary and advanced prostate cancers, but very few MMR mutations have been identified. We speculate that technical limitations have led to an underestimation of MMR gene mutations in prostate cancer.

Specific Aim 2: Determine unique vulnerabilities of hypermutated prostate cancer to therapy in xenograft models.

Aim 2, Subtask 1: *Use xenograft LuCaP hypermutated prostate cancer cells lines 58, 73, and 147 and 3 non-hypermutated control cell lines. Assess xenograft tumor responses to chemotherapy and targeted therapy agents*

Work on aim 2 will largely be done in Year 2 and 3. In Year 1 IACUC approval was obtained to carry out animal studies and preliminary experiments begun. Note that no funding for animal studies is provided by this award. The goal of this aim is to carry out a pilot study using patient-derived xenograft (PDX) preclinical models as 'tumor avatars' to test anti-cancer therapies in comparison to responses in non-hypermutated LuCaP xenograft lines. We are assessing responses to currently used and approved chemotherapeutics including docetaxel, carboplatin and 5-fluorouricil, to determine if the hypermutated subtype is more or less susceptible to drugs that can be immediately used in clinical practice. We have identified 3 hypermutated PDX lines (LuCaP 58, 73, and 147) that we are using to assess selective responses of these therapies, in collaboration with Drs. Colm Morrissey, Robert Vessella, and Eva Corey at the University of Washington GU Cancer Research Laboratory.

For hypermutated PDX tumor LuCaP 147 we obtained 4 different metastatic sites from the patient from whom the xenograft line was derived and found that the same complex *MSH2* structural rearrangements were present in all metastatic sites in the pre-xenografted tumors, demonstrating that the MMR gene structural rearrangements are not an artifact of xenografting.

We begun by testing responses to docetaxel because it is the most commonly used genotoxic chemotherapy in advanced prostate cancer patients. In collaboration with Drs. Corey, Vessella, and Morrissey we evaluated the efficacy of docetaxel in hypermutated LuCaP xenografts (LuCaP 58, 73 and 147) and non–hypermutated LuCaP xenografts (LuCaP 105CR, 96CR, 77, 96 and 35CR). LuCaP tumors were subcutaneously implanted into SCID male mice. When tumor exceeded 100mm^3, animals were randomized and enrolled into following groups: 1) Docetaxel treatment at 10 mg/kg, 2) Docetaxel treatment at 20 mg/kg, 3) Vehicle controls/no treatment animals, and 4) Castration animals. Tumor volumes and body weight were measured once weekly.

Treatment responses for the two different dosages (10 mg/kg and 20 mg/kg) varied across the hypermutated and non-hypermutated tumor models. For hypermutated models, 10 mg/kg treatment responses ranged from major tumor growth inhibition in LuCaP 58 to mostly unimpeded tumor progression in LuCaP 147. At 20 mg/kg, LuCaP 73 exhibited maximal responsiveness as opposed to LuCaP 58 and 147 (**Figure 4**). We also assessed single animal response to docetaxel (20 mg/kg) within the hypermutated LuCaP PDX and found heterogeneity in responses. Similar to hypermutated LuCaP PDX, the non–hypermutated LuCaP PDX exhibited a broad range of susceptibility to docetaxel (see data-rich PowerPoint). Comparing the responses of hypermutated and non–hypermutated LuCaP PDX, we did not find a significant difference in susceptibility to docetaxel, or a differential survival benefit. Our results suggest a range of docetaxel responsiveness among LuCaP PDX lines that is not strongly predicted by hypermutation status.

We have begun similar experiments in the same hypermutated LuCaP lines using carboplatin and plan to test 5-FU and a PARP inhibitor. We anticipate results for additional drugs in Year 2 and 3.

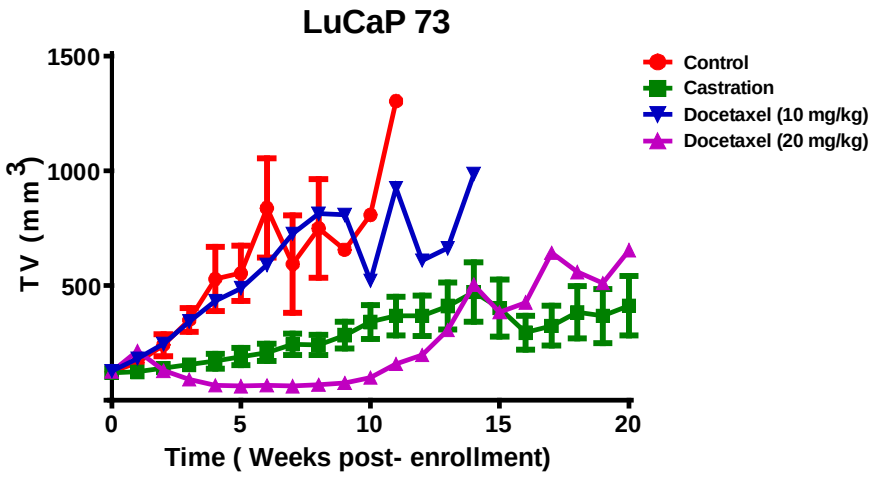

Figure 4. Responses to docetaxel in hypermutated prostate cancer PDX LuCaP 73.

Specific Aim 3: Develop and validate a clinical diagnostic approach to determine hypermutation status in advanced prostate cancer.

Aim 3, Subtask 1: *Develop bioinformatics methods to accurately detect hypermutation and microsatellite instability using the UW-OncoPlex assay*

Work on Aim 3, has been a focus of work in Year 1 and will continue in Year 2. We developed a novel method for inferring MSI and hypermutation from next-generation sequencing data that we call "mSINGS". We recently published a manuscript on this method for which Dr. Pritchard was the senior and corresponding author (Salipante et al. *Clin Chem.* 2014 60:1192-9). A graphical depiction of how the mSINGS method works is given in **Figure 5**.

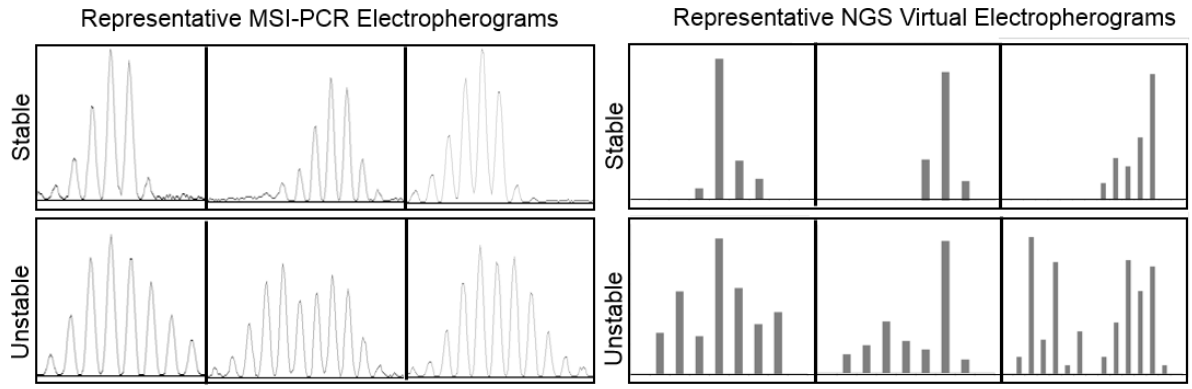

Figure 5: Detection of microsatellite instability by MSI-PCR and next-generation DNA sequencing using "mSINGS". Representative capillary electrophoresis results from MSI-PCR (top panels) and "virtual electropherograms" of next-generation DNA sequencing data (bottom panels), where the length (x-axis) and relative abundance (Y-axis) of variant repeats are plotted. Loci in top and bottom panels are not equivalent, and are from different genomic locations.

We have adapted the mSINGS method to both the BROCA and UW-OncoPlex genomic deep sequencing platforms to accurately detect both phenotypic MSI and hypermutation status, even when matched non-tumor tissue is not available (**Figure 6**). UW-OncoPlex is a clinically-validated diagnostic platform for precision cancer medicine developed by Dr. Pritchard that has been used to test over 1,000 cancer patients to date (for details on the assay see http://tests.labmed.washington.edu/UW-OncoPlex, or Google: "UW-OncoPlex"). We have identified 65 mononucleotide microsatellite loci that are captured in the current UW-OncoPlex assay version (version 4). We established parameters for each locus to be called unstable based on the SD of peak distribution and defined MSI-High as having at 20% unstable loci. Using the mSINGS informatics approach, we correctly identified all known MSI-High cancer samples (7/7) including one hypermutated prostate cancer sample which had 24/65 (37%) loci unstable (autopsy sample 00-010, liver metastasis). MSI-High samples had 35 +/- 12 unstable loci (n=7, mean +/- SD), while known microsatellite stable samples had only 2 +/- 1.5 unstable loci (n=10).

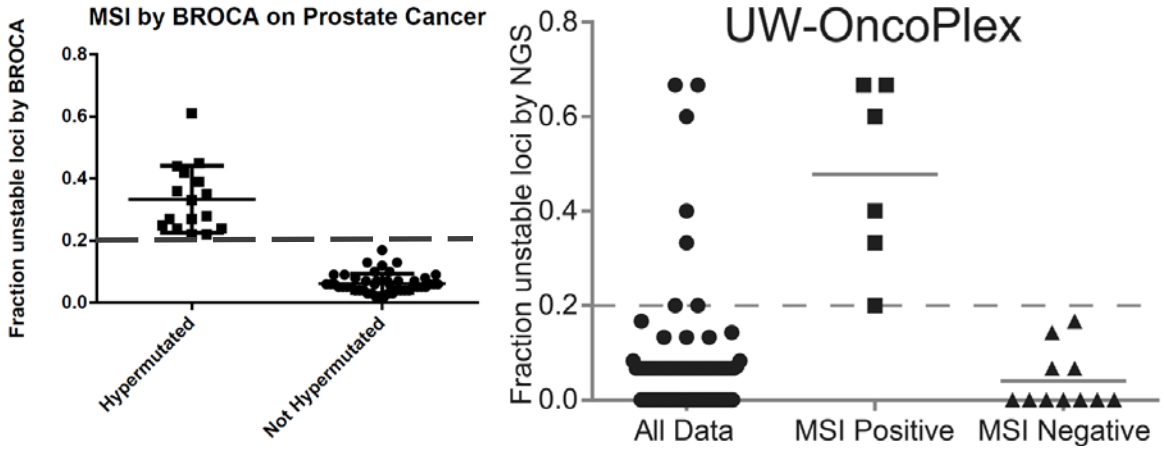

Figure 6: Detection of MSI in prostate cancer samples using mSINGS applied to BROCA and UW-OncoPlex targeted gene sequencing panels. (Left panel) The fraction of unstable microsatellite loci are shown for BROCA (left) and UW-OncoPlex (right) targeted sequencing. Results are stratified by hypermutation or MSI status. The threshold used for interpreting MSI status is indicated by a dashed line, set at a fraction of 0.2 (20% unstable loci). This threshold perfectly separated hypermutated (MSI positive) and not hypermutated (MSI negative) tumors.

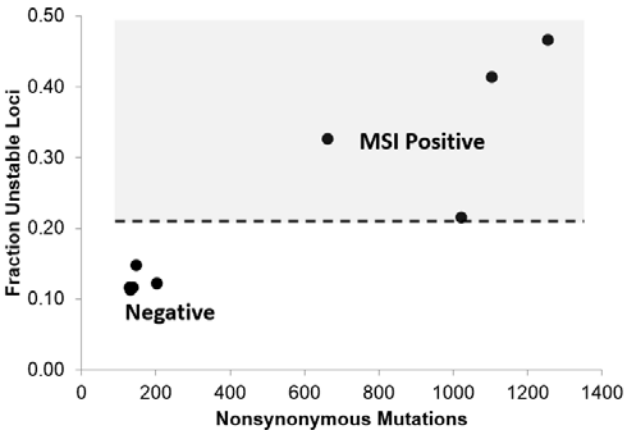

Figure 7. Hypermutated CRPC cases from SU2C international dream team have phenotypic microsatellite instability (MSI) detected by mSINGS. We applied an approach to measure microsatellite instability directly from next-generation sequencing data (mSINGS) to four hypermutated cases, defined as >300 nonsynonymous mutations in exome sequencing. A threshold fraction of 0.2 (20%) unstable loci is the cutoff for microsatellite instability using the mSINGS method (dashed line). All four hypermutated cases were MSI positive and had somatic mutations in mismatch repair genes (*MLH1, MSH2*, or *MSH6*). Selected cases with less than 300 nonsynonymous mutations were MSI negative (bottom).

In Year 1 we developed a simple and rapid clinical diagnostic assay based on the mSINGS method that we call “MSIplus”. This method using amplicon sequencing of 17 microsatellite loci, following by NGS. We validated this method on 81 tumor specimens with known MSI status, including prostate cancer samples. This work has led to a manuscript which is currently in press in the *Journal of Molecular Diagnostics* (see Appendix 4).

Aim 3, Subtask 2: *Establish the performance characteristics of MSI-PCR and IHC-based approaches to detect hypermutation compared to the UW-OncoPlex genomic sequencing*

Work on this subtask has not yet begun. In Year 2 we plan to evaluate MSI detection by MSIplus and UW-OncoPlex in hypermutated and non-hypermutated prostate cancer samples that have been previously characterized by traditional MSI-PCR. Although we have already shown that MSI can be detected in hypermutated prostate cancer samples using MSIplus, we anticipate that a subset of microsatellite loci will be optimal for detection of MSI in prostate cancer. In collaboration with Dr. Stephen Salipante we will identify a set of optimal loci for MSI detection in prostate cancer and develop bioinformatics to adapt the MSIplus assay to evaluate these loci for prostate cancer samples. With help from mentor Dr. Larry True, we also plan to evaluate IHC patterns in hypermutated tumors to determine if IHC may be a reliable screening assay to identify hypermutation.

Specific Aim 4: Implement diagnostic testing for hypermutation status in the UW-OncoPlex program for precision cancer medicine.

Aim 4, Subtask 1: *Establish a clinical trial that includes hypermutation testing by UW-OncoPlex with or without additional MSI-PCR/MSI-IHC tests depending on results of Aim 3*

Work on Aim 4 is in early stages and will be a focus of work in Year 2 and 3. No funds from this award have yet been used for this aim. In year 1 we obtained IRB human subjects approval for this work. We have begun to offer clinical UW-OncoPlex testing (**Table 3**) for prostate cancer patients. Clinical reports are provided and results discussed directly with treating oncologists and urologists at a monthly precision tumor board led by Dr. Pritchard. We are evaluating treatment decision making in prostate cancer patients who have undergone UW-OncoPlex testing. We plan to use this established assay and tumor board framework to formally test the role of hypermutation status as a precision biomarker in a clinical trial in Year 2 and 3 of this research. Recent work suggests that hypermutation and MSI due to DNA mismatch repair deficiency is a predictive biomarker for anti-programmed cell death 1 (PD-1) immunotherapy in several cancers (Le et al. N Engl J Med. 2015 372:2509-20). In collaboration with Dr. Michael Schweizer, we are working on establishing a protocol to screen men with prostate cancer for MSI using MSIplus as a qualifying test for enrollment on anti-PD-1 therapeutic trials. This work is in planning stages.

Aim 4, Subtask 2: *Report hypermutation status results to medical oncologists in prostate cancer precision tumor board meetings and document treatment decisions and short-term outcomes.*

Work on this subtask will largely be done in year 2 and 3. We have already identified one patient with a hypermutated prostate cancer at precision tumor board. This patient had MSI detected by our mSINGS method using UW-OncoPlex and an underlying tumor *MSH6* mutation with associated loss of heterozygosity. The discussion at precision tumor board suggested that the patient may be eligible for an anti-PD-1 checkpoint inhibitor immunotherapy trial. Recent work on MSI-high cancers indicates that hypermutation may predict response to anti-PD1 therapy. Unfortunately, this patient's disease was very aggressive and the patient passed away

before trial enrollment could be accomplished. In year 2 and 3 we anticipate identifying at least 3 to 4 additional hypermutated patients through a 100 patient pilot study.

Table 3: UW-OncoPlex™ genes (assay version 4)

Tier 1: Currently actionable	*ABL1*	*AKT1*	*ALK*	*AR*	*ASXL1*	*AURKA*	*BAP1*	*BCR*	*BCL2L11*
	BRAF	*BRCA1*	*BRCA2*	*CCND1*	*CCNE1*	*CDK4*	*CDK8*	*CEBPA*	*DDR2*
	DNMT3A	*EGFR*	*EML4*	*EPHB2*	*ERBB2*	*FGFR2*	*FGFR4*	*FLT3*	*HIF1A*
	IDH1	*IDH2*	*JAK2*	*KIF5B*	*KIT*	*KRAS*	*MAP2K1*	*MET*	*MLL*
	MPL	*NKX2-1*	*NPM1*	*NRAS*	*PDGFRA*	*PIK3CA*	*PML*	*PTEN*	*RARA*
	NTRK1	*ROS1*	*RET*	*STK11*	*TP53*	*VHL*	*PALB2*	*CALR*	*DNAJB1*
Tier 2: Actionable in the near future	*ABL2*	*AKT2*	*AKT3*	*ATM*	*AURKB*	*BCOR*	*CBL*	*CBLB*	*CDK6*
	CHEK1	*CHEK2*	*ERBB3*	*ERBB4*	*FBXW7*	*FGFR1*	*FLT1*	*FLT4*	*GATA2*
	GNA11	*GNAQ*	*GRM3*	*HDAC4*	*HRAS*	*IGF1R*	*IKZF1*	*JAK3*	*KDM6A*
	KDR	*MAP2K2*	*MAPK1*	*MC1R*	*MCL1*	*MDM2*	*MDM4*	*MEN1*	*MITF*
	MLH1	*MRE11A*	*MSH2*	*MSH6*	*MYC*	*MYCN*	*NF2*	*NOTCH1*	*PAX5*
	PDGFRB	*PIK3R1*	*PMS2*	*RAF1*	*RUNX1*	*SMO*	*SRSF2*	*SUZ12*	*TMPRSS2*
	TSC1	*TSC2*	*TET2*	*TYR*	*WT1*	*POLE*	*POLD1*	*AXL*	*ATRX*
	BARD1	*BRIP1*	*RAD51C*	*RAD51D*	*NBN*	*FAM175A*	*PHF6*	*SHH*	*GLI1*
	DAXX	*H3F3A*	*SUFU*	*TACSTD2*					
Tier 3: Frequently mutated	*APC*	*BAK1*	*BCL2*	*CDH1*	*CDKN2A*	*CREBBP*	*CRLF2*	*CSF1R*	*CTNNB1*
	EPHA3	*EPHA5*	*EPHB6*	*ETV6*	*EZH2*	*FGFR3*	*FOXA1*	*GAB2*	*GATA3*
	GATA1	*GNAS*	*GRIN2A*	*HNF1A*	*IL7R*	*JAK1*	*MAP2K4*	*MED12*	*MUTYH*
	MYCL1	*NF1*	*NOTCH2*	*PBRM1*	*PRPF40B*	*PTCH1*	*PTPN11*	*PTPRD*	*RB1*
	RICTOR	*RPS14*	*SF1*	*SF3B1*	*SMAD2*	*SMAD3*	*SMAD4*	*SMARCA4*	*SMARCB1*
	SPOP	*SPRY4*	*SRC*	*TFG*	*TGFBR2*	*TRRAP*	*U2AF1*	*U2AF65*	*ZRSR2*
	ZBTB16	*CDKN1A*	*CHD1*	*MTAP*	*MLH3*	*PLK1*	*PLK3*	*PLK4*	*PAK1*
	TACC3	*DOCK7*	*DEPDC5*	*NPRL2*	*NPRL3*	*MIOS*			
Germline pharmaco-genomics	*ABCB1*	*ABCC2*	*ABCC4*	*ABCG2*	*C1orf144*	*COMT*	*CYP1B1*	*CYP2C19*	*CYP2C8*
	CYP2D6	*CYP3A4*	*CYP3A5*	*DPYD*	*EIF3A*	*ERCC2*	*ESR1*	*ESR2*	*FCGR1A*
	FCGR2A	*FCGR3A*	*GSTP1*	*GUCY1A2*	*ITPA*	*LRP2*	*MAN1B1*	*MTHFR*	*NQO1*
	NRP2	*SLC19A1*	*SLC22A2*	*SLCO1B3*	*SOD2*	*SULT1A1*	*TPMT*	*TYMS*	*UGT1A1*
	UMPS								

http://tests.labmed.washington.edu/UW-OncoPlex
This is a clinically-available comprehensive gene sequencing platform co-developed and offered clinically by Dr. Pritchard's CLIA-certified genetics and solid tumors laboratory.

3.3 What opportunities for training and professional development has the project provided?

Training-specific tasks from the approved SOW are given below. Detail related to training goals in the first year is provided in the section that follows.

Major Task: Training and educational development in prostate cancer research	**Months**	**Completed in Year 1?**
Subtask 1: Attend the Prostate Cancer Foundation Annual Retreat and the Association of Molecular Pathology Annual Conference	1-36	Yes, see *National Conferences and Committees section below*
Subtask 2: Present research at the monthly mentor group meetings, and at least once per year at Pacific Northwest Prostate Cancer SPORE research conferences	1-36	Yes, *Seminars* and *Interaction with Mentors sections below*
Subtask 3: Lead local prostate cancer precision tumor board, including review of genomic sequencing data and preparation of presentations that integrate prostate cancer patient clinical histories with genomic findings	1-36	Yes, see *Prostate Precision Tumor Board section* below
Subtask 4: Attend face-to-face meetings as part of the Stand-Up-To-Cancer (SU2C) prostate cancer dream team 2 to 3 times/year. Attend monthly conference calls for the SU2C prostate cancer dream team sequencing and analysis group	1-24	Yes, see *National Conferences and Committees section below*
Subtask 5: Lead local "pipeline" journal club focused on application of new genomic technologies in the clinic	1-36	Yes*, see Journal Club section below*
Subtask 6: Train senior pathology residents and fellows in the interpretation and clinical reporting of prostate-cancer focused precision diagnostics	1-36	Yes*, see Teaching section below*
Subtask 7: Serve as PI for the prostate cancer precision medicine component of the local "ACT-SMART" initiative as part of the institute for prostate cancer research	1-36	Yes
Subtask 8: Clinical reporting of UW-OncoPlex testing applied to advanced prostate cancer	12-36	Yes, *see prostate cancer precision tumor board and clinical duties below*
Subtask 9: Hands-on training in prostate cancer with Dr. True in pathology/immunohistochemistry and exposure to preclinical	1-36	Yes, see *Hand's-on training*

prostate cancer models with Drs. Vessella and Morrissey.		section below
Milestone(s) Achieved: Publication of original research	24-36	Yes, *see appendices for publications in the first year*
Milestone(s) Achieved: Presentation of project data at a national meeting	12-36	Yes, see *National Conferences and Committees section below*

National Conferences and Committees: In year 1 I attended the Prostate Cancer Foundation annual retreat where I presented work on mechanisms of hypermutation in advanced prostate cancer. I also attended the Prostate Cancer Foundation Coffey-Holden Prostate Cancer Academy Meeting. This 3-day invite-only meeting was a think tank of leading prostate cancer researchers focused on the question of oligo-metastatic disease. I attended the Association of Molecular Pathology Annual Conference, which is my primary professional society. This year, I was invited to give an opening plenary session at the 2015 Association of Molecular Pathology Annual Conference on the topic of bioinformatics as a new area for the clinical laboratory. I also attended Stand Up to Cancer (SU2C) Prostate Cancer International Dream Team face-to-face meetings and participated in monthly SU2C sequencing and analysis conference calls. As part of my involvement with the SU2C Prostate Cancer International Dream Team I analyzed genomic data, prepared figures for publication, and gave a formal presentation to the SU2C team members.

Seminars: I continue to attend and present at the weekly Pacific Northwest Prostate Cancer SPORE conference series. For example, at the most recent SPORE talk my work on Aim 1 of this research was presented in addition to my collaborative with the SU2C international dream team. I also attend weekly Laboratory Medicine grand rounds and Laboratory Medicine research rounds which include a wide range of topics related to clinical diagnostic medicine.

Teaching: In year 1 of funding I trained 4 senior clinical pathology residents, 2 molecular genetic pathology fellows, and 2 junior molecular pathology faculty (Dr. Eric Konnick and Dr. Tina Lockwood) in the clinical interpretation and reporting of genomic testing for prostate cancer. I have continued to be an active mentor to our molecular genetic pathology (MGP) fellowship director, MGP fellows, and chief resident in prostate cancer-related molecular diagnostics. In addition, I have mentored 2 medical genetics senior residents in molecular oncology diagnostics, including one resident (Dr. Mari Tokita) who spent 9 months of dedicated time in my research laboratory developing circulating tumor DNA diagnostics methods. As part of this work she helped to assemble ctDNA samples for clinical assay validation from patients with metastatic prostate cancer. As associated director of the genetics and solid tumors laboratory at the UW I have also mentored 6 junior clinical pathology residents in 4-week basic genetics training rotations.

Journal Club: I continue to lead the "pipeline" monthly journal club at UW which is attended by about 20-30 faculty and senior trainees and is focused on genomic technologies applied in the clinic. I have recruited several speakers in year 1 of funding. Examples include a speaker (Mary Goldman) who works for the UCSC genome browser and outlined new tools for cancer data visualization, and a speaker who discussed new methods for gene fusion analysis in cancer, including *TMPRSS2-ERG* fusion detection in prostate cancer (David Wu).

***Prostate Precision Tumor Board*:** I lead the local prostate precision tumor board at the University of Washington where we review genome sequencing data from advanced prostate cancer patients and make treatment recommendations to treating oncologists. This activity is a substantial effort in which I prepare detailed PowerPoint presentations for each patient and do a thorough literature review to identify potential or actual therapeutic implications for genomic findings. This monthly tumor board is attended by GU medical oncologists, pathologists (including co-mentor Dr. Larry True), urologists, research coordinators, genetic counselors, and trainees including our junior faculty and molecular genetic pathology fellows.

***Clinical Duties*:** I am a primary faculty member responsible for clinical reporting of BROCA and UW-OncoPlex tests that are available through my CLIA-certified laboratory. I have already trained 2 other junior molecular pathology faculty to assist me, and will continue to mentor and train new junior faculty to assist with these clinical duties. My clinical work includes close mentorship from Dr. Mary-Claire King, who personally consults on all BROCA cases. We have weekly "signout" meetings that last 1 to 2 hours. I interpret and write clinical reports for approximately 1,000 genomic sequencing cases per year. As part of my clinical work I interpret and report on UW-OncoPlex clinical testing for all prostate cancer patients tested.

***Grant Writing*:** In year 1, in collaboration with Dr. Peter Nelson and Dr. Bruce Montgomery, I am a partnering PI for a DOD IMPACT proposal focused on DNA repair defects as a predictive biomarker for advanced prostate cancer. I am also preparing an R01 application in collaboration with Heather Hampel at The Ohio State University focused on genomic sequencing as a tool for Lynch syndrome screening. This application benefits from the work we have done to develop robust methods to detect hypermutation and MSI in cancer.

***Hand's-on training*:** With Dr. True I have received personal tutorials in prostate cancer pathology, including one-on-one formal lectures followed by teaching slide review. In addition, Dr. True provides helpful feedback on prostate pathology-related issues at the monthly prostate precision tumor board that I lead. I have also received 'hand's on' exposure to preclinical prostate cancer models with Drs. Eva Corey, Robert Vessella and Colm Morrissey in the University of Washington GU Cancer Research Laboratory.

Interaction with Mentors: I am **co-mentored by Dr. Larry True and Dr. Mary-Claire King** for this training award. Dr. True is an internationally prominent genitourinary pathologist with over 30 years-experience mentoring junior academic researchers. He and I have worked together since 2000, and he has effectively mentored me in aspects of prostate cancer pathology, and molecular biomarker development. For example, I served on the NCI Tissue-Based biomarker subcommittee of the Investigational Drug Steering Committee that Dr. True chaired. Dr. King is an internationally famous geneticist who discovered the *BRCA1* locus, and has mentored dozens of highly successful faculty in the area of cancer genetics. She has mentored me since 1998 as part of the medical scientist training program and has been an even closer ongoing

mentor to me over the past 3 years in the clinical implementation of the BROCA assay that was developed in her laboratory by Dr. Tom Walsh. I meet more than once a month at length with Dr. King to discuss BROCA test results and discuss research directions, and I meet with Dr. True at the monthly prostate cancer precision tumor board. In addition, I meet with Dr. True for formal prostate cancer pathology training.

3.4 How were the results disseminated to communities of interest?

Through the Institute for Prostate Cancer Research (IPCR) we have reached out to patient advocates in the region. This has included a formal presentation on prostate cancer precision medicine that I gave to a lay audience for the IPCR on the topic of the UW-OncoPlex program for prostate cancer precision medicine. In year 2 we plan to work on a segment to air on UWTV that highlights the prostate cancer precision tumor board that I lead.

3.5 What do you plan to do during the next reporting period to accomplish the goals?

Plans in Year 2

Research-specific tasks

- Evaluate all available tumor and matched normal samples from the UW rapid autopsy program by BROCA to identify additional hypermutated cases.
- Continue work in Aim 2 to test carboplatin and 5-FU therapies in hypermutated PDX tumors (no funds from this award used for animal studies).
- Implement MSIplus as a routine clinical assay through Dr. Pritchard's CLIA-certified lab. Evaluate performance characteristics of MSIplus for prostate cancer and determine the optimal loci.
- Validate mSINGS analysis by UW-OncoPlex for clinical use and reporting in prostate cancer.
- Test additional SU2C international dream team CRPC cases by mSINGS and correlate with MMR mutation status.
- Work on 50 patient pilot project using clinical UW-OncoPlex for men with prostate cancer. Use experience gained from clinical testing to inform a future clinical trial for men with hypermutated prostate cancer.
- Evaluate treatment decision making in prostate cancer patients who have undergone UW-OncoPlex testing through review with treating oncologists at the precision tumor board. The primary measured outcome will be treatment decisions specifically influenced by hypermutation status results. We will use this data to plan future clinical trials to more formally test the role of hypermutation status as a precision biomarker.
- Investigate protocols to refer men with hypermutated MSI prostate cancer to existing clinical trials, including trials of anti PD-1 immunotherapy.

Training-specific tasks

- Attend PCF annual meeting and AMP annual meetings as well as SU2C prostate international dream team face-to-face meetings.
- Present data at SPORE conference and at national conferences.
- Continue resident and fellow training of genomic testing in prostate cancer
- Continue hand's on training meetings with Dr. True in prostate cancer pathology

- Continue frequent genomic sequencing signout sessions in cancer genetics with Dr. Mary-Claire King (about 2 to 3 times per month).
- Continue to lead monthly Prostate Precision Tumor Board
- Continue to lead monthly pipeline journal club
- Continue grant writing activities

4. IMPACT

4.1 What was the impact on the development of the principal discipline(s) of the project?

The work in year 1 of this research has led to the discovery of the mechanism of hypermutation in advanced prostate cancer. We found that complex somatic *MSH2* and *MSH6* mismatch DNA repair mutations resulting in microsatellite instability are the chief cause of hypermutation. We also found that hypermutation is more common in advanced prostate cancer than previously expected, with 7/60 (12%) patients identified in our series. Our discovery identifies parallels and differences in the mechanisms of hypermutation in prostate cancer compared with other microsatellite instability-associated cancers. Our findings have important implications for prognosis and treatment. If hypermutation can be targeted, a substantial minority of patients with advanced prostate cancer may benefit. For example, cancers with mismatch DNA repair deficiency have recently been shown to be responsive to anti-PD-1 immunotherapy. Our research has also facilitated microsatellite instability and immunohistochemistry-based testing as screening tools for hypermutation in advanced prostate cancer.

Our work in year 1 has also led to the development of highly innovative and robust methods to detect microsatellite instability (MSI) that is associated with hypermutation. We recently developed the "mSINGS" method for detection of MSI directly from NGS. This has facilitated MSI analysis of exome data from the SU2C prostate cancer international dream team consortium, proving that all hypermutated prostate cancer cases in that series also have MSI associated with underlying mismatch DNA repair mutations.

4.2 What was the impact on other disciplines?

Our work builds bridges between research in colorectal and endometrial cancer and research in prostate cancer. Hypermutation and MSI are well-studied in colorectal and endometrial cancer. We have applied the mSINGS method we developed to both colorectal and endometrial cancer, resulting in the first ever tumor-based DNA sequencing test for Lynch syndrome, ColoSeq Tumor. We collaborate closely with colleagues at the Ohio State University on Lynch syndrome screening research (Heather Hampel and Albert de la Chapelle), resulting in a recent NIH R01 grant submission that harnesses the mSINGS method.

4.3 What was the impact on technology transfer?

Nothing to Report

4.4 What was the impact on society beyond science and technology?

Nothing to Report

5. CHANGES/PROBLEMS

5.1 Changes in approach and reasons for change

Due to cost constraints we were required to slightly modify our planned experimental design for aim 2 to evaluate only 3 different therapies in the hypermutated and non-hypermutated LuCaP xenograft models. The three therapies chosen are docetaxel, carboplatin, and 5-FU. Note that this change does not affect the budget of this award because no vertebrate animal work is funded through this training award.

5.2 Actual or anticipated problems or delays and actions or plans to resolve them

Based on prior experience by the GU cancer research laboratory we anticipate potential problems with carboplatin toxicity in future LuCaP xenograft animal studies. This is particularly a problem for the LuCaP 58 hypermutated line in which frequent ulceration may occur. To address this, we will lower the dose and dosing frequency of carboplatin for this arm of the study.

5.3 Changes that had a significant impact on expenditures

Nothing to report.

5.4 Significant changes in use or care of human subjects, vertebrate animals, biohazards, and/or select agents

Nothing to report.

6. PRODUCTS

6.1 Publications, conference papers, and presentations

6.11 Journal publications

Pritchard CC (corresponding author), Morrissey C, Kumar A, Zhang X, Smith C, Coleman I, Salipante SJ, Milbank J, Tait JF, Corey E, Vessella RL, Walsh T, Shendure J, Nelson PS; Complex *MSH2* and *MSH6* Mutations in Hypermutated Microsatellite Unstable Advanced Prostate Cancer; *Nature Communications*; 5: 2014; 4988; published; acknowledgement of federal support (yes).
See Appendix 1 and 2

Robinson D, Van Allen EM, Wu Y, Schultz N., Lonigro RJ, Mosquera J, Montgomery R, Taplin ME, **Pritchard CC (co-second author)**, Attard G, Beltran H, Abida WM, Bradley RK, Vinson J, Cao X, Vats P, Kunju LP, Hussain M, Feng FY, Tomlins SA, Cooney KA, Smith DC, Brennan C, Siddiqui J, Mehra R, Scher HI, Chen Y, Rathkopf DE, Morris MJ, Solomon SB, Durack JC, Reuter VE, Gopalan A, Gao J, Loda M, Lis RT, Bowden M, Balk SP, Gaviola G, Sougnez C, Gupta M, Yu EY, Mostaghel EA, Cheng HH, Chew FS, True LD, Plymate SR, Dvinge H,

Ferraldeschi R, Flohr P, Miranda S, Zafeiriou Z, Tunariu N, Mateo J, Demichelis F, Elemento O, Robinson BD, Sboner A, Schiffman MA, Nanus DM, Tagawa ST, Sigaras A, Eng KW, Heath E, Pienta KJ, Kantoff P, de Bono JS, Rubin MA, Nelson PS, Garraway LA, Sawyers CL, Chinnaiyan AM; Integrative clinical sequencing analysis of metastatic castration resistant prostate cancer reveals a high frequency of clinical actionability; *Cell*. 161: 2015; 1215–1228; published; acknowledgement of federal support (yes).
See Appendix 3

Hempelmann JA, Scroggins SM, **Pritchard CC**, Salipante SJ; MSIplus: integrated colorectal cancer molecular testing by next-generation sequencing; *Journal of Molecular Diagnostics*. 2015; in press; acknowledgement of federal support (yes).
See Appendix 4

6.12 Books or other non-periodical, one-time publications.

Nothing to report.

6.13 Other publications, conference papers, and presentations.

*Pritchard CC, Morrissey C, Kumar A, Zhang X, Smith C, Coleman I, Salipante S, Grady WM, Tait JF, Vessella R, Walsh T, Shendure J, and Nelson PS. Mechanisms of Microsatellite Instability in Hypermutated Advanced Prostate Cancer. (2014) Prostate Cancer Foundation Annual Scientific Retreat.

*Salipante S, Scroggins S, Hampel HL, Turner EH, and **Pritchard CC**. Microsatellite Instability Detection By Next-Generation Sequencing. (2014) Academy of Clinical Laboratory and Physician Scientists Annual Meeting.

6.2 Website(s) or other Internet site(s)

Nothing to report.

6.3 Technologies or techniques

We have developed the mSINGS method for detection of microsatellite instability from targeted next-generation sequencing data. The source code for this bioinformatics method is freely available for academic users and can be found at: https://bitbucket.org/uwlabmed/msings. This source code has already been shared with multiple national and international researchers.

6.4 Inventions, patent applications, and/or licenses

Nothing to report.

6.5 Other Products

The genomic sequencing dataset we generated as part of the research on aim 1 to identify mechanisms of hypermutation is publically available at GenBank/EMBL/DDBJ under the accession code SRP044943.

7. PARTICIPANTS & OTHER COLLABORATING ORGANIZATIONS

7.1 What individuals have worked on the project?

Name: Colin C. Pritchard
Project Role: PI
Researcher Identifier: ORCID ID: 0000-0002-2461-1557
Nearest person month worked: 5
Contribution to Project: Dr. Pritchard has obtained funding support, designed experiments, and written manuscripts related to this work
Funding Support: (this award)

Name: Robert Livingston
Project Role: Senior Research Scientist
Researcher Identifier: ORCID ID: 0000-0002-7424-2956

Nearest person month worked: 1
Contribution to Project: Dr. Livingston has coordinated coordinating genomic sequencing library preparation and assisted in data analysis.
Funding Support: (this award)

Name: Christina Smith
Project Role: Senior Clinical Technologist
Nearest person month worked: 3
Contribution to Project: Ms. Smith has helped perform genomic sequencing assays including BROCA and UW-OncoPlex.
Funding Support: (this award)

Name: Mallory Beightol
Project Role: Research Technician
Nearest person month worked: 3
Contribution to Project: Ms. Beightol has helped perform genomic sequencing assays including BROCA and UW-OncoPlex.
Funding Support: Institutional, PNW Prostate Cancer SPORE pilot funds

Name: Geetika Sethi
Project Role: Senior Research Fellow
Nearest person month worked: 5
Contribution to Project: Dr. Sethi has helped plan animal experiments and performed NGS data analysis of prostate cancer datasets
Funding Support: Prostate Cancer Foundation

7.2 Has there been a change in the active other support of the PD/PI(s) or senior/key personnel since the last reporting period?

Colin Pritchard: Changes in current support since last reporting period:

RAF-CA14-004 (R33)

Title: Advanced Development Advanced Development and validation of targeted molecular counting methods for precise and ultrasensitive quantitation of low prevalence somatic mutations (Salipante, PI)
Time Commitment: 0.6 Calendar Months (5% effort)
Role: Co-investigator
Supporting Agency: NIH
Address of Funding Agency: grants.gov
Performance Period 4/1/15-3/31/18
Level of Funding: $295,868

Project Goals: The ultrasensitive detection of clinically relevant somatic alterations in cancer genomes has great potential for impacting patient care, e.g. for early detection, establishing diagnoses, refining prognoses, guiding treatment, and monitoring recurrence. However, current technologies are poorly suited to the robust detection of somatic mutations present at very low frequencies (<1%). Massively parallel sequencing represents an advantageous path forward, but its sensitivity to detect very rare events is fundamentally constrained by the sequencing error rate. We have recently developed a new experimental paradigm that overcomes this limitation. In our approach, each copy of a target sequence that is present in a sample is molecularly tagged during the first cycle of a multiplex capture reaction with a unique random sequence. After amplification, target amplicons and their corresponding molecular tags are subjected to massively parallel sequencing. During analysis, the molecular tags are used to associate sequence reads sharing a common origin. The availability of robust, cost-effective, quantitative, and generically applicable tools for the ultrasensitive, multiplex detection of rare somatic events in the clinical setting will provide enhanced, transformative capabilities in the diagnosis and monitoring of cancers. The methodology will also have application to basic science cancer research.

No overlap

7.3 What other organizations were involved as partners?

Nothing to report.

8. SPECIAL REPORTING REQUIREMENTS

Nothing to report.

9. APPENDICES

Appendix 1: Reprint of Pritchard CC et al.; Complex *MSH2* and *MSH6* Mutations in Hypermutated Microsatellite Unstable Advanced Prostate Cancer; *Nature Communications*; 5: 2014; 4988.

Appendix 2: Supplemental Figures from Pritchard CC et al.; Complex *MSH2* and *MSH6* Mutations in Hypermutated Microsatellite Unstable Advanced Prostate Cancer; *Nature Communications*; 5: 2014; 4988.

Appendix 3: Reprint of Robinson D et al.; Integrative clinical sequencing analysis of metastatic castration resistant prostate cancer reveals a high frequency of clinical actionability; *Cell*. 161: 2015; 1215–1228.

Appendix 4: Draft of Hempelmann JA et al.; MSIplus: integrated colorectal cancer molecular testing by next-generation sequencing; *Journal of Molecular Diagnostics*. 2015; in press.

nature COMMUNICATIONS

ARTICLE

Received 13 Mar 2014 | Accepted 14 Aug 2014 | Published 25 Sep 2014

DOI: 10.1038/ncomms5988 OPEN

Complex *MSH2* and *MSH6* mutations in hypermutated microsatellite unstable advanced prostate cancer

Colin C. Pritchard[1], Colm Morrissey[2], Akash Kumar[3], Xiaotun Zhang[2], Christina Smith[1], Ilsa Coleman[4], Stephen J. Salipante[1,3], Jennifer Milbank[3], Ming Yu[5], William M. Grady[5], Jonathan F. Tait[1], Eva Corey[2], Robert L. Vessella[2], Tom Walsh[6], Jay Shendure[3] & Peter S. Nelson[4]

A hypermutated subtype of advanced prostate cancer was recently described, but prevalence and mechanisms have not been well-characterized. Here we find that 12% (7 of 60) of advanced prostate cancers are hypermutated, and that all hypermutated cancers have mismatch repair gene mutations and microsatellite instability (MSI). Mutations are frequently complex *MSH2* or *MSH6* structural rearrangements rather than *MLH1* epigenetic silencing. Our findings identify parallels and differences in the mechanisms of hypermutation in prostate cancer compared with other MSI-associated cancers.

[1] Department of Laboratory Medicine, University of Washington, Seattle, Washington 98195, USA. [2] Department of Urology, University of Washington, Seattle, Washington 98195, USA. [3] Department of Genome Sciences, University of Washington, Seattle, Washington 98195, USA. [4] Division of Human Biology, Fred Hutchinson Cancer Research Center, Seattle, Washington 98109, USA. [5] Division of Clinical Research, Fred Hutchinson Cancer Research Center, Seattle, Washington 98109, USA. [6] Division of Medical Genetics, Department of Medicine, University of Washington, Seattle, Washington 98195, USA. Correspondence and requests for materials should be addressed to C.C.P. (email: cpritch@uw.edu).

Recently exome sequencing of metastatic prostate cancers revealed that a subset of patients harboured tumors with markedly elevated single-nucleotide mutation rates, defining a new hypermutated subtype[1]. This phenotype was subsequently observed in primary prostate cancer in a tumour that harboured an *MSH6* mutation[2]. However, mechanisms that lead to hypermutation and the prevalence of this distinct subtype have not been completely defined. Comprehensive cancer genomics efforts recently published by The Cancer Genome Atlas Research Network (TCGA) reported that 16% of colon cancers and up to 35% of endometrial cancers exhibit hypermutation[3,4]. For both colon and endometrial cancers, about three quarters of hypermutated tumors were associated with phenotypic microsatellite instability (MSI) and loss-of-function DNA mismatch repair genes via mutation or epigenetic silencing. Therefore, we hypothesized that hypermutated prostate cancer may also be associated with DNA mismatch repair (MMR) gene defects and MSI.

In this study we identified hypermutation in 7 of 60 patients with advanced prostate cancer. Using a targeted deep sequencing approach we find that all hypermutated tumors have somatic mutations in MMR genes and associated MSI. In four of seven hypermutated cases MMR mutations were complex structural rearrangements in *MSH2* and *MSH6*. We conclude that somatic rearrangements in *MSH2* and *MSH6* are an important mechanism leading to hypermutation and MSI in advanced prostate cancer.

Results

Prevalence of hypermutation. We identified hypermutated cases in exome sequencing data sets of advanced prostate cancer samples from two sources: a panel of patient-derived xenografts (PDX) and metastatic specimens obtained through a rapid autopsy programme (Supplementary Table 1). Exome data for PDX tumors was from Kumar *et al.*[1], where hypermutation was previously characterized. In the autopsy samples where hypermutation status had not been previously established, we defined hypermutation as >300 somatic protein altering mutations based on the distribution of total mutation burden in metastatic tumors, which had matched normal tissue available (Supplementary Fig. 1; Supplementary Table 1). We identified hypermutation in 3 of 15 PDX tumors (Table 1), and in metastatic tumors from 5 of 50 autopsy patients (Table 2). There was partial overlap between the two patient groups: five of the PDX tumors were derived from autopsy patients, including one with a hypermutated genome (LuCaP 147). Therefore, there were a total of 7/60 unique patients with hypermutated tumors, for an overall prevalence of 11.6%. Hypermutation status was 100% concordant at different metastatic sites, and was also concordant between primary tumour and metastasis in two patients where primary prostate tumors were available (Table 2).

Identification of *MSH2* and *MSH6* rearrangements. Because exome sequencing has limitations in detecting structural rearrangements and larger insertion/deletion (indel) mutations, we investigated alterations in DNA MMR pathway genes in hypermutated and non-hypermutated cases using a targeted deep sequencing approach (BROCA assay) that included capture of intronic and flanking DNA sequences (Supplementary Table 2)[5,6]. We developed a bioinformatics pipeline to accurately detect structural variation, copy number variation and indel mutations of all sizes[7].

All three PDX hypermutated tumors had complex structural rearrangements in *MSH2*, *MSH6* or both genes (Table 1; Fig. 1a; Supplementary Figs 2–4), while only 1 of 20 non-hypermutated xenografts had mutations in these genes (LuCaP 145, derived from a patient with neuroendocrine prostate cancer, Supplementary Fig. 5). A second loss-of-function mutation in *MSH2* or *MSH6* was detected in the three hypermutated PDX tumors, but not in LuCaP 145, supporting a requirement for bi-allelic gene inactivation underlying the hypermutated genome.

We detected mutations with predicted loss-of-function in *MSH2*, *MSH6* or both genes in four of five rapid autopsy patients

Table 1 | MMR gene mutations in prostate cancer PDX.

PDX tumour*	Patient-derived from	Hypermutated?†	MSI	MMR gene mutation(s)‡
LuCaP 58		Yes	Yes	(1) *MSH6* del exon 8 to 3′UTR (2) *MSH6* frameshift (c.3799_3800del)
LuCaP 73		Yes	Yes	(1) *MSH2* and *MSH6* copy loss (del 3 Mb) (2) *MSH2-FBXO11* inversion
LuCaP 147, 147CR	05-165	Yes	Yes	(1) *MSH2-C2orf61* 343 kb inversion (2) *MSH2-KCNK12* 74 kb inversion (3) *MSH2-KCNK12* 40 kb inversion
LuCaP 23.1, 23.1CR		No	No	None
LuCaP 35, 35CR		No	No	None
LuCaP 70, 70CR		No	No	None
LuCaP 77, 77CR		No	No	None
LuCaP 78	98-328	No	No	None
LuCaP 81	98-362	No	No	Chr2 copy losses
LuCaP 86.2, 86.2CR		No	No	None
LuCaP 92	99-069	No	No	None
LuCaP 96, 96CR		No	No	None
LuCaP 105, 105CR		No	No	None
LuCaP 141		No	No	None
LuCaP 145.1, 145.2	05-144	No	No	(1) *MSH2* exon 8-16 del (2) *MSH6-TESC* t(2;12)

MMR, mismatch repair; MSI, microsatellite instability; PDX, patient-derived xenografts.
*Matched pairs of androgen-sensitive and castration-resistant sublines (for example, LuCaP 35 and LuCaP 35CR) and tumour lines derived from the same patient are listed numerically and grouped in the same row.
†Hypermutation status was previously determined in these samples in Kumar *et al.*[1]
‡Mosaic *MSH6* frameshift mutations observed in a poly G tract in exon 5 (c.3261dup/del) and poly A tract in exon 7 (c.3573del) were detected in several hypermutated samples and are not included in the table because they are presumed to be due to MSI.

Table 2 | MMR gene mutations in rapid autopsy patients.

Autopsy patient*	Tumour site(s) tested by BROCA targeted sequencing	Mutation burden† (exome)	Hypermutated?	MSI	MMR gene mutation(s)‡
05-165*	Bone, adrenal, liver and lymph node	855	Yes	Yes	(1) *MSH2-C2orf61* 343 kb inversion (2) *MSH2-KCNK12* 74 kb inversion (3) *MSH2-KCNK12* 40 kb inversion
03-130	Lymph node	647	Yes	Yes	(1) *MSH2* translocation splits the gene t(2;18) (2) *MSH2* copy loss (3) *MSH6* frameshift (c.2690del) (4) *MSH6* copy loss
06-134	Kidney and lymph node	314	Yes	Yes	*MLH1* homozygous copy loss
00-010	Prostate and liver	673	Yes	Yes	*MSH2* frameshift (c.2364_2365insTACA)
05-123	Prostate and lymph node	807	Yes	Yes	(1) *MSH2* frameshift (c.1124_1125insG) (2) *MSH2* frameshift (c.1082del) (3) *MLH1* frameshift (c.1310del), lymph node only
01-095	Liver and lymph node	149	No	No	None
05-144*	Bone, adrenal, liver and lymph node	57	No	No	(1) *MSH2* exon 8-16 del (2) *MSH6-TESC* t(2;12)
05-214	Bone, liver and lymph node (two sites)	46	No	No	None
05-116	Bone, adrenal, liver and lung	47	No	No	None
00-029	Liver	37	No	No	None
00-090	Lymph node	69	No	No	None

MMR, mismatch repair; MSI, microsatellite instability.
*Fifty total unique autopsy patients were assessed by exome sequencing (see Supplementary Table 1). Listed are a subset of cases that were followed up by targeted deep sequencing for MMR genes. Clinical data for this patient subset is provided in Supplementary Table 6. Patient-matched non-cancer tissue was tested in every case and did not exhibit MSI or MMR mutations. LuCaP 147 and 147CR are derived from autopsy patient 05-165. LuCaP 145.1 and 145.2 are derived from autopsy patient 05-144.
†Number of protein altering somatic mutations by exome sequencing with removing of germline variants from matched-non-tumour samples.
‡Mutations were detected at every tumour site unless otherwise indicated. Mosaic *MSH6* frameshift mutations observed in a poly G tract in exon 5 (c.3261dup/del) and poly A tract in exon 7 (c.3573del) were detected in several hypermutated samples and are not included in the table because they are presumed to be due to MSI.

with hypermutated tumors. Mutations included complex structural rearrangements, copy losses and frameshift mutations (Table 2; Supplementary Figs 4 and 6–9). Two hypermutated patients had mutations in the MMR gene *MLH1*. We interrogated a subset of six non-hypermutated patients by deep sequencing and did not detect MMR gene mutations except in patient 05–144 from which the PDX LuCaP 145 was derived (Table 2). Like hypermutation status, MMR mutations were concordant at different metastatic sites in the same patient. MMR mutations were also concordant between primary tumour and metastasis except for a single *MLH1* frameshift mutation in patient 05–123 not found in the primary tumour (Table 2; Supplementary Fig. 9). Patient-matched non-tumour tissues were tested for the autopsy patients (Supplementary Table 1 and Supplementary Data 1). No MMR mutations were detected in patient-matched non-tumour tissue, indicating that none of the MMR mutations were inherited in the germline. Mutations in additional DNA repair genes are given in Supplementary Table 3.

Hypermutated tumors have phenotypic MSI. *MSH2* and *MSH6* are mismatch DNA repair genes that act together as a heterodimer, and bi-allelic inactivating mutations of either gene are predicted to result in MSI. PCR of microsatellite loci revealed MSI in all hypermutated tumors, from both PDX and autopsy patients (Fig. 1b; Supplementary Data 1). Phenotypic MSI was also detected directly from targeted next-generation data for all hypermutated tumors, and not detected in any non-hypermutated tumors (Supplementary Data 1; Supplementary Fig. 10). Immunohistochemistry (IHC) for DNA MMR proteins in hypermutated tumors demonstrated complete loss of MSH2 and/or MSH6 in a pattern consistent with the inactivating mutations detected by sequencing (Fig. 1c; Supplementary Fig. 11). Non-hypermutated tumors were microsatellite stable (Tables 1 and 2; Supplementary Data 1) and had intact MSH2 and MSH6 proteins, except LuCaP 145, which exhibited heterogeneous loss of MSH6 protein (Fig. 1c). *MLH1* methylation was not detected in any of the MSI positive tumors (Supplementary Fig. 12), and MLH1 protein expression was intact by IHC in MSI-positive tumors except in 06–134 that had homozygous *MLH1* gene deletion (Supplementary Fig. 13), arguing that *MLH1* epigenetic silencing was not responsible for MSI in any of the tumors in our series.

Discussion

Our findings support the conclusion that the hypermutated subtype of prostate cancer is chiefly due to loss-of-function mutations in *MSH2* and *MSH6* that result in MSI. Mutations were predicted to be bi-allelic in all cases except 00–010, which may harbour a second undetected mutation. Most interestingly, four of seven hypermutated cases had complex structural rearrangements in *MSH2* and *MSH6* that were not detected by exome sequencing in the same samples, and would also not be expected to be detected by traditional exon-based Sanger sequencing methods. Several previous studies have reported MMR protein loss and MSI in both primary and advanced prostate cancers, but very few MMR mutations have been identified[8–15]. We speculate that technical limitations have led to an underestimation of MMR gene mutations in prostate cancer.

Our finding of predominantly *MSH2* and *MSH6* mutations is in contrast to colon and endometrial cancer, where MSI is most often due to *MLH1* epigenetic silencing[3,4]. This supports an alternate mechanism by which MSI is acquired in prostate cancer. A recent study demonstrated that DNA translocations and deletions in advanced prostate cancer occur in a highly

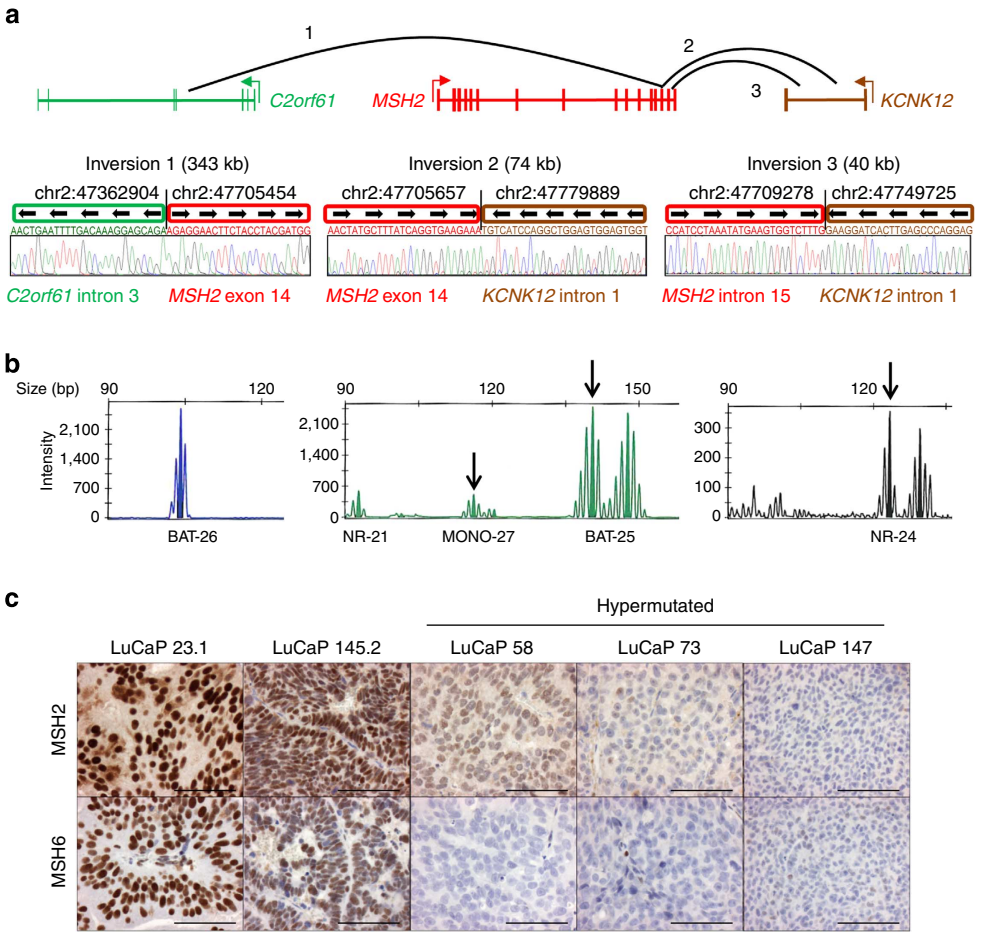

Figure 1 | *MSH2* and *MSH6* rearrangements are associated with loss of protein expression and MSI. (**a**) Four of seven hypermutated cases had complex rearrangements in *MSH2* and *MSH6* or both genes. Shown is a representative complex *MSH2* rearrangement present in hypermutated cases LuCaP 147 and 05-165 (LuCaP 147 was derived from autopsy patient 05-165). Breakpoints were confirmed by Sanger sequencing. Genomic coordinates are hg19. Detail on additional structural rearrangements and other mismatch repair gene mutations is provided in Tables 1 and 2 and Supplementary Figs 2–9. (**b**) Hypermutated tumors exhibited microsatellite instability by PCR. Shown is representative data for LuCaP 58, which is positive for MSI in 3/5 mononucleotide marker systems (MONO-27, BAT-25 and NR-24, arrows). All hypermutated tumors tested were MSI-PCR positive in at least 2/5 loci (Supplementary Data 1). (**c**) Hypermutated tumors LuCaP 58, 73 and 147 have loss of MSH2 and MSH6 proteins by IHC. Similar results were observed in hypermutated tumors from rapid autopsy patients (Supplementary Fig. 11). A representative non-hypermutated tumour (LuCaP 23.1) has intact expression. LuCaP 145 had mono-allelic mutations in *MSH2* and *MSH6* but was not hypermutated. IHC shows loss of MSH6 protein expression in some tumour cells. Scale bars, 0.1 mm.

interdependent manner, a process termed 'chromoplexy'[16]. This process may play a role in the genesis of *MSH2* and *MSH6* structural rearrangements and deserves future study. Androgen receptor (AR) function may also play a role in the formation of *MSH2* and *MSH6* structural alterations. AR has recently been implicated in the genesis of gene rearrangements in prostate cancer by facilitating double-strand DNA breaks and inducing non-homologous end-joining (reviewed in refs 17,18).

In summary, we have shown that complex structural rearrangements in mismatch DNA repair genes *MSH2* and *MSH6* are a major mechanism underlying hypermutation in advanced prostate cancer. Future studies should focus on determining if patients with MMR gene defects exhibit a distinct clinical course and are differentially responsive to genotoxic therapy.

Methods

Patients and specimens. The LuCaP series of prostate cancer xenografts were obtained from the University of Washington Prostate Cancer Biorepository.

Human primary and metastatic prostate cancer tissues were obtained as part of the University of Washington Prostate Cancer Donor Rapid Autopsy Programme. A haematoxylin and eosin slide was reviewed and scrolls from tissue blocks with >50% estimated tumour purity were used. The Institutional Review Board of the University of Washington approved all procedures involving human subjects, and all subjects signed written informed consent. The sample size was chosen based on the number of cases with suitable tissues for exome sequencing.

Genomic DNA was prepared from either formalin-fixed paraffin-embedded tissue or from fresh-frozen tissue (for bone metastases) with the Gentra Puregene DNA Isolation Kit (Qiagen, Catalogue #158489).

Immunohistochemistry. Expression of MMR proteins was determined by IHC using a tissue microarray (UWTMA55), that consisted of 155 metastatic prostate cancer sites from 50 patients, including 77 soft tissue metastases and 83 bone metastases), UWTMA52 consisting of primary prostate cancer obtained at the time of radical prostatectomy from 127 patients, and UWTMA 63 that consisted of prostate cancer tissue from 32 different LuCaP xenograft lines. All the tissue cores were duplicated.

Formalin-fixed paraffin-embedded tissue sections (5 μm) were deparaffinized and rehydrated with three changes of xylene and graded ethanol. Antigen retrieval was performed with heat-induced epitope retrieval for 20 min. Endogenous peroxide and avidin/biotin was blocked and sections were then blocked with 5% normal goat-horse-chicken serum at room temperature for 1 h, and incubated with primary antibody (listed in table below) at 4 °C overnight. After washing three times with 1 × PBS, slides were incubated with biotinylated secondary antibody (Vector Laboratories Inc.), followed by ABC reagent (Vector Laboratories Inc.)

and stable diaminobenzidine (Invitrogen Corp.). All sections were lightly counterstained with haematoxylin and mounted with Cytoseal XYL (Richard Allan Scientific). Mouse or rabbit immunoglobulin-G was used at the same concentration as the primary antibody for negative controls. Antibodies and dilutions used for IHC are given in Supplementary Table 4.

Immunostaining was assessed using a quasi-continuous score system, created by multiplying each intensity level ('0' for no brown colour, '1' for faint and fine brown chromogen deposition and '2' for clear and coarse granular chromogen clumps) with the corresponding percentage of cells expressing the particular intensity, and then summing all values to get a final score for each sample (scores ranging from 0 to 200). Only nuclear staining was evaluated. Samples with damaged tissue core, missing tissue core or poor quality of tissue were excluded from finial analysis.

Microsatellite instability PCR. MSI-PCR testing was performed by the University of Washington (UW) clinical genetics and solid tumors laboratory using the Promega MSI analysis kit (Promega, Madison, WI, USA) following the manufacturer's instructions. Specimens demonstrating instability within two or more of the five mononucleotide markers included in this panel were considered 'MSI positive', others were considered 'MSI negative'. The microsatellite loci tested in the Promega MSI analysis kit were NR-21, BAT-26, BAT-25, NR-24 and MONO-27 (Genbank Accession # XM_033393, U41210, L04143, X60152, AC007684, respectively).

***MLH1* methylation analysis.** Two to four hundred nanograms of DNA from each sample was bisulfite converted using the EZ DNA Methylation Kit (Zymo Research, Irvine, CA, USA) and eluted in 20 µl volume, according to manufacturer's protocol.

SYBR Green qPCR to detect methylated and unmethylated *MLH1* was performed using a CFX 96 Touch Real-Time PCR Detection System (Bio-Rad, Hercules, CA, USA) with a final reaction volume of 20 µl, consisting of 500 nM each primer, 9 ng of bisulfite-converted genomic DNA and iTaq Universal SYBR Green Supermix at the following conditions: 95 °C for 3.5 min, followed by 40 cycles at 95 °C for 5 s and 60 °C for 30 s. The unique primer sequences for methylated *MLH1* were 5′-CGGATAGCGATTTTTAACGC-3′ (forward) and 5′-CCTAAAACGACTACTACCCG-3′ (reverse), and for unmethylated *MLH1* were 5′-AATGAATTAATAGGAAGAGTGGATAGT-3′ (forward) and 5′-TCTCT TCATCCCTCCCTAAAACA-3′ (reverse) (ref. 19). The four primers each also included a 20 bp GC-rich tail (5′-GCGGTCCCAAAAGGGTCAGT-3′) at their 5′ end. Repetitive Alu sequence ('AluC4') was used to normalize for the amount of input DNA2. The absolute quantitation of methylated and unmethylated *MLH1* in each sample was determined by using the Epitect human methylated and unmethylated DNA (Qiagen, Germantown, MD, USA) to create a standard curve. The SYBR Green assay results are expressed as ratios between methyl-*MLH1* or unmethyl-*MLH1* values and the ALUC4 control values. The error bars represent the s.e.m.

Exome sequencing. Exome sequencing for autopsy samples was performed using the Nimblegen EZ SeqCap kit (Roche)[1,20]. Shotgun libraries were constructed by shearing DNA and ligating sequencing adaptors. Libraries were hybridized to either the EZSeqCap V1 or V2 solution-based probe, amplified and sequenced on either the Illumina GAIIx or HiSeq platform. For all metastases, somatic mutations were called using Mutect using default parameters with matched normal (non-tumour) samples. To remove common polymorphisms and other artifacts, we imposed a number of additional requirements, including requiring variants to be observed with a variant allele fraction of at least 10% within a tumour, removing variants present within dbSNP v137 that had first been stripped of all disease-associated variants and removing variants that were present at an allele balance of 40% or more in any germline sample. All exome sequencing was performed on fresh-frozen tissue samples.

Exome data for PDX samples was from Kumar *et al.*[1], where hypermutation status was previously characterized based on the distribution of mutations across samples. For the xenografts, because corresponding normal germline DNA was not available, tumour sequences were compared against a database of common germline variants. The variants remaining were termed novel single-nucleotide variants SNVs ('novSNV') and the estimated the contribution of germline variants was ~200 and sometimes more per individual. novSNV counts from Kumar *et al.*[1] are provided in Supplementary Table 1.

Targeted deep sequencing by BROCA. Targeted deep sequencing of DNA repair pathway genes was performed using the BROCA assay in the UW clinical genetics and solid tumors laboratory[5]. Three micrograms of DNA was sonicated to a peak of 200 bp on a Covaris S2 instrument (Covaris, Woburn, MA, USA). Following sonication, DNA was purified with AMPure XP beads (Beckman Coulter, Brea CA, USA) and subjected to three enzymatic steps: end repair, A-tailing and ligation to Illumina paired-end adaptors as described in the SureSelectXT Target Enrichment for Illumina multiplexed sequencing, which is available for free download. Adapter-ligated library was PCR amplified for five cycles with Illumina primers 1.0 and 2.0 and individual paired-end libraries (500 ng) were hybridized to a custom design of complementary RNA biotinylated oligonucleotides targeting 53 genes in 52 genomic regions (Supplementary Table 2). The 120-mer oligonucleotide baits were designed in Agilent's eArray web portal with the following parameters: centred tiling, 3 × bait overlap and a maximum overlap of 20 bp into repetitive regions. The custom design targets a total of 1.4 Mb of DNA. Following capture, each library was PCR amplified for 13 cycles with primers containing a unique 6 bp index. Equimolar concentrations of 96 libraries were pooled to a final concentration of 10 pM, denatured with 3 N NaOH, and cluster amplified with a cBot instrument on a single lane of an Illumina v3 flowcell. Sequencing was performed with 2 × 101 bp paired-end reads and a 7 bp index read using SBS v3 chemistry on a HiSeq2500 (Illumina, SanDiego, CA, USA).

We used our targeted tumour sequencing bioinformatics pipeline for data analysis[21]. Reads were mapped to human reference genome (hg19/GRCh37) and alignment performed using BWA v0.6.1-r10419 and SAMtools v0.1.1820. SNV and indel calling was performed through the GATK Universal Genotyper using default parameters and using VarScan v2.3.2 and PINDEL version 0.2.42. Structural variants were identified using CREST v1.0 and BreakDancer v1.1. For copy number variant (CNV) analysis, copy number states for individual probes were initially called using CONTRA v2.0.32 with reference to a CNV control comprised of reads from two independent rounds of library preparation and sequencing of HapMap individual NA12878. CNV calls were made at the resolution of individual exons using custom Perl scripts. CNV plots were visualized using the R package ggplot2.

Phenotypic MSI was assessed directly from BROCA next-generation sequencing data using mSINGS (MSI by NGS)[22]. This method evaluated up to 146 mononucleotide microsatellite loci that are captured by BROCA in both matched normal non-tumour and tumour samples. For each specimen, microsatellite loci covered by a read depth of < 30 × were excluded as not passing quality filter. For each microsatellite locus passing quality filter, the distribution of size lengths were compared with a population of normal controls. Loci were considered unstable if the number of repeats is statistically greater than in the control population. A fraction of > 0.20 (20% unstable loci) was considered MSI-high by mSINGS based on validation with 324 tumour specimens, in which 108 cases had MSI-PCR data available as a gold standard[22].

Confirmation of *MSH2* and *MSH6* structural rearrangements. To validate structural rearrangement calls, we designed primers against regions flanking putative breakpoints using either PrimerBlast (http://www.ncbi.nlm.nih.gov/tools/primer-blast/) or Primer3 (http://bioinfo.ut.ee/primer3-0.4.0/primer3/input.htm). We used the iProof High-Fidelity PCR kit (Bio-Rad) to perform PCR under the following conditions: 98 °C for 35 s followed by 30–40 cycles of 55–69 °C for 30 s, 72 °C for 30 s and 72 °C for 10 min. Primers are listed in Supplementary Table 5. We submitted resulting PCR products to Genewiz for Sanger sequencing and aligned fragments to the human genome reference sequence (hg19) using BLAT from the UCSC Genome Browser (http://genome.ucsc.edu/cgi-bin/hgGateway).

Copy number changes were confirmed by genomic microarray. One microgram of high molecular weight genomic DNA from each sample was labelled by random priming using the Agilent Genomic DNA Enzymatic Labelling Kit (Cy3-dUTP.) A pool of reference normal DNA (Promega) was labelled with Cy5-dUTP. Cy3 and Cy5 probes were combined and hybridized to Agilent 2 × 400K SurePrint G3 CGH Microarrays and washed following the manufacturer's specifications. Fluorescent array images were collected using the Agilent DNA microarray scanner G2505C and Agilent Feature Extraction software. Data analysis was performed with Biodiscovery Nexus Copy Number 6.0 software. The FASST2 segmentation algorithm and default Agilent settings for significance, gain and loss thresholds, with at least six probes per segment were used to identify regions of CNV for each sample. Results of copy number analysis by genomic microarray are given in Supplementary Fig. 14.

References

1. Kumar, A. *et al.* Exome sequencing identifies a spectrum of mutation frequencies in advanced and lethal prostate cancers. *Proc. Natl Acad. Sci. USA* **108,** 17087–17092 (2011).
2. Barbieri, C. E. *et al.* Exome sequencing identifies recurrent SPOP, FOXA1 and MED12 mutations in prostate cancer. *Nat. Genet.* **44,** 685–689 (2012).
3. Cancer Genome Atlas Network. Comprehensive molecular characterization of human colon and rectal cancer. *Nature* **487,** 330–337 (2012).
4. Kandoth, C. *et al.* Integrated genomic characterization of endometrial carcinoma. *Nature* **497,** 67–73 (2013).
5. Pritchard, C. C. *et al.* ColoSeq provides comprehensive lynch and polyposis syndrome mutational analysis using massively parallel sequencing. *J. Mol. Diagn.* **14,** 357–366 (2012).
6. Walsh, T. *et al.* Detection of inherited mutations for breast and ovarian cancer using genomic capture and massively parallel sequencing. *Proc. Natl Acad. Sci. USA* **107,** 12629–12633 (2010).
7. Pritchard, C. C. *et al.* Validation and implementation of targeted capture and sequencing for the detection of actionable mutation, copy number variation, and gene rearrangement in clinical cancer specimens. *J. Mol. Diagn.* **16,** 56–67 (2014).

8. Jarzen, J., Diamanduros, A. & Scarpinato, K. D. Mismatch repair proteins in recurrent prostate cancer. *Adv. Clin. Chem.* **60,** 65–84 (2013).
9. Burger, M. *et al.* Elevated microsatellite instability at selected tetranucleotide repeats does not correlate with clinicopathologic features of bladder cancer. *Eur. Urol.* **50,** 770–775 (2006).
10. Chen, Y. *et al.* Defects of DNA mismatch repair in human prostate cancer. *Cancer Res.* **61,** 4112–4121 (2001).
11. Velasco, A. *et al.* Differential expression of the mismatch repair gene hMSH2 in malignant prostate tissue is associated with cancer recurrence. *Cancer* **94,** 690–699 (2002).
12. Sun, X., Chen, C., Vessella, R. L. & Dong, J. T. Microsatellite instability and mismatch repair target gene mutations in cell lines and xenografts of prostate cancer. *Prostate* **66,** 660–666 (2006).
13. Chen, Y. *et al.* Alterations in PMS2, MSH2 and MLH1 expression in human prostate cancer. *Int. J. Oncol.* **22,** 1033–1043 (2003).
14. Dahiya, R. *et al.* High frequency of genetic instability of microsatellites in human prostatic adenocarcinoma. *Int. J. Cancer* **72,** 762–767 (1997).
15. Watanabe, M. *et al.* Microsatellite instability in human prostate cancer. *Br. J. Cancer* **72,** 562–564 (1995).
16. Baca, S. C. *et al.* Punctuated evolution of prostate cancer genomes. *Cell* **153,** 666–677 (2013).
17. White, N. M., Feng, F. Y. & Maher, C. A. Recurrent rearrangements in prostate cancer: causes and therapeutic potential. *Curr. Drug Targets* **14,** 450–459 (2013).
18. Wu, D., Zhang, C., Shen, Y., Nephew, K. P. & Wang, Q. Androgen receptor-driven chromatin looping in prostate cancer. *Trends Endocrinol. Metab.* **22,** 474–480 (2011).
19. Petko, Z. *et al.* Aberrantly methylated CDKN2A, MGMT, and MLH1 in colon polyps and in fecal DNA from patients with colorectal polyps. *Clin. Cancer Res.* **11,** 1203–1209 (2005).
20. O'Roak, B. J. *et al.* Exome sequencing in sporadic autism spectrum disorders identifies severe de novo mutations. *Nat. Genet.* **43,** 585–589 (2011).
21. Pritchard, C. C. *et al.* Validation and implementation of targeted capture and sequencing for the detection of actionable mutation, copy number variation, and gene rearrangement in clinical cancer specimens. *J. Mol. Diagn.* **16,** 56–67 (2014).
22. Salipante, S. J., Scroggins, S. M., Hampel, H. L., Turner, E. H. & Pritchard, C. C. Microsatellite instability detection by next-generation sequencing. *Clin. Chem.* 24987110 (2014).

Acknowledgements

We thank Karen Koehler and Tatyana Marushchak for help with library preparation and sequencing. We thank Deborah Barden, Rachel Slusher, Laura Akagi and Youly Welt for their help in preparing the genomic DNA and with MSI-PCR. We thank Emily Turner for help with data analysis. We thank the University of Washington Rapid Autopsy team members and most importantly the patients and families who participated in research studies. This work was supported by awards P50CA097186, CA085859 and CA163227 from the National Cancer Institute, CDMRP awards PC131820 and PC093372P1 and a 2013 Young Investigator Award from the Prostate Cancer Foundation.

Author contributions

C.C.P. conceived and designed the study, coordinated sample acquisition and processing and performed primary data analyses. C.M., A.K. and P.S.N. assisted with the study design. T.W., J.S., R.L.V., E.C. and J.F.T. assisted with the study design and reviewed the manuscript. R.L.V., C.M. and E.C. were involved in metastasis and PDX tissues collection and selection. A.K., J.M. and S.J.S. performed confirmatory Sanger sequencing studies. C.M. and X.Z. performed and analyzed the IHC studies. C.S., I.C. and A.K. assisted with the genomic sequencing. I.C., S.J.S., C.C.P. and A.K. coordinated informatics analyses. W.M.G. and M.Y. performed *MLH1* methylation studies. C.C.P., P.S.N., R.L.V., T.W. and J.S. directed the research. C.C.P. wrote the manuscript, with contributions from P.S.N., A.K. and C.M.

Additional information

Accession codes: Sequencing data reported in this manuscript have been deposited in GenBank/EMBL/DDBJ under the accession code SRP044943.

Supplementary Information accompanies this paper at http://www.nature.com/naturecommunications

Competing financial interests: The authors declare no competing financial interests.

Reprints and permission information is available online at http://npg.nature.com/reprintsandpermissions/

How to cite this article: Pritchard, C. C. *et al.* Complex *MSH2* and *MSH6* mutations in hypermutated microsatellite unstable advanced prostate cancer. *Nat. Commun.* 5:4988 doi: 10.1038/ncomms5988 (2014).

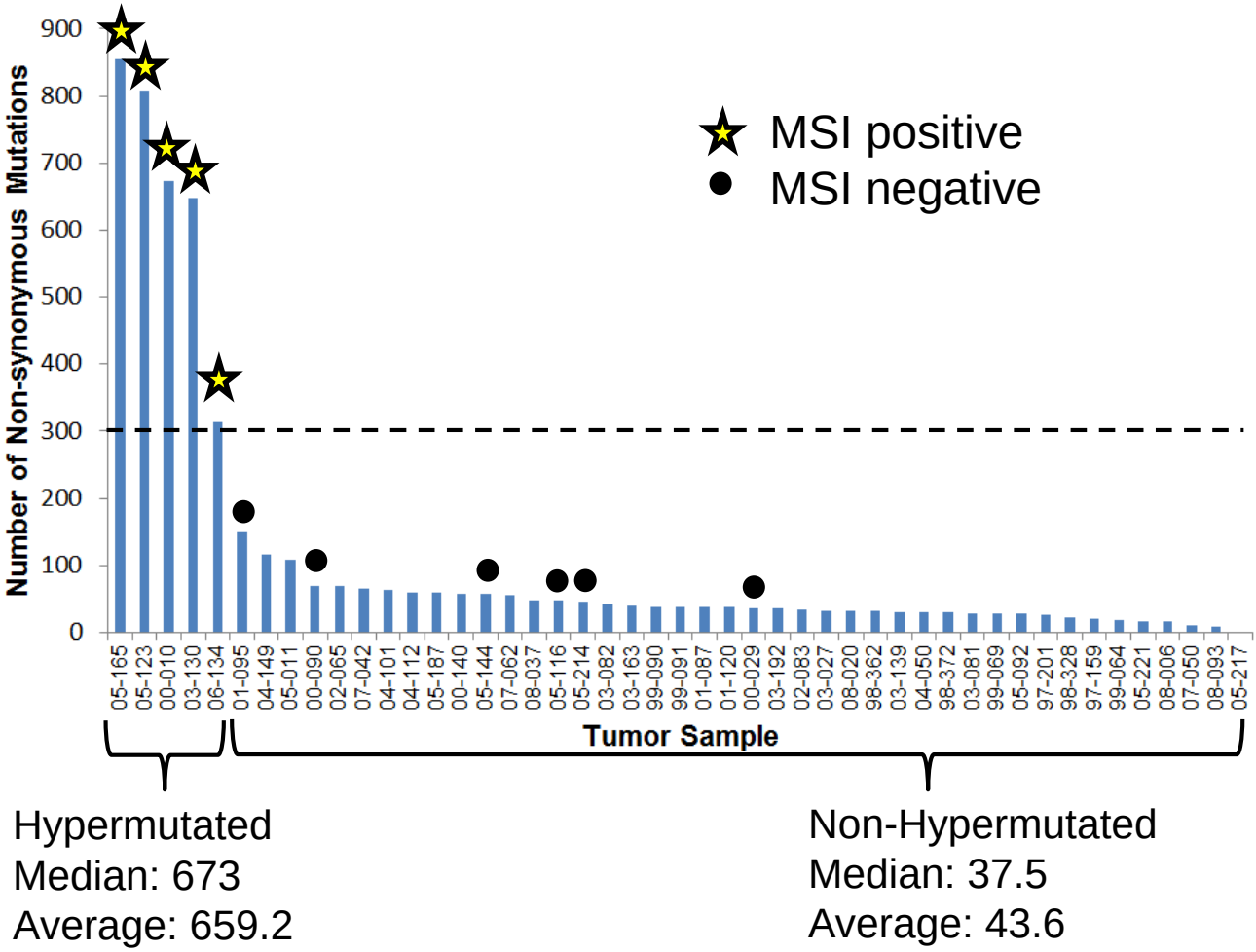

Supplementary Figure 1: Somatic Mutation Burden in Autopsy Cases by Exome Sequencing. Total number of somatic nonsynonymous mutations by exome sequencing for rapid autopsy cases. The threshold of 300 mutations used to determine hypermutation status is shown with the dashed line. Median and average mutation burden is given for both groups. Cases that had microsatellite instability testing are shown with yellow stars (positive) and black circles (negative).

LuCaP 58

1) *MSH6* del exon 8 through 3'UTR

2) *MSH6* frameshift (c.3799_3800del)

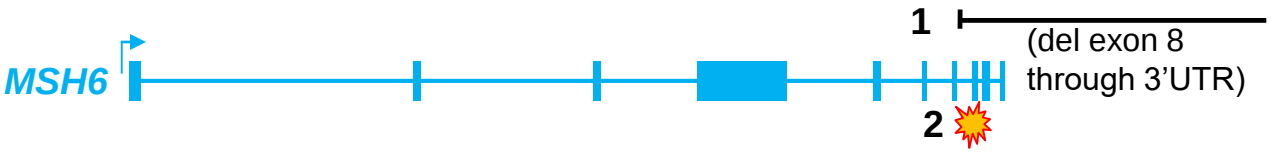

1)

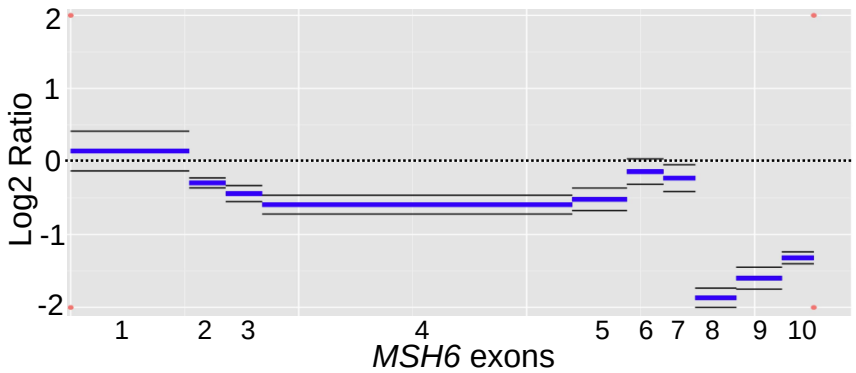

Deletion of exon 8 through 3'UTR

2) *MSH6* c.3799_3800del, p.M1267Gfs*7

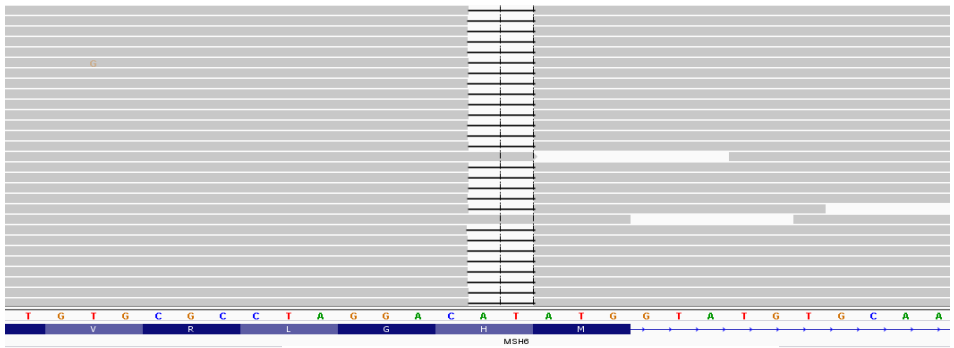

chr2:48033493-48033494delAT

Supplementary Figure 2: Detail on Mismatch Repair Gene Mutations in LuCaP 58. Two inactivating mutations were detected in *MSH6*. The first (1) is a deletion of exon 8 through the 3'UTR (top). Copy number was calculated from normalized depth of coverage of BROCA sequencing data and confirmed by genomic microarray (data not shown). The blue bars indicate exons 1-10 (from left to right) and black bars are the standard deviation of the measurement of Log2 ratio. The second (2) is a 2bp deletion resulting in a frameshift and premature truncation of the MSH6 protein (c.3799_3800del, bottom). Shown is a screenshot from the integrated genomics viewer of representative sequencing reads. The black bars indicated the deleted bases. The frameshift was detected in 314 out of a total of 360 sequencing reads, strongly supporting that there is bi-allelic inactivation of *MSH6*.

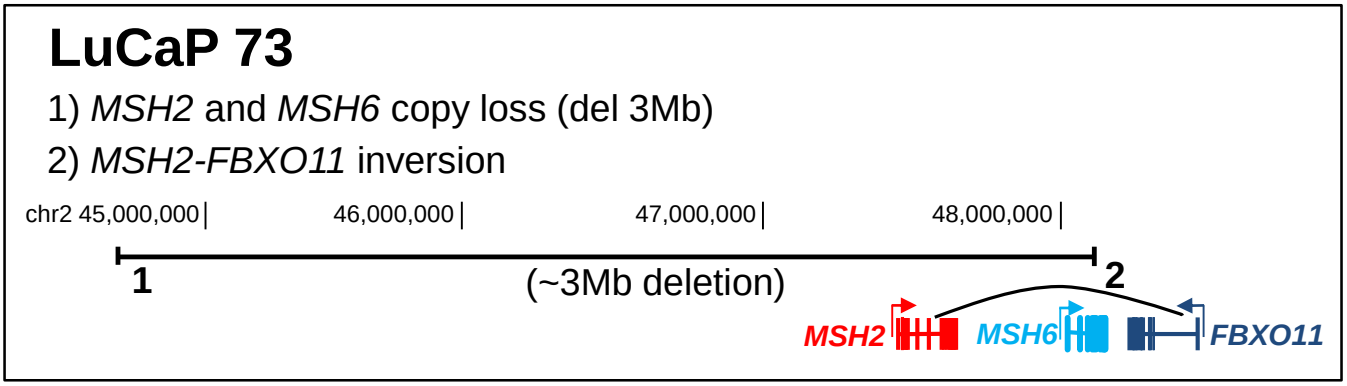

1) ~3MB deletion deletes *MSH2* and most of *MSH6*

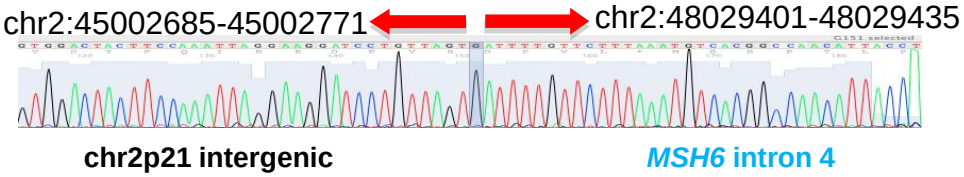

2) 440kb inversion splits the *MSH2* gene

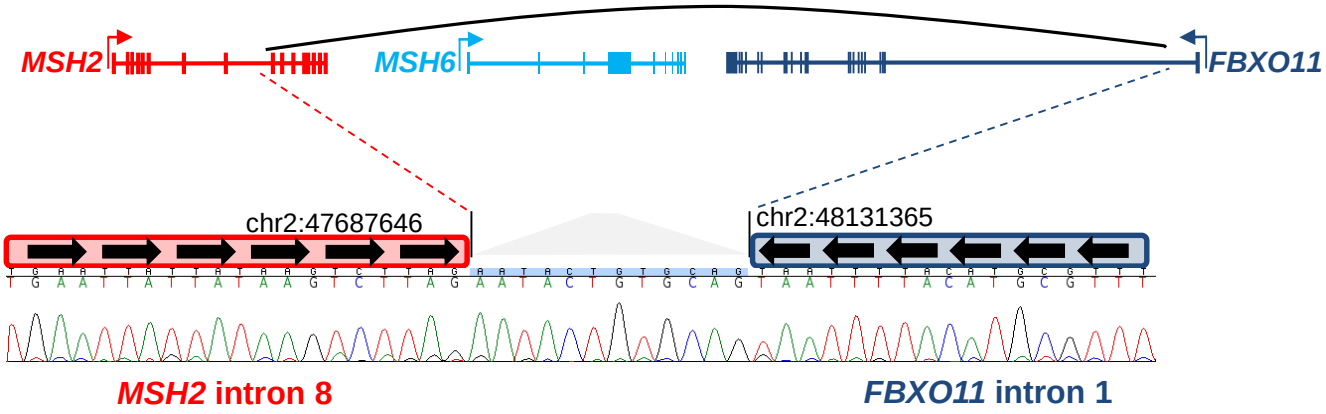

Supplementary Figure 3: Detail on Mismatch Repair Gene Mutations in LuCaP 73. Two large rearrangement mutations were detected at the *MSH2/MSH6* locus on chromosome 2 predicted to result in bi-allelic inactivation of *MSH2*. The first (1) is a 3Mb deletion that deletes both the MSH2 and MSH6 genes. The breakpoints where confirmed by Sanger sequencing as chr2:45,002,771-48,029,401 in hg19 genomic coordinates (top). The second (2) is a 440kb inversion mutation between *MSH2* intron 8 and *FBXO11* intron 1 that splits the *MSH2* gene and is predicted to result in loss of function. The breakpoints of the inversion were confirmed by Sanger sequencing as chr2:47687644-chr2:48131365 (bottom). There is a short inserted sequence between the two breakpoints.

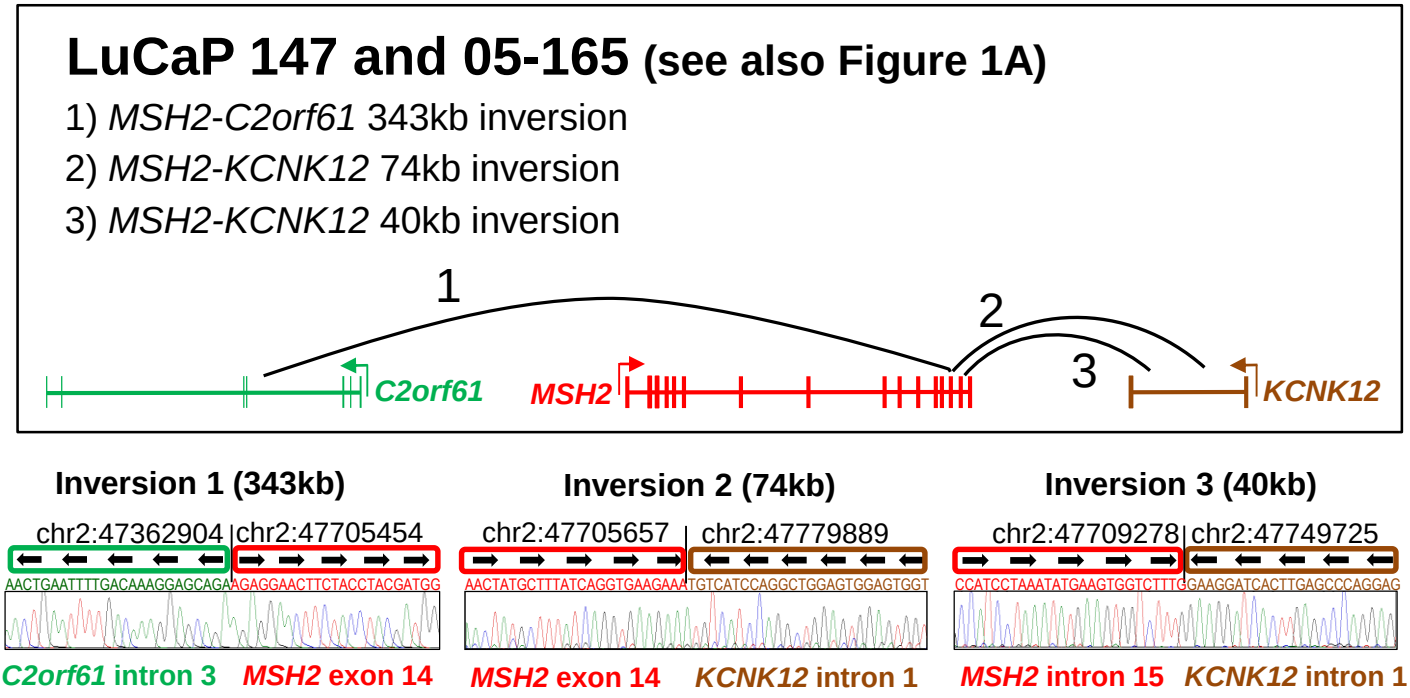

Supplementary Figure 4: Detail on Mismatch Repair Gene Mutations in LuCaP 147 and 05-165. Three different inversion mutations were detected involving the *MSH2* gene that are predicted to result in loss-of-function. The inversions were detected in all metastatic sites (bone, adrenal, liver, and lymph node). Each inversion was confirmed by Sanger sequencing with breakpoints given in hg19 genomic coordinates. LuCaP 147 was derived from autopsy patient 05-165 and the same mutations were detected in both, indicating that the *MSH2* structural rearrangements are not a result of xenografting.

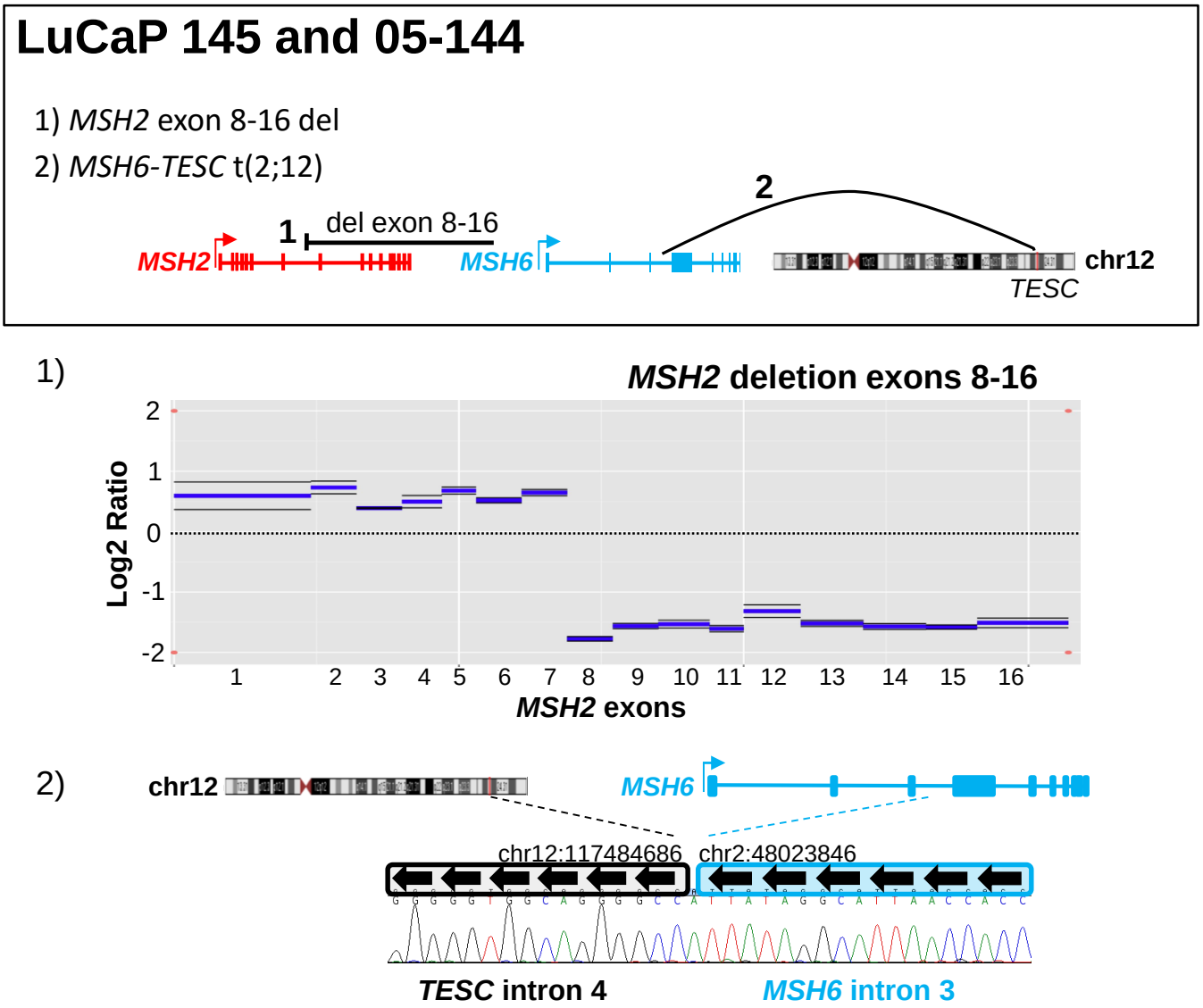

Supplementary Figure 5: Detail on Mismatch Repair Gene Mutations in LuCaP 145 and 05-144. Two mutations were detected. The first (1) is copy loss of exons 8-16 of *MSH2* (top). Copy number was calculated from normalized depth of coverage of BROCA sequencing data and confirmed by genomic microarray (data not shown). The blue bars indicate *MSH2* exons 1-16 (from left to right) and black bars are the standard deviation of the measurement of Log2 ratio. The second (2) is a translocation between *MSH6* intron 3 and *TESC* intron 4 on chromosome 12 q24.22. The breakpoints of the translocation were confirmed by Sanger sequencing. These tumors had neuroendocrine differentiation. Unlike the other tumors *MSH2/MSH6* rearrangements these tumors were not hypermutated and did not demonstrate MSI, most likely because one copy of *MSH2* and *MSH6* remain functionally intact. One hypothesis is that the cancer was 'transitioning' to a hypermutated state when the patient died, with a second hit in the *MSH2* or *MSH6* gene not yet acquired. LuCaP 145 was derived from autopsy patient 05-144 and the same mutations were detected in both, indicating that the structural rearrangements are not a result of xenografting.

Supplementary Figure 6

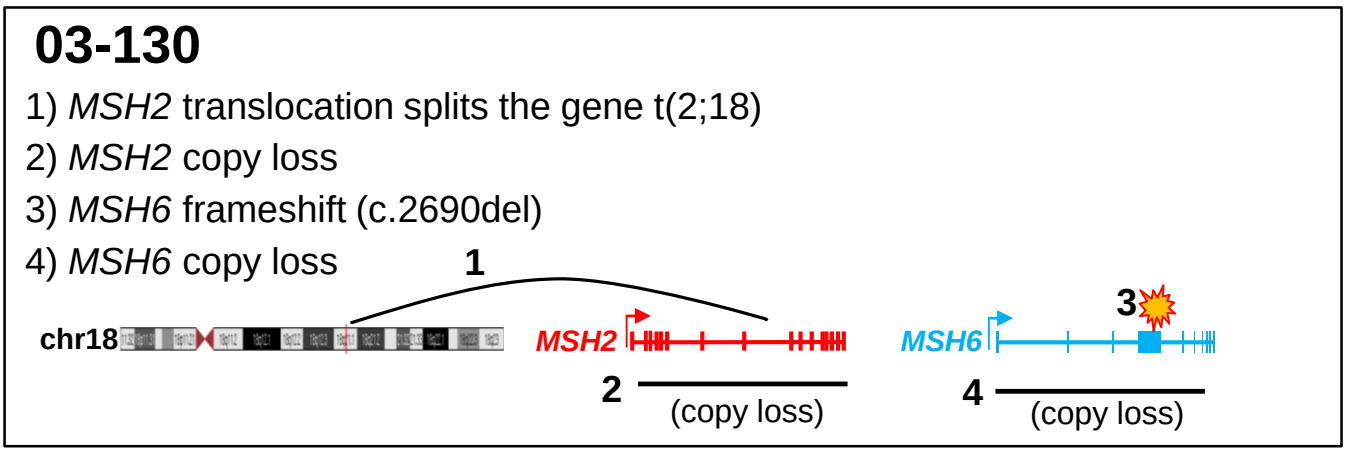

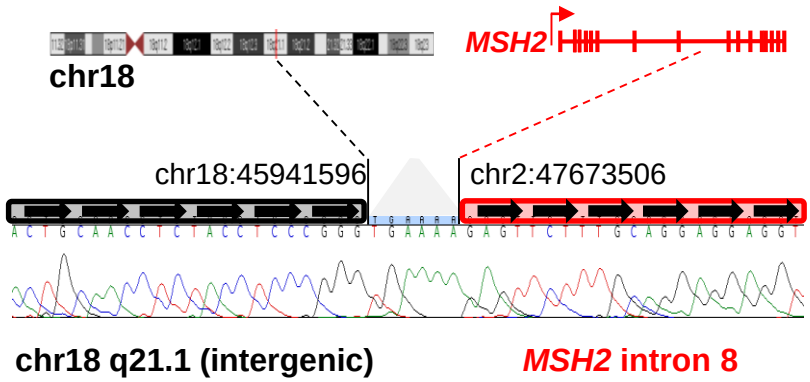

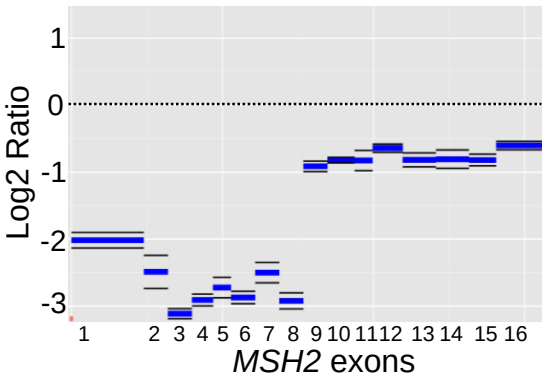

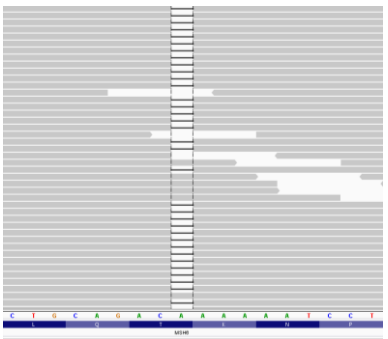

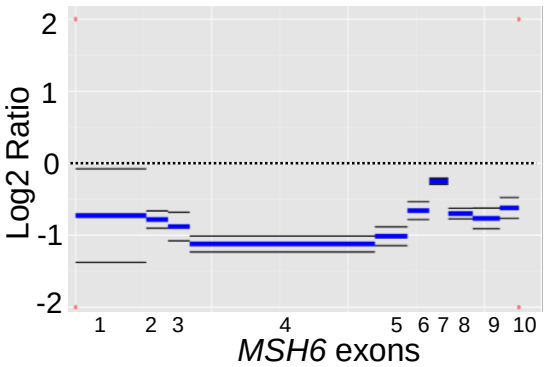

Supplementary Figure 6: Detail on Mismatch Repair Gene Mutations in 03-130. There was evidence of bi-allelic loss-of-function mutations in *MSH2* and *MSH6*. The first mutation (1) is a translocation between *MSH2* intron 8 *and* chr18 q21.1 (top left), in which the breakpoints were confirmed by Sanger sequencing. The second (2) is copy loss of *MSH2* (top right, homozygous in exons 1-8, likely as a result of the *MSH2* translocation). The third (3) is frameshift mutation in exon 4 of MSH6 (c.2690del, p.N897IfsX9). The black bars indicated the deleted bases. The frameshift was detected in 366 out of a total of 547 sequencing reads (67%), despite admixture of tumor with normal cells in the sample tested, supporting that there is bi-allelic inactivation of *MSH6* in tumor. The fourth (4) is copy loss of *MSH6*, probably single copy. In copy number plots blue bars indicate exons and black bars are the standard deviation of the measurement of Log2 ratio. Copy number was calculated by normalized depth of coverage of BROCA sequencing and confirmed by genomic microarray (data not shown)

06-134

MLH1 homozygous copy loss

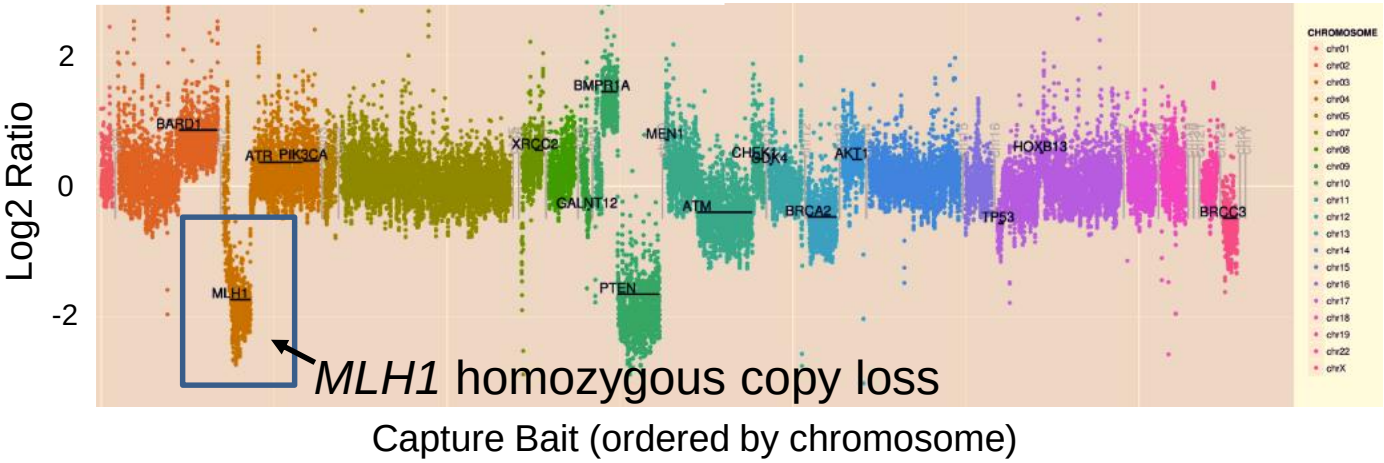

Supplementary Figure 7: Detail on Mismatch Repair Gene Mutations in 06-134. The sample tested had *MLH1* copy loss which is very likely to be homozygous and result in complete loss of MLH1 protein function. Depicted is copy number analysis by BROCA targeted deep sequencing. *MLH1* deletion was confirmed by genomic microarray (data not shown). The Log2 ratio in relationship to a normal female control patient. *BRCC3* (far right) on the X chromosome can be used to calibrate the Log2 ratio expected with heterozygous copy loss because this is a male patient. *PTEN* is also deleted in this patient's tumor, a common event in metastatic prostate cancer.

00-010

MSH2 frameshift (c.2364_2365insTACA, p.A789YfsX11)

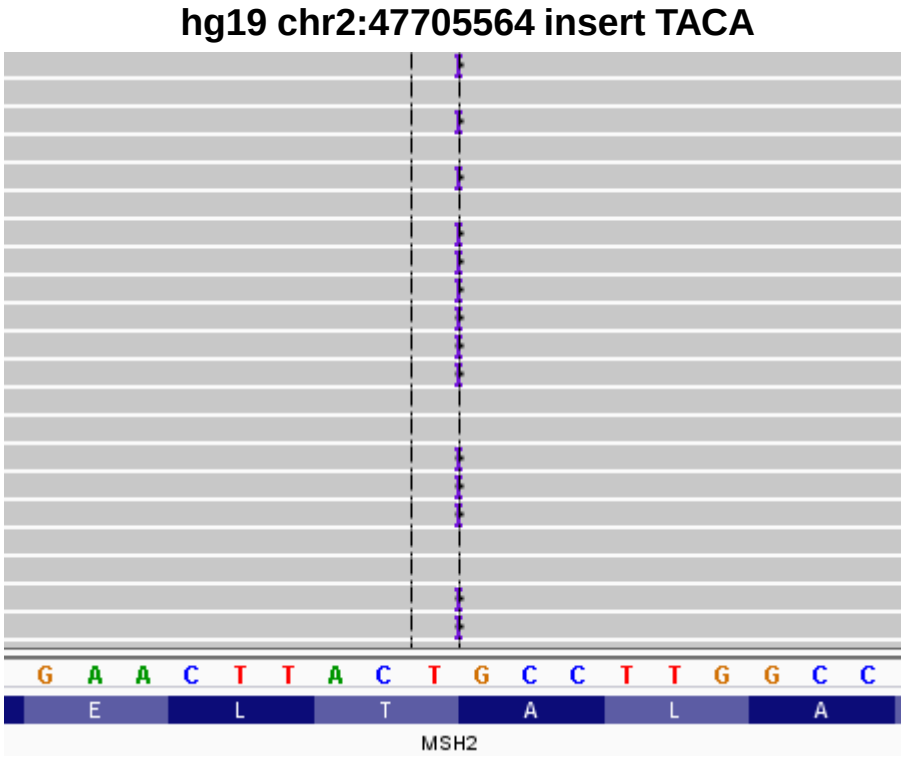

Supplementary Figure 8: Detail on Mismatch Repair Gene Mutations in 00-010. The primary prostate and liver tumor metastasis samples tested had a frameshift loss-of-function mutation in *MSH2* (c.2364_2365insTACA, p.A789YfsX11). The purple "I" indicates the position of the inserted bases, visualized in the integrated genomics viewer. A second loss-of-function mutation was not detected. It is suspected a second *MSH2* loss-of-function mutation is present because the case was MSI high, had loss of MSH2 and MSH6 protein by IHC, was *MLH1* unmethylated, and had intact MLH1 protein IHC (see separate figures).

05-0123

1) *MSH2* frameshift (c.1124_1125insG)
2) *MSH2* frameshift (c.1082del)
3) *MLH1* frameshift (c.1310del), lymph node only

MSH2 c.1082del, p.N361IfsX2
chr2:47656885delA

MSH2 c.1124_1125insG, p.L376FfsX13
chr2:47656928insG

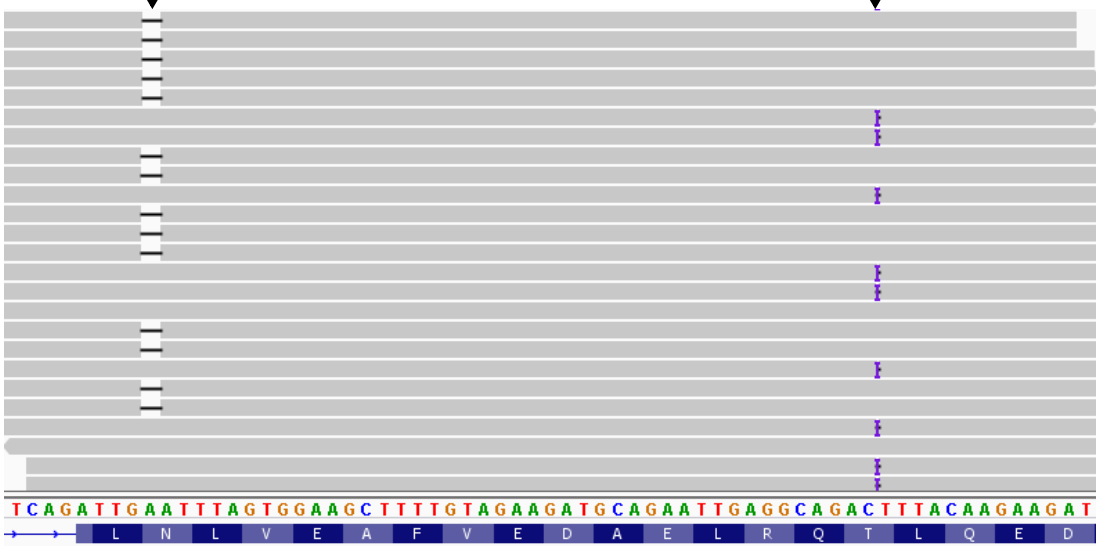

MSH2 exon 7

chr3:37067396delC

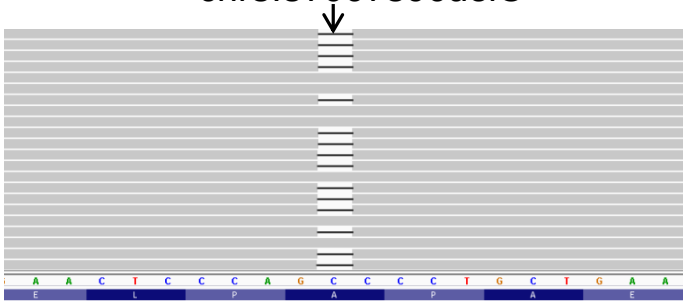

MLH1 exon 12

MLH1 c.1310del, p.P437LfsX54
(Lymph node metastasis only)

Supplementary Figure 9: Detail on Mismatch Repair Gene Mutations in 05-123. The primary prostate and lymph node metastasis tumor samples tested had bi-allelic frameshift loss-of-function mutations in *MSH2* exon 7 (c.1082del and c.1124_1125insG, top). The black bars indicate sequencing reads with the c.1082del deletion; the purple "I" indicates the position of the inserted bases in the c.1124_1125insertion, visualized in the integrated genomics viewer. Note that these two mutations do not occur on sequencing reads from the same allele, strongly supporting that they are *in trans (*bi-allelic). In addition, an *MLH1* frameshift mutation in exon 12 (c.1310delC) was detected in the lymph node metastasis sample only (bottom).

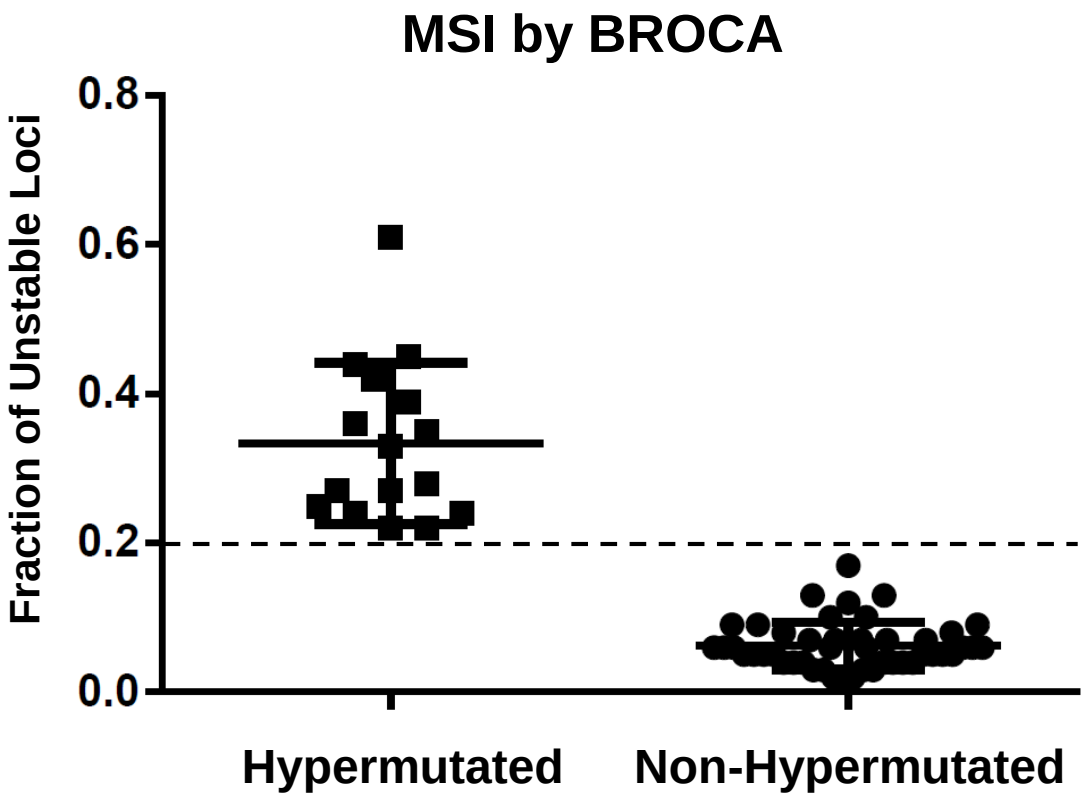

Supplementary Figure 10: Microsatellite Instability Results by BROCA Next-Generation Sequencing. We developed an approach to measure microsatellite instability directly from next-generation sequencing data that we call mSINGS. This method is described in the methods section (Salipante et al. 2014 *Clinical Chemistry*, in press). The fraction of unstable microsatellite loci out of a maximum of 146 mononucleotide microsatellite loci captured by BROCA is given on the y-axis. A threshold of 0.2 (20%) unstable loci was established as a cutoff for microsatellite instability (dashed line). Solid lines represent the median fraction of unstable loci for hypermutated and non-hyermutated cases. The raw data used to generate this summary figure, including which loci were unstable by BROCA in each sample is given in Supplementary Data 3.

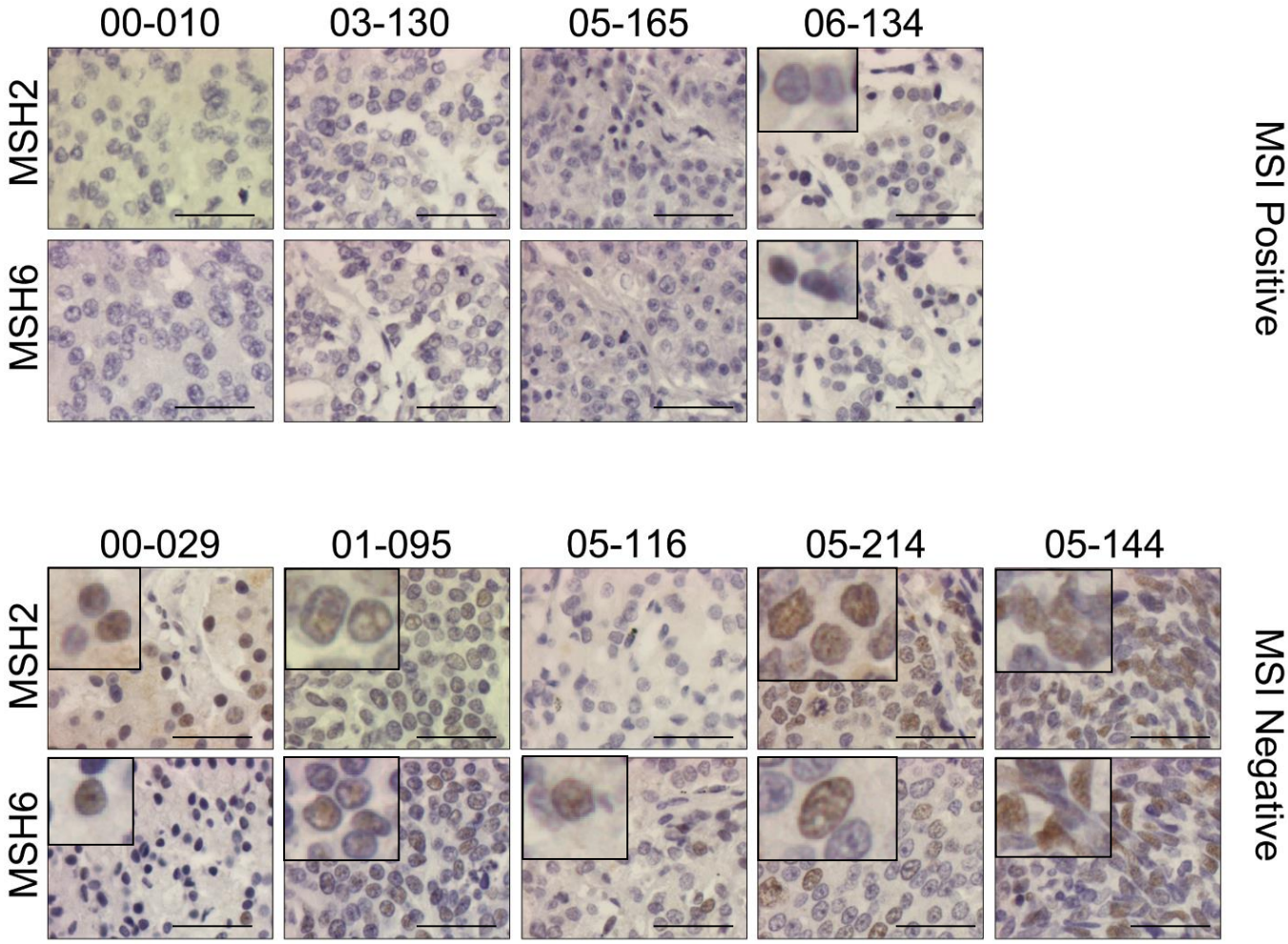

Supplementary Figure 11: IHC results for prostate rapid autopsy metastasis samples. Hypermutated MSI positive autopsy cases 00-010, 03-130, 05-165, which harbored somatic mutations in *MSH2*, *MSH6* or both genes show complete loss of MSH2 and MSH6 expression by IHC using a tissue microarray (top panels). Tissue was not available for IHC studies in hypermutated case 05-123. Hypermutated MSI positive case 06-134, which had somatic deletion of *MLH1*, has focal intact nuclear expression of MSH2 and MSH6 protein (top left, insets). By contrast, MSH2 and MSH6 nuclear staining is intact in MSI-negative autopsy cases 00-029, 01-095, 05-214, and 05-144 (bottom panels, examples of positive nuclear staining in insets). MSH6, but not MSH2 protein expression was detected MSI-negative case 05-116, a case that also had absent MLH1 protein (see separate figure). This could reflect a false negative result due to poor quality tissue for this sample on the tissue microarray. For MSH2 and MSH6, heterogeneity of immunostaining is common in tumor tissue, and protein expression is generally considered intact if any cells display positive nuclear staining. Because MSH2 and MSH6 function as a heterodimer, mutations in one gene frequently result in loss of expression of both proteins, particularly when there are *MSH2* mutations. All samples are from metastases and not primary tumors. Scale bar: 0.1mm.

Supplementary Figure 12

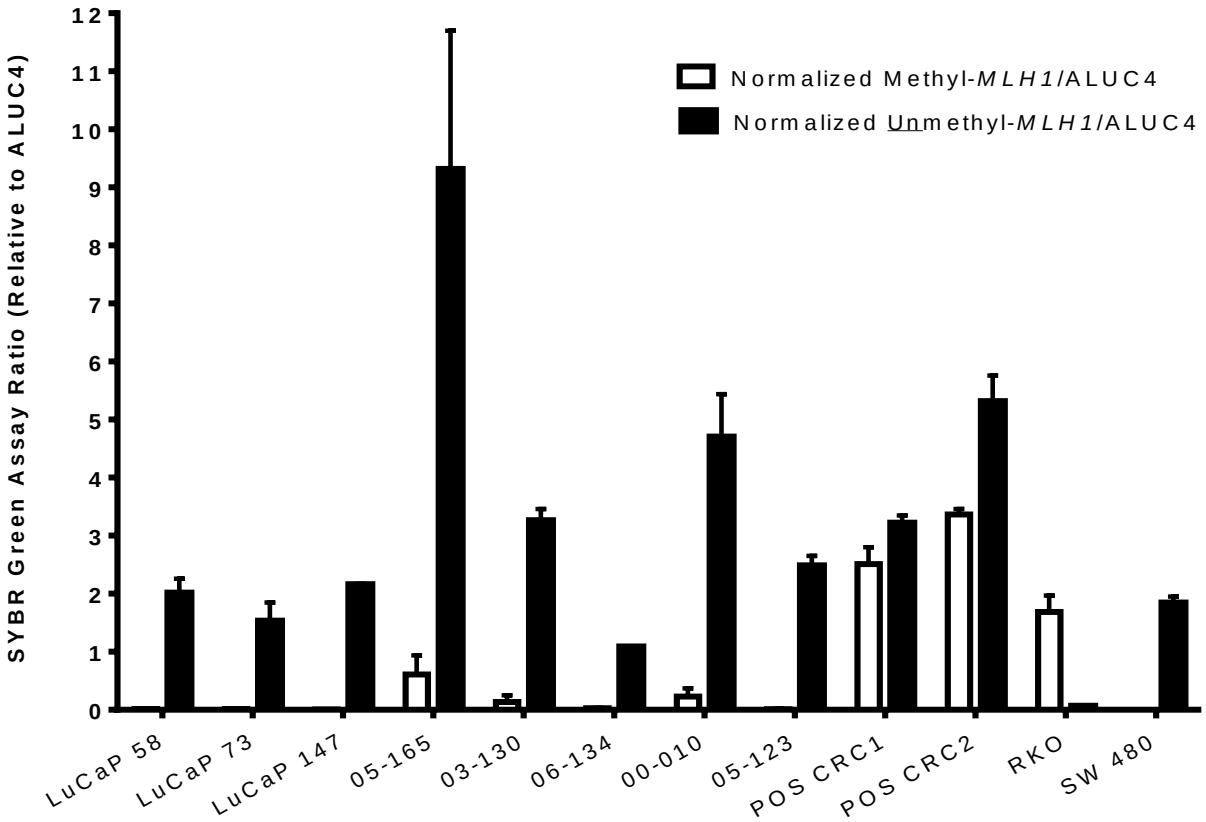

Sample	*MLH1* methylation status
LuCaP 58	Unmethylated
LuCaP 73	Unmethylated
LuCaP 147	Unmethylated
05-165-K3	Unmethylated
03-130-L2	Unmethylated
06-134-P1	Unmethylated
00-010	Unmethylated
05-123-D1	Unmethylated
POS CRC 1 (known methylated colon tumor)	Methylated
POS CRC 2 (known methylated colon tumor)	Methylated
RKO (positive control cell line)	Methylated
SW 480 (negative control cell line)	Unmethylated

Supplementary Figure 12: Hypermutated Prostate Tumors Do Not Exhibit *MLH1* Methylation. Results of a *MLH1* methylation-specific SYBR green assay are expressed as ratios between Methyl-MLH1 or Unmethyl-MLH1 values and the ALUC4 control values. Genomic DNA samples were bisulfite-treated with EZ DNA Methylation Kit (Zymo Research, Irvine, CA) according to manufacturer's protocol. The primers used in the SYBR Green Assay were previously described (see methods). The error bars represent the standard error of the mean. DNA samples from 2 known *MLH1* methylated colon cancer tumors (POS CRC1 and POS CRC2) and cancer cell lines RKO (methylated) and SW480 (unmethylated) are used as controls for the assay.

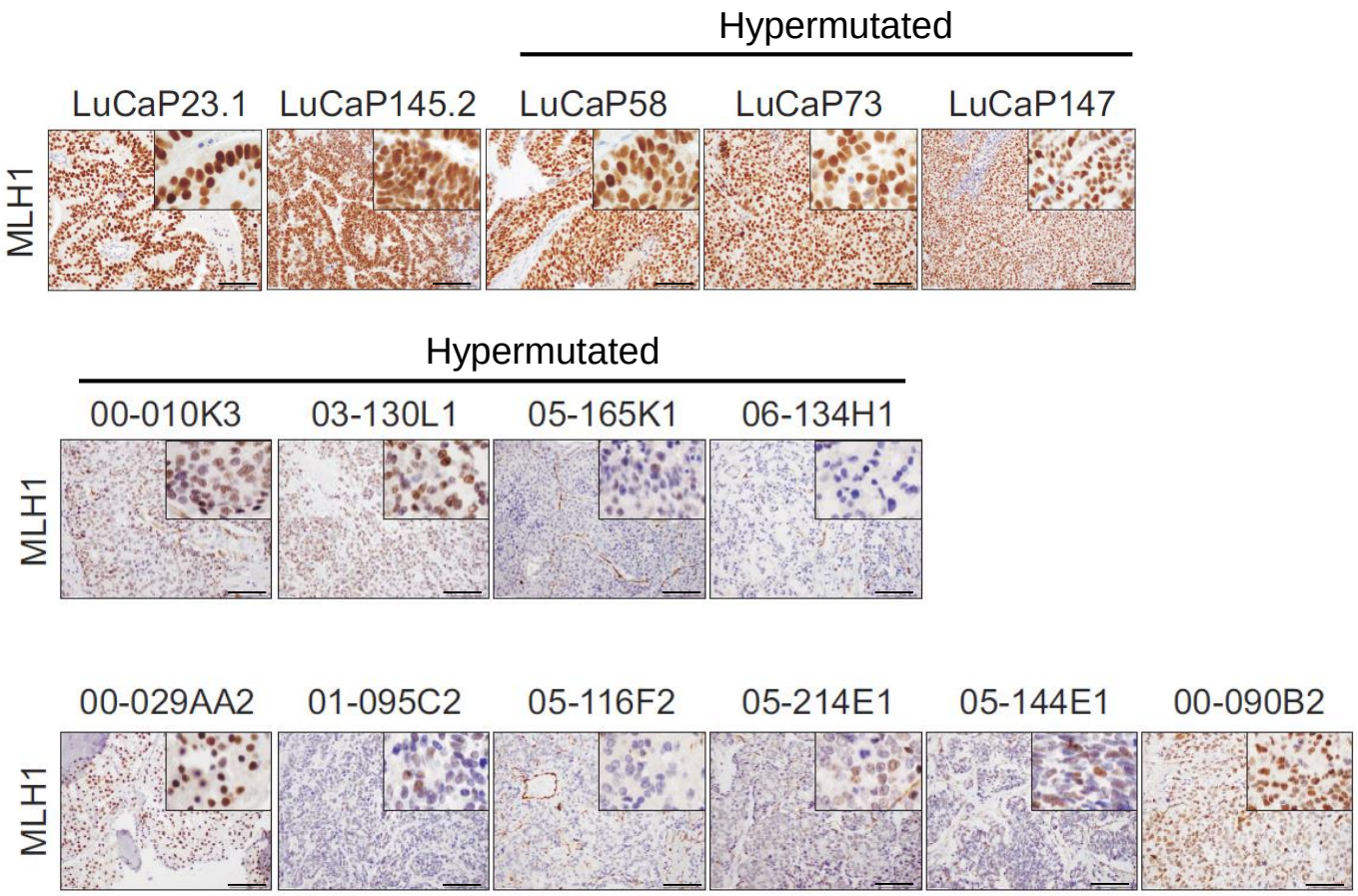

Supplementary Figure 13: Hypermutated MSI Positive Prostate Tumors With *MSH2* or *MSH6* mutations have intact MLH1 protein by IHC. Hypermutated MSI positive cases LuCaP 58, LuCaP 73, LuCaP 147 (top) and autopsy cases 00-010, 03-130, 05-165 (middle), which harbored somatic mutations in *MSH2*, *MSH6* or both have intact MLH1 expression by IHC using a tissue microarray. This corroborates the *MLH1* methylation studies and strongly argues against *MLH1* epigenetic silencing as a mechanism of MSI in these tumors. Hypermutated MSI positive case 06-134 that had homozygous deletion of *MLH1* has absent MLH1 protein. Tissue was not available for IHC studies in hypermutated case 05-123. MLH1 protein expression was not detected MSI-negative case 05-116 (bottom), a case that also had absent MSH2 protein (see separate figure). This could reflect a false negative result due to poor quality tissue for this sample on the tissue microarray. For MLH1, heterogeneity of immunostaining is common in tumor tissue, and protein expression is generally considered intact if any cells display positive nuclear staining. Scale bar: 0.1mm.

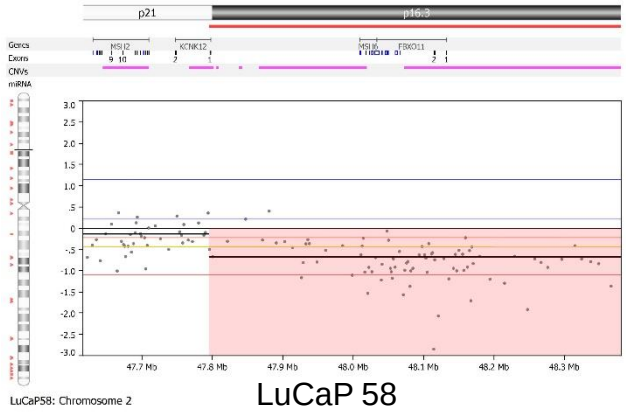

LuCaP 58

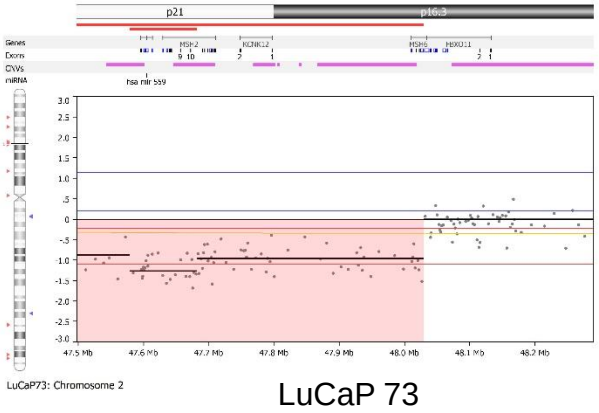

LuCaP 73

LuCaP 147 and 05-165

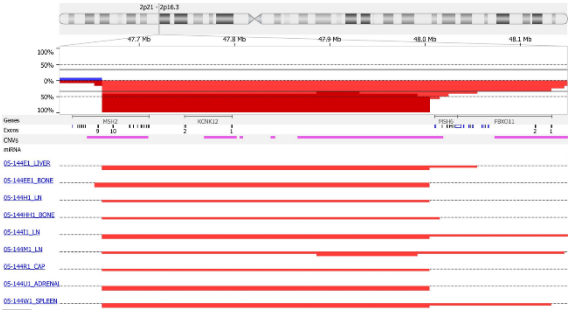

05-144

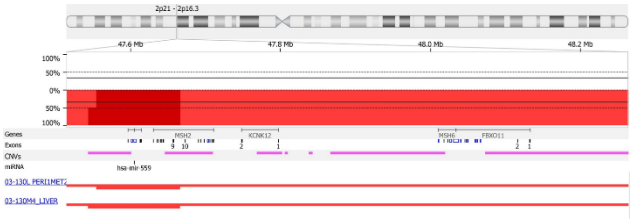

03-130

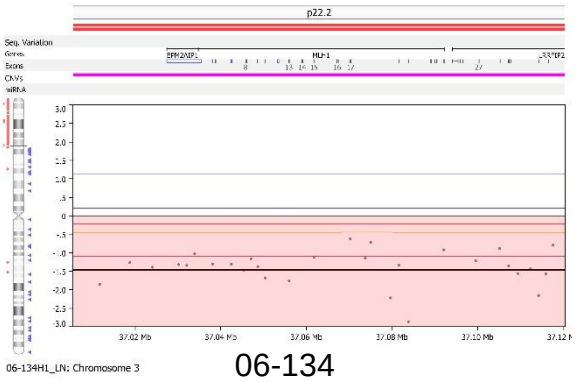

06-134

Supplementary Figure 14: Confirmation of *MSH2*, *MSH6*, and *MLH1* Copy Number Status by Genomic Microarray. Genomic microarray (array CGH) was performed for all cases that had *MSH2* and *MSH6* structural rearrangements and also for case 06-134 with *MLH1* homozygous gene deletion. The genomic loci are given along the top of each panel. Y axes are log2 ratio compared to normal control. Red indicates deletion. The results are concordant with copy number status as assessed by BROCA next-generation sequencing.

Resource

Cell

Integrative Clinical Genomics of Advanced Prostate Cancer

Graphical Abstract

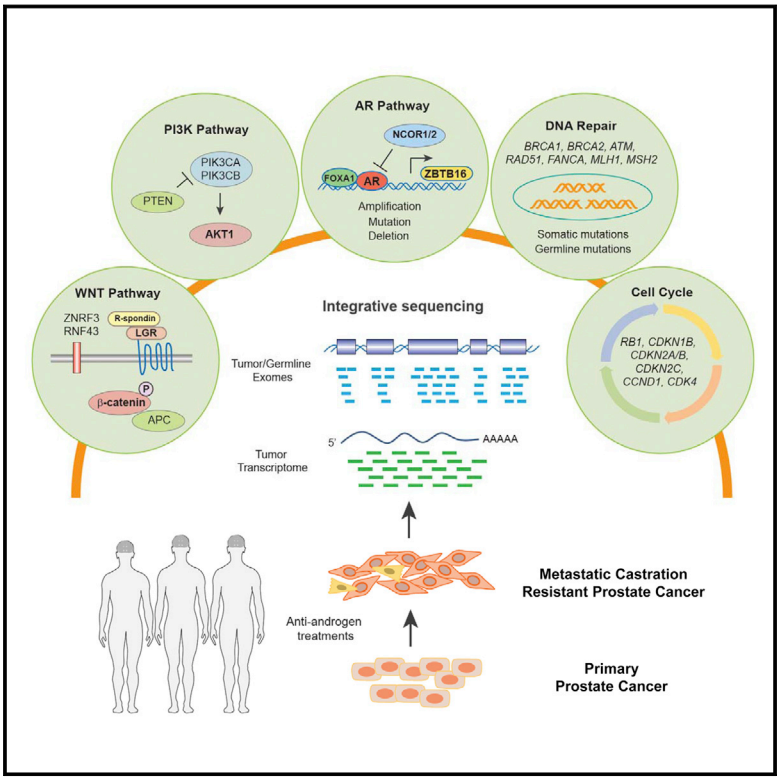

Highlights

- A multi-institutional integrative clinical sequencing of mCRPC
- Approximately 90% of mCRPC harbor clinically actionable molecular alterations
- mCRPC harbors genomic alterations in *PIK3CA/B*, *RSPO*, *RAF*, *APC*, β-catenin, and *ZBTB16*
- 23% of mCRPC harbor DNA repair pathway aberrations, and 8% harbor germline findings

Authors

Dan Robinson, Eliezer M. Van Allen, ..., Charles L. Sawyers, Arul M. Chinnaiyan

Correspondence

sawyersc@mskcc.org (C.L.S.), arul@umich.edu (A.M.C.)

In Brief

A multi-institutional integrative clinical sequencing analysis reveals that the majority of affected individuals with metastatic castration-resistant prostate cancer harbor clinically actionable molecular alterations, highlighting the need for genetic counseling to inform precision medicine in affected individuals with advanced prostate cancer.

Robinson et al., 2015, Cell *161*, 1215–1228
May 21, 2015
http://dx.doi.org/10.1016/j.cell.2015.05.001

CellPress

Cell

Integrative Clinical Genomics of Advanced Prostate Cancer

Dan Robinson,[1,2,43] Eliezer M. Van Allen,[3,4,43] Yi-Mi Wu,[1,2] Nikolaus Schultz,[5,40] Robert J. Lonigro,[1] Juan-Miguel Mosquera,[6,7,8,38] Bruce Montgomery,[9,10] Mary-Ellen Taplin,[3] Colin C. Pritchard,[26] Gerhardt Attard,[11,12] Himisha Beltran,[7,8,13,38] Wassim Abida,[14,20] Robert K. Bradley,[9] Jake Vinson,[15] Xuhong Cao,[1,42] Pankaj Vats,[1] Lakshmi P. Kunju,[1,2,17] Maha Hussain,[16,17,18] Felix Y. Feng,[1,17,19] Scott A. Tomlins,[1,2,17,18] Kathleen A. Cooney,[16,17,18] David C. Smith,[16,17,18] Christine Brennan,[1] Javed Siddiqui,[1] Rohit Mehra,[1,2] Yu Chen,[13,14,20] Dana E. Rathkopf,[13,20] Michael J. Morris,[13,20] Stephen B. Solomon,[21] Jeremy C. Durack,[21] Victor E. Reuter,[22] Anuradha Gopalan,[22] Jianjiong Gao,[40] Massimo Loda,[3,4,23,39] Rosina T. Lis,[3,23] Michaela Bowden,[3,23,39] Stephen P. Balk,[24] Glenn Gaviola,[25] Carrie Sougnez,[4] Manaswi Gupta,[4] Evan Y. Yu,[10] Elahe A. Mostaghel,[9,10] Heather H. Cheng,[9,10] Hyojeong Mulcahy,[27] Lawrence D. True,[28] Stephen R. Plymate,[10] Heidi Dvinge,[9] Roberta Ferraldeschi,[11,12] Penny Flohr,[11,12] Susana Miranda,[11,12] Zafeiris Zafeiriou,[11,12] Nina Tunariu,[11,12] Joaquin Mateo,[11,12] Raquel Perez-Lopez,[11,12] Francesca Demichelis,[7,29] Brian D. Robinson,[6,7,8,38] Marc Schiffman,[7,31,38] David M. Nanus,[7,8,13,38] Scott T. Tagawa,[7,8,13,38] Alexandros Sigaras,[7,30,32] Kenneth W. Eng,[7,30,32] Olivier Elemento,[30] Andrea Sboner,[6,7,30,38] Elisabeth I. Heath,[33,34] Howard I. Scher,[13,20] Kenneth J. Pienta,[35] Philip Kantoff,[3,44] Johann S. de Bono,[11,12,44] Mark A. Rubin,[6,7,8,38,44] Peter S. Nelson,[10,36,37,38,44] Levi A. Garraway,[3,4,44] Charles L. Sawyers,[14,41,44,*] and Arul M. Chinnaiyan[1,2,17,18,42,44,*]

[1]Michigan Center for Translational Pathology, University of Michigan Medical School, Ann Arbor, MI 48109, USA
[2]Department of Pathology, University of Michigan Medical School, Ann Arbor, MI 48109, USA
[3]Department of Medical Oncology, Dana-Farber Cancer Institute, Boston, MA 02215, USA
[4]Broad Institute of Massachusetts Institute of Technology and Harvard, Cambridge, MA 02142, USA
[5]Department of Epidemiology and Biostatistics, Memorial Sloan Kettering Cancer Center, New York, NY 10065, USA
[6]Department of Pathology and Laboratory Medicine, Weill Medical College of Cornell University, New York, NY 10021, USA
[7]Institute for Precision Medicine, Weill Medical College of Cornell University, New York, NY 10021, USA
[8]New York Presbyterian Hospital, New York, NY 10021, USA
[9]Computational Biology Program, Public Health Sciences Division and Basic Science Division, Fred Hutchinson Cancer Center, University of Washington, Seattle, WA 98109, USA
[10]Department of Medicine and VAPSHCS, University of Washington, Seattle, WA 98109, USA
[11]Cancer Biomarkers Team, Division of Clinical Studies, The Institute of Cancer Research, London SM2 5NG, UK
[12]Prostate Cancer Targeted Therapy Group and Drug Development Unit, The Royal Marsden NHS Foundation Trust, London SM2 5NG, UK
[13]Department of Medicine, Weill Medical College of Cornell University, New York, NY 10021, USA
[14]Human Oncology and Pathogenesis Program, Memorial Sloan Kettering Cancer Center, New York, NY 10065, USA
[15]Prostate Cancer Clinical Trials Consortium, Memorial Sloan Kettering Cancer Center, New York, NY 10065, USA
[16]Department of Internal Medicine, Division of Hematology Oncology, University of Michigan Medical School, Ann Arbor, MI 48109, USA
[17]Comprehensive Cancer Center, University of Michigan Medical School, Ann Arbor, MI 48109, USA
[18]Department of Urology, University of Michigan Medical School, Ann Arbor, MI 48109, USA
[19]Department of Radiation Oncology, University of Michigan Medical School, Ann Arbor, MI 48109, USA
[20]Genitourinary Oncology Service, Department of Medicine, Sidney Kimmel Center for Prostate and Urologic Cancers, Memorial Sloan Kettering Cancer Center, New York, NY 10065, USA
[21]Interventional Radiology, Department of Radiology Service, Memorial Sloan Kettering Cancer Center, New York, NY 10065, USA
[22]Department of Pathology, Memorial Sloan Kettering Cancer Center, New York, NY 10065, USA
[23]Center for Molecular Oncologic Pathology, Dana-Farber Cancer Institute, Boston, MA 02215, USA
[24]Division of Hematology-Oncology, Department of Medicine, Beth Israel Deaconess Cancer Center, Beth Israel Deaconess Medical Center, Harvard Medical School, Boston, MA 02215, USA
[25]Department of Musculoskeletal Radiology, Brigham and Women's Hospital, Boston, MA 02115, USA
[26]Department of Laboratory Medicine, University of Washington, Seattle, WA 98195, USA
[27]Department of Radiology, University of Washington, Seattle, WA 98109, USA
[28]Department of Pathology, University of Washington Medical Center, Seattle, WA 98109, USA
[29]Laboratory of Computational Oncology, CIBIO, Centre for Integrative Biology, University of Trento, 38123 Mattarello TN, Italy
[30]Institute for Computational Biomedicine, Department of Physiology and Biophysics, Weill Medical College of Cornell University, New York, NY 10021, USA
[31]Division of Interventional Radiology, Department of Radiology, New York-Presbyterian Hospital/Weill Cornell Medical Center, New York, NY 10021, USA
[32]Department of Physiology & Biophysics, Weill Medical College of Cornell University, New York, NY 10021, USA
[33]Department of Oncology, Wayne State University School of Medicine, Detroit, MI 48201, USA
[34]Molecular Therapeutics Program, Barbara Ann Karmanos Cancer Institute, Detroit, MI 48201, USA
[35]The James Buchanan Brady Urological Institute and Department of Urology, Johns Hopkins School of Medicine, Baltimore, MD 21205, USA
[36]Division of Human Biology, Fred Hutchinson Cancer Research Center, Seattle, WA 98109, USA
[37]Division of Clinical Research, Fred Hutchinson Cancer Research Center, Seattle, WA 98109, USA
[38]Meyer Cancer, Weill Medical College of Cornell University, New York, NY 10021, USA

[39]Department of Pathology, Brigham & Women's Hospital, Boston, MA 02115, USA
[40]Marie-Josée and Henry R. Kravis Center for Molecular Oncology, Memorial Sloan Kettering Cancer Center, New York, NY 10065, USA
[41]Howard Hughes Medical Institute, Memorial Sloan Kettering Cancer Center, New York, NY 10065, USA
[42]Howard Hughes Medical Institute, University of Michigan, Ann Arbor, MI 48109, USA
[43]Co-first author
[44]Co-senior author
*Correspondence: sawyersc@mskcc.org (C.L.S.), arul@umich.edu (A.M.C.)
http://dx.doi.org/10.1016/j.cell.2015.05.001

SUMMARY

Toward development of a precision medicine framework for metastatic, castration-resistant prostate cancer (mCRPC), we established a multi-institutional clinical sequencing infrastructure to conduct prospective whole-exome and transcriptome sequencing of bone or soft tissue tumor biopsies from a cohort of 150 mCRPC affected individuals. Aberrations of *AR*, ETS genes, *TP53*, and *PTEN* were frequent (40%–60% of cases), with *TP53* and *AR* alterations enriched in mCRPC compared to primary prostate cancer. We identified new genomic alterations in *PIK3CA/B*, R-spondin, *BRAF/RAF1*, *APC*, β-catenin, and *ZBTB16/PLZF*. Moreover, aberrations of *BRCA2*, *BRCA1*, and *ATM* were observed at substantially higher frequencies (19.3% overall) compared to those in primary prostate cancers. 89% of affected individuals harbored a clinically actionable aberration, including 62.7% with aberrations in AR, 65% in other cancer-related genes, and 8% with actionable pathogenic germline alterations. This cohort study provides clinically actionable information that could impact treatment decisions for these affected individuals.

INTRODUCTION

Prostate cancer is among the most common adult malignancies, with an estimated 220,000 American men diagnosed yearly (American Cancer Society, 2015). Some men will develop metastatic prostate cancer and receive primary androgen deprivation therapy (ADT). However, nearly all men with metastatic prostate cancer develop resistance to primary ADT, a state known as metastatic castration-resistant prostate cancer (mCRPC). Multiple ''second generation'' ADT treatments, like abiraterone acetate (de Bono et al., 2011; Ryan et al., 2013) and enzalutamide (Beer et al., 2014; Scher et al., 2012), have emerged for mCRPC affected individuals; however, nearly all affected individuals will also develop resistance to these agents. In the U.S., an estimated 30,000 men die of prostate cancer yearly.

Multiple studies have identified recurrent somatic mutations, copy number alterations, and oncogenic structural DNA rearrangements (chromoplexy) in primary prostate cancer (Baca et al., 2013; Barbieri et al., 2012; Berger et al., 2011; Cooper et al., 2015; Pflueger et al., 2011; Taylor et al., 2010; Tomlins et al., 2007; Wang et al., 2011). These include point mutations in *SPOP*, *FOXA1*, and *TP53*; copy number alterations involving *MYC*, *RB1*, *PTEN*, and *CHD1*; and E26 transformation-specific (ETS) fusions, among other biologically relevant genes. Although certain primary prostate cancer alterations or signatures have prognostic clinical significance (Hieronymus et al., 2014; Lalonde et al., 2014), the therapeutic impact of primary prostate cancer genomic events has not yet been realized.

Genomic studies of metastatic prostate cancers demonstrated additional alterations in *AR* (Taplin et al., 1995) and in the androgen signaling pathway (Beltran et al., 2013; Grasso et al., 2012; Gundem et al., 2015; Hong et al., 2015), although these studies were performed predominantly using autopsy samples or preclinical models with limited cohort sizes. Prospective genomic characterization of fresh biopsy samples from living mCRPC affected individuals has been limited due to challenges in obtaining adequate tumor tissue, especially from bone biopsies (Mehra et al., 2011; Van Allen et al., 2014a), which is the most common site of metastatic disease. Thus, the landscape of genomic alterations in mCRPC disease remains incompletely characterized. Moreover, the low frequency of actionable genomic alterations in primary prostate cancer has limited the inclusion of mCRPC among cohorts wherein precision cancer medicine approaches have been piloted to guide treatment or clinical trial enrollment.

We conducted a systematic and multi-institutional study of mCRPC tumors obtained from living affected individuals to determine the landscape of somatic genomic alterations in this cohort, dissect genomic differences between primary prostate cancer and mCRPC, and discover the potential relevance of these findings from a biological and clinical perspective.

RESULTS

Clinical, Biopsy, and Pathology Parameters

An international consortium consisting of eight academic medical center clinical sites was established to capture fresh clinical mCRPC affected individual samples as part of standard-of-care approaches or through a cohort of prospective clinical trials (Figures 1A and 1B). Standard-of-care approaches for mCRPC included abiraterone acetate or enzalutamide. Clinical trials included in this study focused on combination strategies involving abiraterone acetate or enzalutamide, inhibitors of poly ADP ribose polymerase (PARP), or inhibitors of aurora kinase. Here, we report the results of genomic profiling from

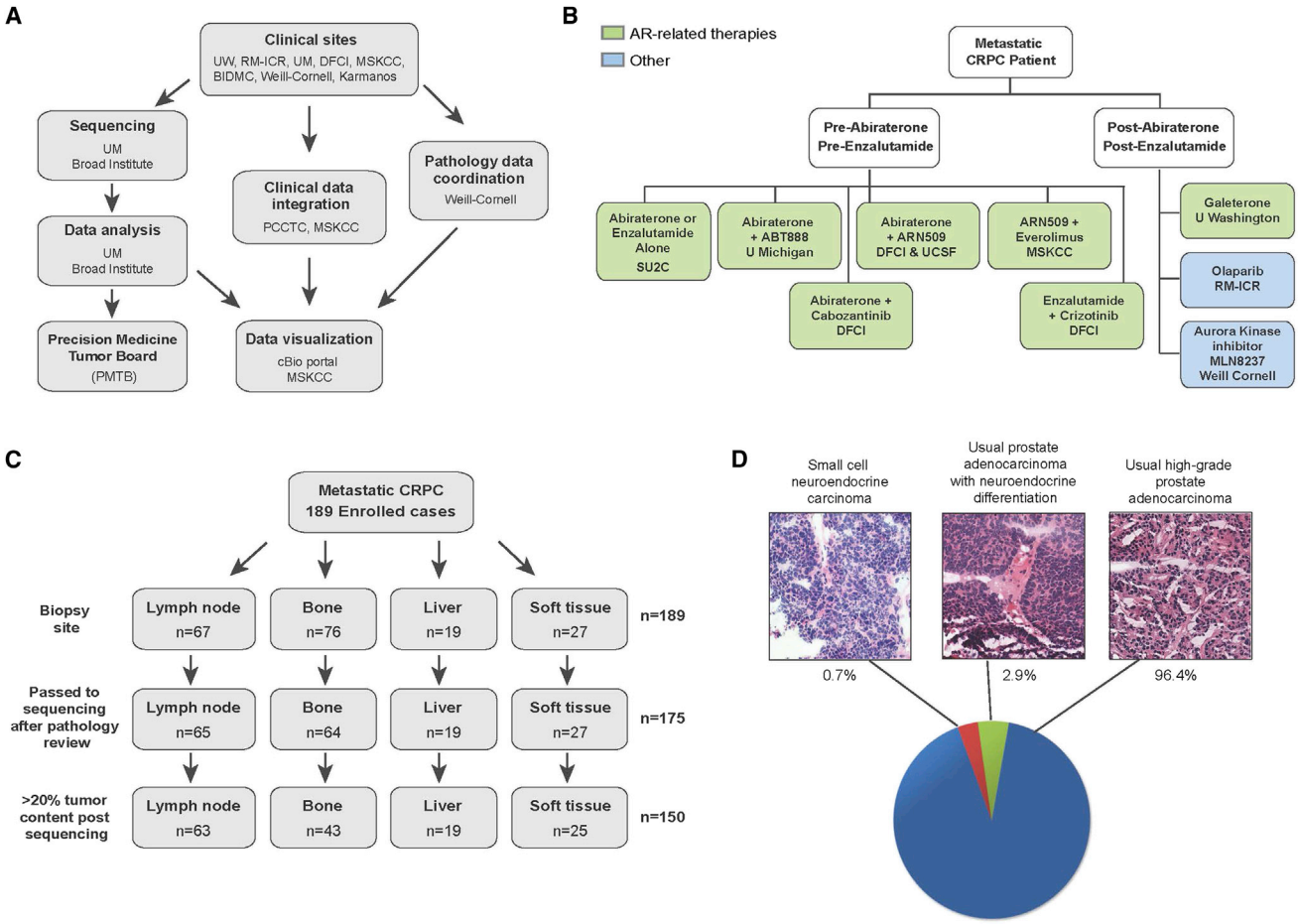

Figure 1. Overview of the SU2C-PCF IDT Multi-Institutional Clinical Sequencing of the mCRPC Project

(A) Schema of multi-institutional clinical sequencing project work flow.

(B) Clinical trials associated with the SU2C-PCF mCRPC project.

(C) Biopsy sites of the samples used for clinical sequencing.

(D) Histopathology of the cohort. Representative images of morphological analysis of mCRPC are shown along with prevalence in our cohort.

mCRPC biopsy samples obtained at time of entry into the cohort study. Future reports will include longitudinal clinical data such as treatment response. The consortium utilized two sequencing and analysis centers, one centralized digital pathology review center, and one centralized data visualization portal (Cerami et al., 2012; Gao et al., 2013; Robinson et al., 2011; Thorvaldsdóttir et al., 2013). Cross-validation of sequencing data from the two original sequencing sites demonstrated comparable variant calls for adequately powered genetic loci (E.M.V.A., D.R., C. Morrissey, C.C.P., S.L. Carter, M. Rosenberg, A. McKenna, A.M.C., L.A.G., and P.S.N., unpublished data).

Here, we describe 150 affected individuals with metastatic disease with complete integrative clinical sequencing results (whole-exome, matched germline, and transcriptome data) (Figure 1C) and summarized in Table S1. 189 affected individuals were enrolled in the study, and 175 cases were sequenced after pathology review and assessment of tumor content. Of these, 150 biopsies had >20% tumor content as defined by computational analysis, based on mutant allele variant fractions and zygosity shifts. The biopsies sequenced were from lymph node (42%), bone (28.7%), liver (12.7%), and other soft tissues (16.7%). Baseline clinical information is available in Table S2. A majority of cases (96.4%) displayed typical high-grade prostate adenocarcinoma features, whereas 2.9% of cases showed neuroendocrine differentiation. One case (0.7%) exhibited small-cell neuroendocrine features (Epstein et al., 2014) (Figure 1D).

Landscape of mCRPC Alterations

Somatic aberrations in a panel of 38 statistically or clinically significant genes are illustrated in Figure 2. Mean target coverage for tumor exomes was 160× and for matched normal exomes was 100×. Although the average mutation rate for mCRPC was 4.4 mutations/Mb, there were four cases that exhibited a mutation rate of nearly 50 per Mb, three of which are likely due to alterations in the mismatch repair genes *MLH1* and *MSH2*, as discussed later.

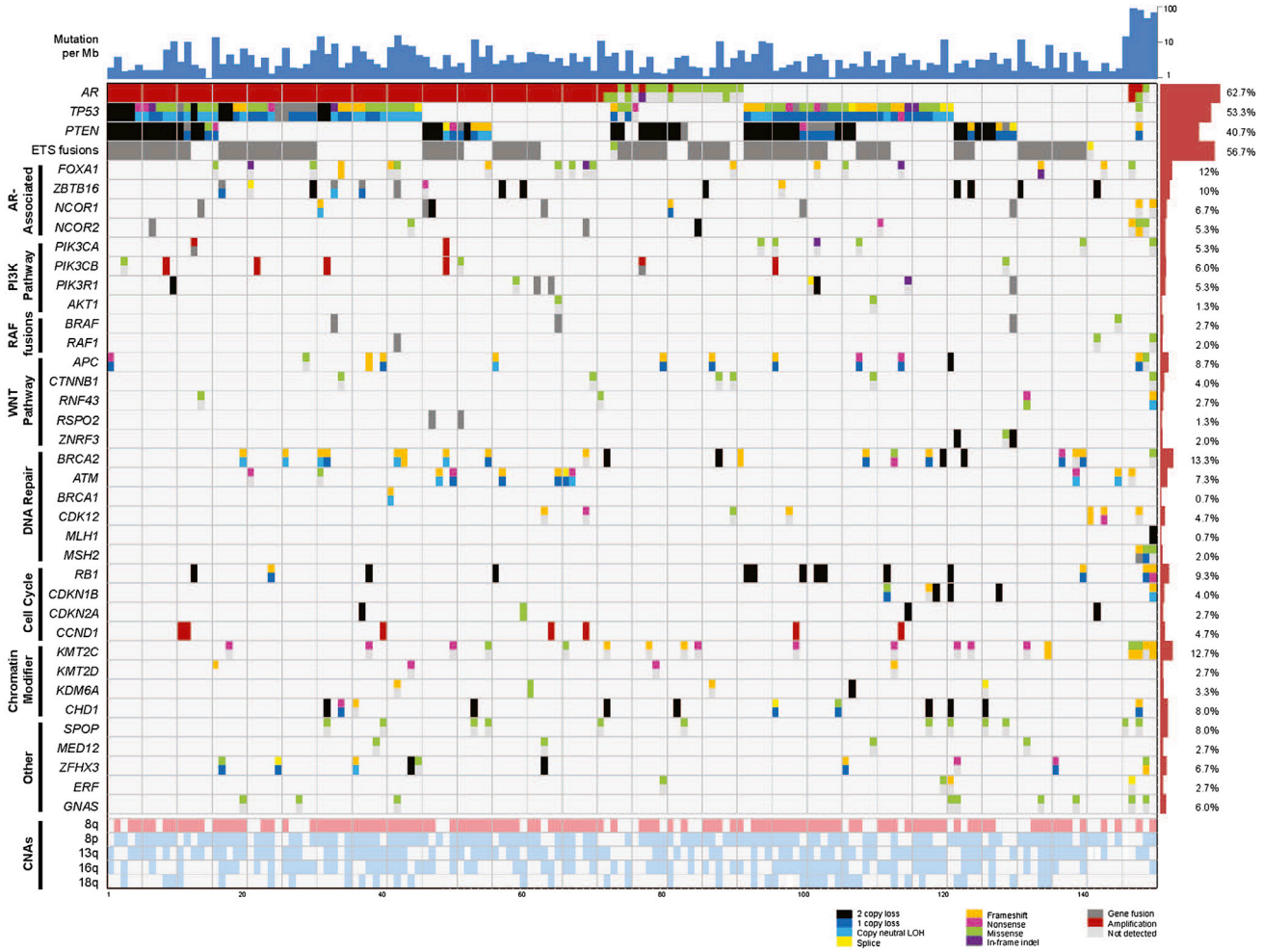

Figure 2. Integrative Landscape Analysis of Somatic and Germline Aberrations in Metastatic CRPC Obtained through DNA and RNA Sequencing of Clinically Obtained Biopsies

Columns represent individual affected individuals, and rows represent specific genes grouped in pathways. Mutations per Mb are shown in the upper histogram, and incidence of aberrations in the cohort is in the right histogram. Copy number variations (CNVs) common to mCRPC are shown in in the lower matrix, with pink representing gain and light blue representing loss. Color legend of the aberrations represented including amplification, two copy loss, one copy loss, copy neutral loss of heterozygosity (LOH), splice site mutation, frameshift mutation, missense mutation, in-frame indel, and gene fusion. Cases with more aberration in a gene are represented by split colors.

Frequent copy number gains of 8q, as well as copy number losses of 8p, 13q, 16q, and 18q, were also observed. The mean number of identified biologically relevant genetic aberrations per case was 7.8 (Figure 2). All mutations identified are presented in Table S3. The landscape of copy number alterations demonstrated expected recurrent amplification peaks (frequent *AR*, 8q gain) and deletion peaks (*CHD1*, *PTEN*, *RB1*, *TP53*) (Figure 3A). Additional frequent focal amplifications were observed in regions encompassing *CCND1* and *PIK3CA* and *PIK3CB*. A new recurrent focal homozygous deletion event was observed in chr11q23, encompassing the transcriptional repressor *ZBTB16*.

To identify gene fusions, analysis of 215 transcriptome libraries derived from the 150 tumor RNAs was performed and identified 4,122 chimeras with at least 4 reads spanning the fusion junction. These fusion junctions resulted from 2,247 gene pairs, an average of 15 gene fusions per tumor (Table S4). Among chimeric fusion transcripts identified, recurrent ETS fusions (Tomlins et al., 2005) were observed in 84 cases (56%), of which the majority were fused to *ERG* and others to *FLI1*, *ETV4*, and *ETV5* (Figure 3B). In addition, potential clinically actionable fusions (involving *BRAF*, *RAF1*, *PIK3CA/B*, or *RSPO2*) were seen in eight cases (Figure S1 and covered subsequently).

To place the mCRPC mutation landscape in the context of primary prostate cancer somatic genomics, we performed a selective enrichment analysis to compare somatic point mutations and short insertion/deletions observed in this cohort with those observed in somatic whole-exome mutation data from 440 primary prostate cancer exomes (Barbieri et al., 2012; The Cancer

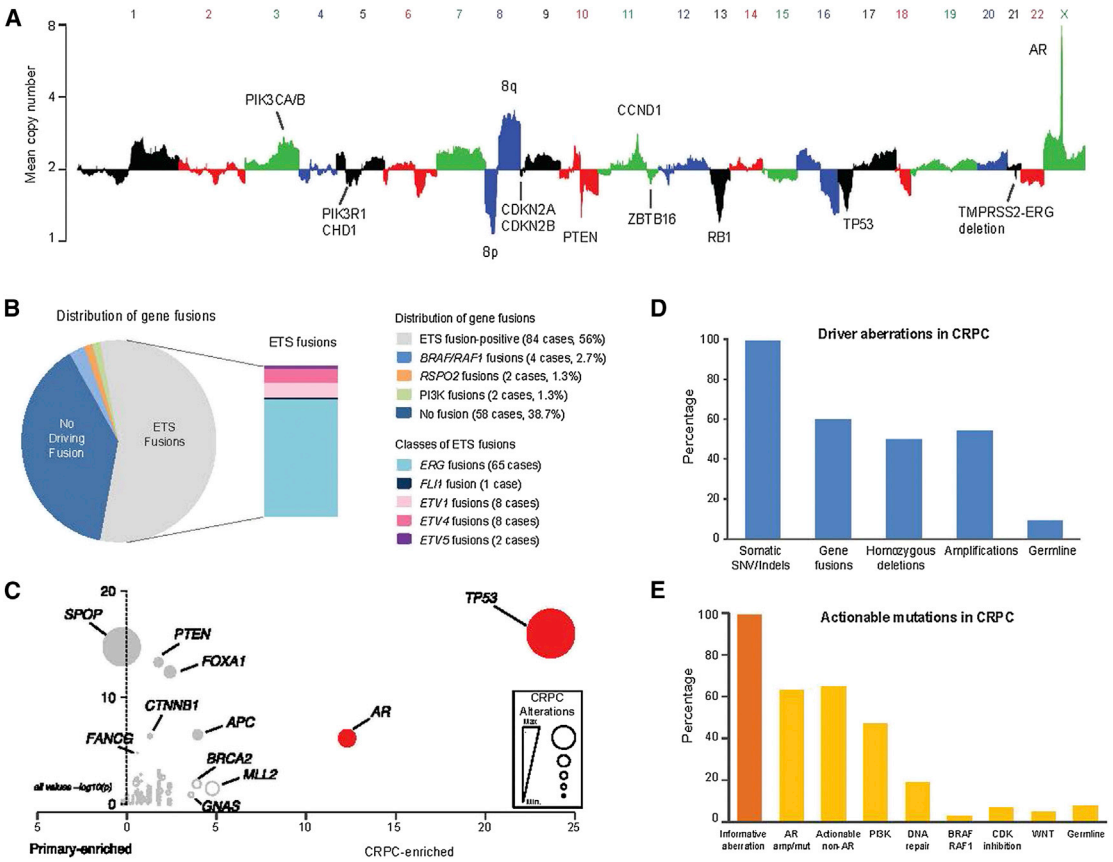

Figure 3. Classes of Genomic Aberrations Seen in mCPRC

(A) Copy number landscape of the SU2C-PCF mCRPC cohort. Individual chromosomes are represented by alternating colors, and key aberrant genes are indicated.

(B) The gene fusion landscape of mCRPC. Pie chart of all driver fusions identified and the box plot represents specific ETS fusions.

(C) Mutations enriched in mCRPC relative to hormone naive primary prostate cancer. Primary prostate cancer data derived from published studies (Barbieri et al., 2012; The Cancer Genome Atlas, 2015). Level of CRPC enrichment is represented by the x axis, and MutSig CRPC significance analysis is provided by the y axis. Diameters are proportional to the number of cases with the specific aberration. Genes of interest are highlighted.

(D) Classes of driver aberrations identified in mCRPC.

(E) Classes of clinically actionable mutations identified in mCRPC.

Genome Atlas, 2015) (Figure 3C and Table S5). Focusing on genes previously implicated in cancer (n = 550), somatic *TP53* mutations were the most selectively mutated ($q < 0.001$; Benjamini-Hochberg), followed by *AR*, *KMT2D*, *APC*, *BRCA2*, and *GNAS* ($q < 0.1$; Benjamini-Hochberg; Table S6). Both *AR* and *GNAS* were mutated exclusively in mCRPC. We found no genes selectively mutated in primary prostate cancer compared to mCRPC.

We identified an established biological "driver" aberration in a cancer-related gene (i.e., known oncogene or tumor suppressor; Table S7) in nearly all the cases (Figure 3D). Although 99% of the mCPRC cases harbored a potential driver single-nucleotide variant (SNV) or indel, other classes of driver aberrations were also highly prevalent. These include driver gene fusions in 60%, driver homozygous deletions in 50% and driver amplifications in 54%. Although informative mutations were present in virtually all mCRPC cases, 63% harbored aberrations in *AR*, an expected finding in castrate-resistant disease but with higher frequency than in prior reports (Figure 3E). Interestingly, even when *AR* was not considered, 65% of cases harbored a putatively clinically actionable alteration (defined as predicting response or resistance to a therapy, having diagnostic or prognostic utility across tumor types) (Table S8) (Roychowdhury et al., 2011; Van Allen et al., 2014c). Non-AR related clinically actionable alterations included aberrations in the PI3K pathway (49%), DNA repair pathway (19%), RAF kinases (3%), CDK inhibitors (7%), and the WNT pathway (5%). In addition to somatic alterations, clinically actionable pathogenic germline variants were seen in 8% of mCRPC affected individuals, potentially emphasizing the need for genetic counseling in affected individuals with prostate cancer.

Genomically Aberrant Pathways in mCRPC

Integrative analysis using both biological and statistical frameworks (Lawrence et al., 2013, 2014) of somatic point mutations,

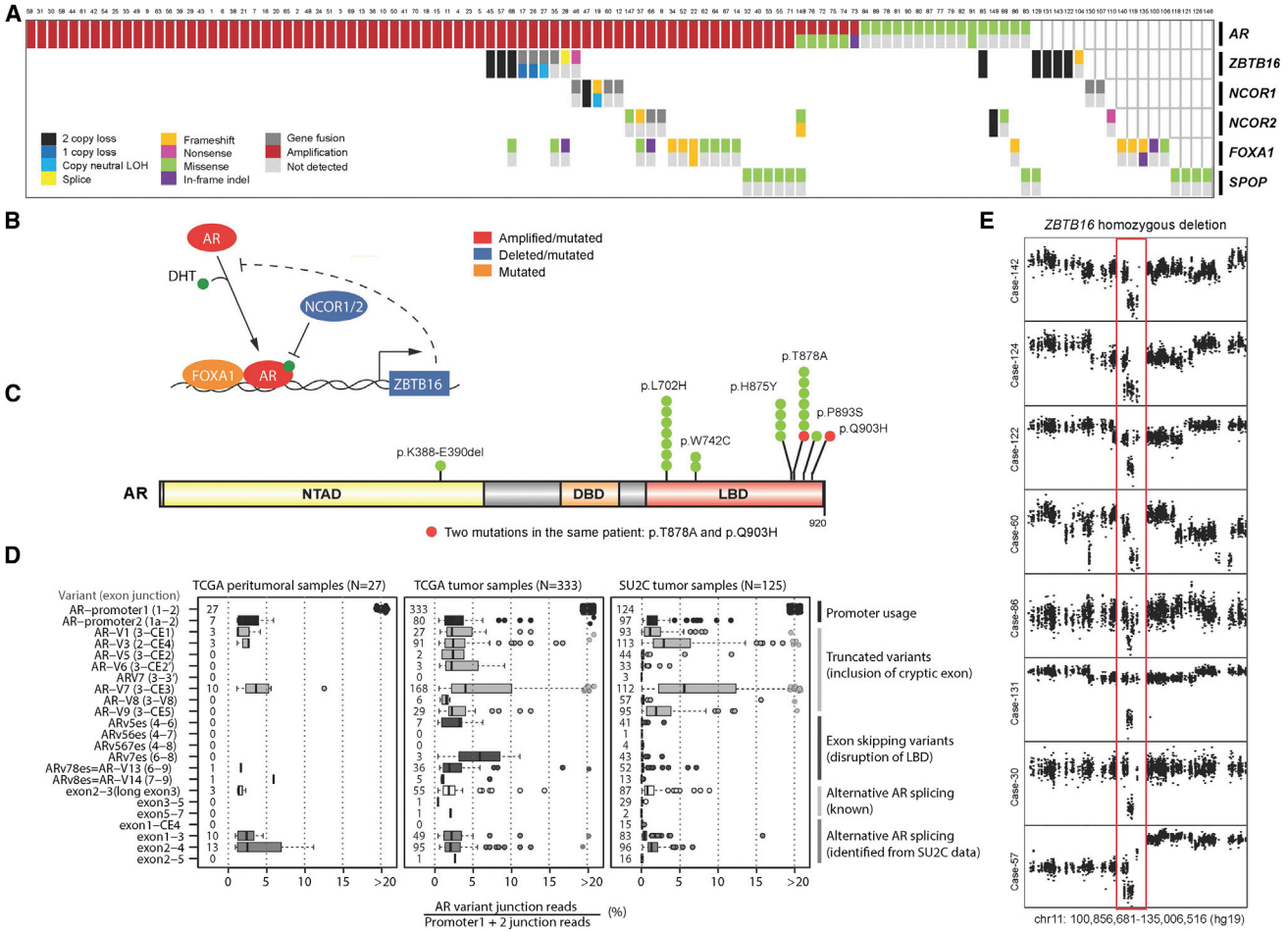

Figure 4. Aberrations in the AR Pathway Found in mCRPC

(A) Cases with aberrations in the AR pathway. Case numbering as in Figure 2.

(B) Key genes found altered in the AR pathway of mCRPC. DHT, dihydrotestosterone.

(C) Point mutations identified in *AR*. Amino acids altered are indicated. NTAD, N-terminal activation. DBD, DNA-binding. LBD, ligand binding.

(D) Splicing landscape of *AR* in mCRPC. Specific splice variants are indicated by exon boundaries, and junction read level is provided. SU2C, this mCRPC cohort. PRAD tumor, primary prostate cancer from the TCGA. PRAD normal, benign prostate from the TCGA.

(E) Homozygous deletion of *ZBTB16*. Copy number plots with x axis representing chromosomal location and the y axis referring to copy number level. Red outline indicates region of *ZBTB16* homozygous loss.

short insertion/deletions, copy number alterations, fusion transcripts, and focused germline variant analysis identified discrete molecular subtypes of mCRPC (Figure 2). These subtypes were classified based on alteration clustering and existing biological pathway knowledge and implicated the *AR* signaling pathway, phosphatidylinositol-4,5-bisphosphate 3-kinase (PI3K), WNT, DNA repair, cell cycle, and chromatin modifier gene sets, among others. The most frequently aberrant genes in mCRPC included *AR* (62.7%), ETS family (56.7%), *TP53* (53.3%), and *PTEN* (40.7%) (Figure 2).

AR Signaling Pathway

In aggregate, 107/150 (71.3%) of cases harbored *AR* pathway aberrations, the majority of which were direct alterations affecting *AR* through amplification and mutation (Figure 4A). Figure 4B summarizes the key genes altered in AR signaling, including *AR* itself, *FOXA1* as a pioneer transcription factor, *NCOR1/2* as negative regulators of AR, *SPOP* as a putative androgen receptor transcriptional regulator (Geng et al., 2013), and *ZBTB16* as an AR inducible target gene that may also negatively regulate *AR*. Recurrent hotspot mutations in *AR* were observed at residues previously reported to confer agonism to AR antagonists such as flutamide (T878A) and bicalutamide (W742C), as well as to glucocorticoids (L702H). Some, but not all, of these affected individuals had documented prior exposures that could explain enrichment for these mutations. Additional clinical data collection is ongoing (Figure 4C). Rare *AR* mutations not previously described were seen in our cohort, although these are of unclear functional significance. Furthermore, one affected individual (Case 89) harbored two putatively

functional *AR* mutations (T878A and Q903H), which may further suggest intra-tumor heterogeneity emerging in the CRPC setting (Carreira et al., 2014). Analysis of *AR* splice variants from RNA-seq data demonstrated a distribution of splice variants observed throughout these mCRPC tumor cases (Figure 4D). Analysis of the TCGA prostate dataset revealed that many of these variants were also present at varying levels in primary prostate cancer and benign prostate tissue. AR-V7, which has been implicated in abiraterone acetate and enzalutamide resistance (Antonarakis et al., 2014), was observed in a majority of pre-abiraterone/enzalutamide cases but at very low ratios relative to full length AR. Implications for treatment response are unknown at this time.

In addition to AR mutations itself, we observed alterations in AR pathway members (Figure 4A). These included known alterations in *NCOR1*, *NCOR2*, and *FOXA1* that have been previously reported in primary prostate cancers and mCRPC (Barbieri et al., 2012; Grasso et al., 2012). In this cohort, truncating and missense mutations in FOXA1 form a cluster near the end of the Forkhead DNA binding domain (Figure S2).

Recurrent homozygous deletions of the androgen-regulated gene *ZBTB16* (also known as PLZF) were seen in 8 (5%) cases (Figure 4E) not previously reported in clinical mCRPC biopsies. Analysis of the minimally deleted region seen in this cohort narrowed the candidate genes in the chr11q23 region to *ZBTB16* (Figure S3). *ZBTB16* has been previously implicated in prostate cancer tumorigenesis and androgen resistance in preclinical models (Cao et al., 2013; Kikugawa et al., 2006), with loss of *ZBTB16* upregulating the MAPK signaling pathway (Hsieh et al., 2015).

New PI3K Pathway Discoveries

The PI3K pathway was also commonly altered, with somatic alterations in 73/150 (49%) of mCRPC affected individuals (Figure 5A). This included biallelic loss of *PTEN*, as well as hotspot mutations, amplifications and activating fusions in *PIK3CA*, and p.E17K activating mutations in *AKT1* (Figure S2). Of note, *PIK3CA* amplifications resulted in overexpression compared to the remaining cohort (Figure S3).

Interestingly, mutations in another member of the PI3K catalytic subunit, *PIK3CB*, were observed in this cohort for the first time, at equivalent positions to canonical activating mutations in PIK3CA (Figure 5B). PIK3CB mutations appeared in the context of PTEN-deficient cases, which is consistent with a previous report demonstrating that some PTEN-deficient cancers are dependent on PIK3CB, rather than PIK3CA (Wee et al., 2008). Furthermore, two affected individuals harbored fusions involving PIK3CA/B, with these events resulting in overexpression of the gene relative to other tumors in the cohort (Figures 5C and 5D).

New Wnt Pathway Discoveries

27/150 (18%) of our cases harbored alterations in the Wnt signaling pathway (Figure 6A). Hotspot activating mutations in *CTNNB1* were seen (Figure 6B), as previously described (Voeller et al., 1998). Notably, recurrent alterations in *APC* were also observed, which have not been previously described in clinical mCRPC affected individuals. This prompted a broader examination of Wnt signaling genes (Figure 6B). Through integrative analysis, we identified alterations in *RNF43* and *ZNRF3*, which were recently described in colorectal, endometrial, and adrenocortical cancers (Assié et al., 2014; Giannakis et al., 2014) and were mutually exclusive with *APC* alterations (Figure 6A). Moreover, we also discovered R-spondin fusions involving *RSPO2*, as previously observed in colorectal carcinoma (Seshagiri et al., 2012) in association with RSPO2 overexpression in these cases (Figure 6C). RSPO2 is a key factor in prostate cancer organoid methodology (Gao et al., 2014). Affected individuals s with aberrations in *RNF43*, *ZNRF3*, or *RSPO2* (overall 6% of affected individuals) are predicted to respond to porcupine inhibitors (Liu et al., 2013).

Cell-Cycle Pathway

We observed *RB1* loss in 21% of cases (Figure S4). Expanding the scope of cell-cycle genes implicated in mCRPC, we noted focal amplifications involving *CCND1* in 9% of cases, as well as less common (< 5%) events in *CDKN2A/B*, *CDKN1B*, and *CDK4* (Figure S4). Cell-cycle derangement, such as through CCND1 amplification or CDKN2A/B loss, may result in enhanced response to CDK4 inhibitors in other tumor types (Finn et al., 2015), and preclinical mCRPC models predict similar activity in prostate cancer (Comstock et al., 2013).

DNA Repair Pathway

Integrative analysis of both the somatic and pathogenic germline alterations in *BRCA2* identified 19/150 (12.7%) of cases with loss of BRCA2, of which ~90% exhibited biallelic loss (Figure 7A). This was commonly a result of somatic point mutation and loss of heterozygosity, as well as homozygous deletion. One of the clinical trials in our consortium is evaluating poly(-ADP-ribose) polymerase (PARP) inhibition in unselected mCRPC affected individuals. Importantly, multiple affected individuals in this trial who experienced clinical benefit harbored biallelic *BRCA2* loss, providing further evidence of clinical actionability (Mateo et al., 2014). Eight affected individuals (5.3%) harbored pathogenic germline *BRCA2* mutations (Figure 7B) with a subsequent somatic event that resulted in biallelic loss, revealing a surprisingly high frequency relative to primary prostate cancer.

We therefore expanded the focus to other DNA repair/recombination genes and identified alterations in at least 34/150 (22.7%) of cases. These include recurrent biallelic loss of *ATM* (Figure 7B), including multiple cases with germline pathogenic alterations. ATM mutations were also observed in affected individuals who achieved clinical responses to PARP inhibition (Mateo et al., 2014). In addition, we noted events in *BRCA1*, *CDK12*, *FANCA*, *RAD51B*, and *RAD51C*. If aberrations of *BRCA2*, *BRCA1*, and *ATM* all confer enhanced sensitivity to PARP inhibitors, 29/150 (19.3%) of mCRPC affected individuals would be predicted to benefit from this therapy. Interestingly, three out of four mCRPC tumors exhibited hypermutation and harbored alterations in the mismatch repair pathway genes *MLH1* or *MSH2* (Figures 2 and 7C), corroborating a recent report identifying structural alterations in *MSH2* and *MSH6* mismatch repair genes in hypermutated prostate cancers (Pritchard et al., 2014).

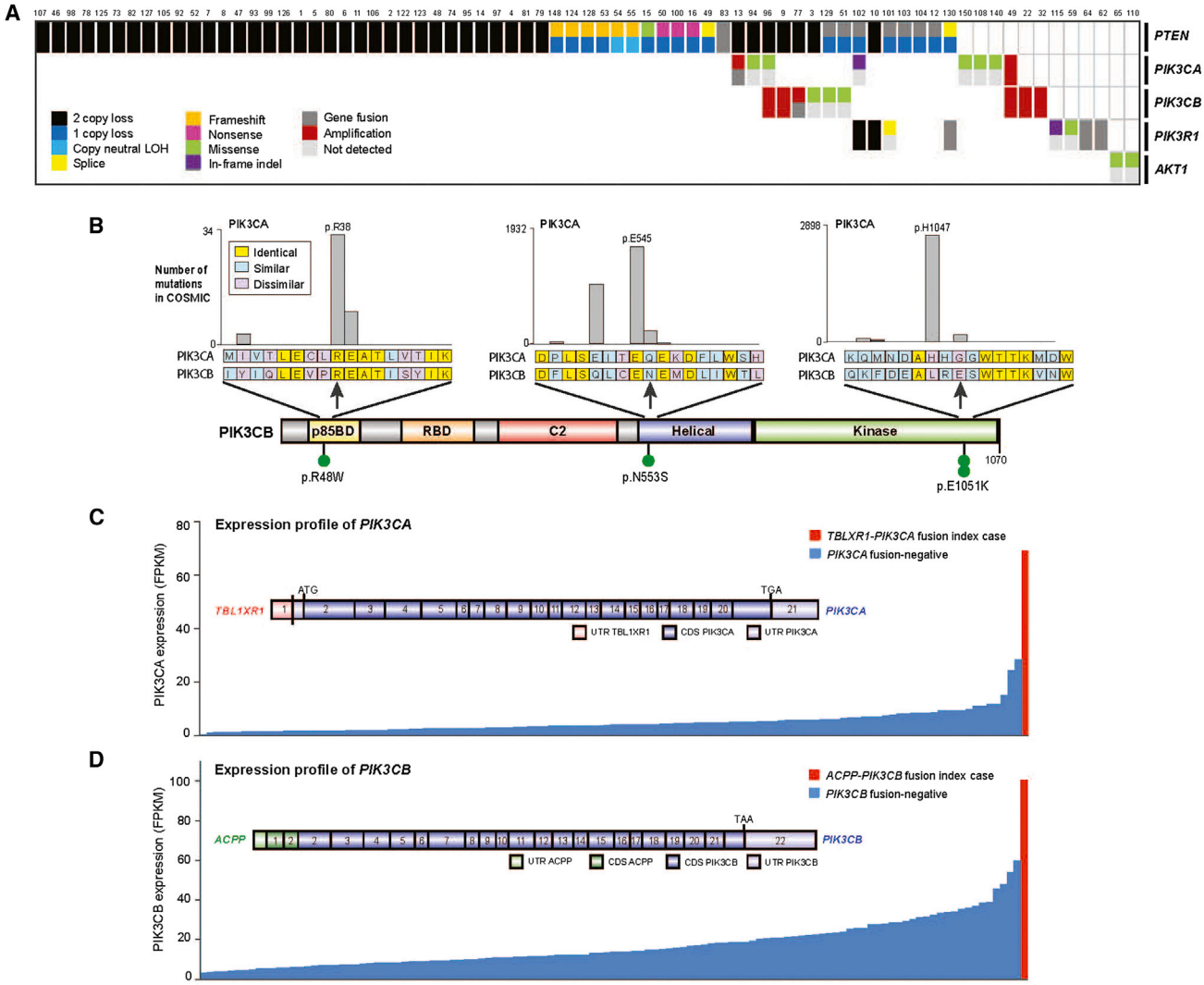

Figure 5. Aberrations in the PI(3)K Pathway Found in mCRPC

(A) Cases with aberrations in the PIK3 pathway. Case numbering as in Figure 2.

(B) Point mutations identified in PIK3CB. Amino acids altered are indicated. Analogous, recurrent COSMIC mutations in PIK3CA are shown as expansion views.

(C) Outlier expression of PK3CA in CRPC case harboring the TBL1XR1-PIK3CA gene fusion. Structure of the gene fusion is inset. UTR, untranslated region. CDS, coding sequence.

(D) As in (C), except for PIK3CB and the ACPP-PIK3CB gene fusion.

DISCUSSION

To effectively implement precision cancer medicine, prospective identification of predictive biomarkers should be performed with information derived from the most contemporary tumor assessments that reflect the affected individual's prior therapies and treatment opportunities. In mCRPC, precision cancer medicine activities have been limited by difficulties obtaining clinical samples from mCRPC affected individuals and a lack of comprehensive genomic data for potentially actionable alterations. By demonstrating the feasibility of prospective genomics in mCRPC and defining the mutational landscape in a focused metastatic clinical cohort, this report may inform multiple genomically driven clinical trials and biological investigations into key mediators of mCRPC. In nearly all of the mCRPC analyzed in this study, we identified biologically informative alterations; almost all harbored at least one driver SNV/indel, and approximately half harbored a driver gene fusion, amplification, or homozygous deletion. Remarkably, in nearly 90% of mCRPC affected individuals, we identified a potentially actionable somatic or germline event.

The high frequency of AR pathway alterations in this cohort strongly implies that the vast majority of mCRPC affected individuals remain dependent on AR signaling for viability. The "second-generation" AR-directed therapies (e.g., abiraterone acetate and enzalutamide) may select for distinct phenotypes that may be indifferent to AR signaling, and prospective

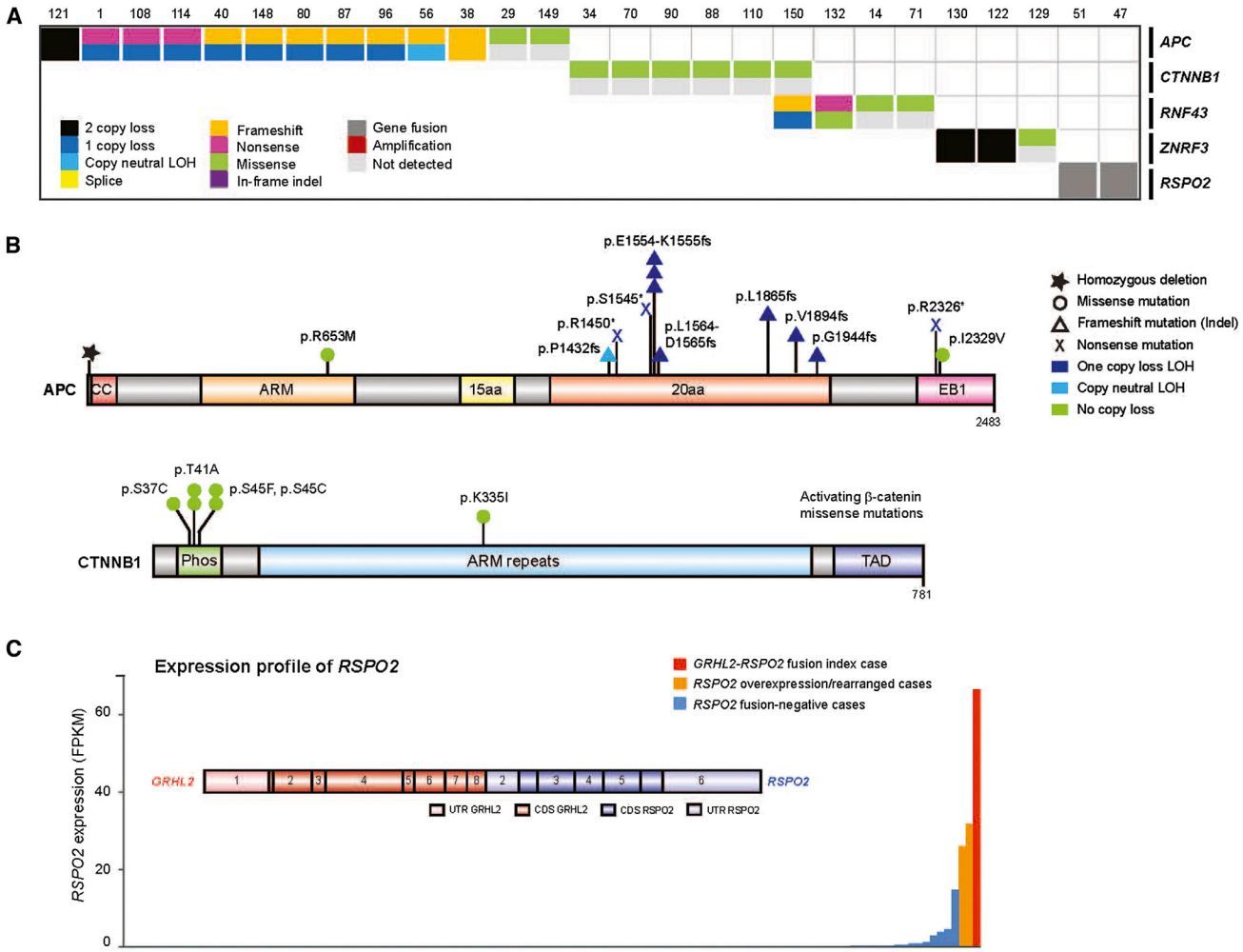

Figure 6. Aberrations in the WNT Pathway Found in mCRPC

(A) Cases with aberrations in the WNT pathway. Case numbering as in Figure 2.

(B) Aberrations identified in APC and CTNNB1. Amino acids altered are indicated. ARM, armadillo repeat. Phos, phosphorylation domain. TAD, *trans*-activating domain. EB1, end binding protein-1 domain. CC, coiled coil.

(C) Outlier expression of *RSPO2* in CRPC and the *GRHL2-RSPO2* gene fusion. RNA-seq expression across our CRPC cohort. Structure of the gene fusion is inset. UTR, untranslated region. CDS, coding sequence.

characterization of such cases will be of particular interest. We hypothesize that affected individuals with acquired *AR* mutations, including new *AR* mutations discovered in this cohort, will harbor differential responses to these second-generation ADT therapies. As the number of affected individuals in this cohort with *AR* mutations increases, we will subsequently be able to link specific AR mutations with clinical phenotypes to determine which mutations confer selective response or resistance to subsequent AR-directed therapy.

Moreover, these data identify multiple therapeutic avenues warranting clinical investigation in the CRPC population. Excluding AR aberrations, 65% of mCRPC have a potentially actionable aberration that may suggest an investigational drug or approved therapy. For example, focusing on the PI3K pathway, PIK3CB-specific inhibitors may have utility in affected individuals with mutation, amplification, and/or fusion of this gene (Schwartz et al., 2015); multiple affected individuals who achieved durable (>1 year) responses to PIK3CB-specificin inhibition harbored activating mutation or amplification in *PIK3CB* (J.S. de Bono et al., 2015, 106th Annual Meeting of the American Association for Cancer Research, abstract). RAF kinase fusions in 3% of mCPRC affected individuals would suggest the use of pan-RAF inhibitors or MEK inhibitors (Palanisamy et al., 2010). In addition, the emergence of porcupine inhibitors (Liu et al., 2013) and R-spondin antibodies may warrant investigation in mCRPC tumors harboring Wnt pathway alterations or specifically R-spondin fusions, respectively. These observations will need to be prospectively assessed in the clinical trials.

Additionally, biallelic inactivation of *BRCA2*, *BRCA1*, or *ATM* was observed in nearly 20% of affected individuals. Previous work in other cancer types suggests that these affected individuals may benefit from PARP inhibitors (Fong et al., 2009;

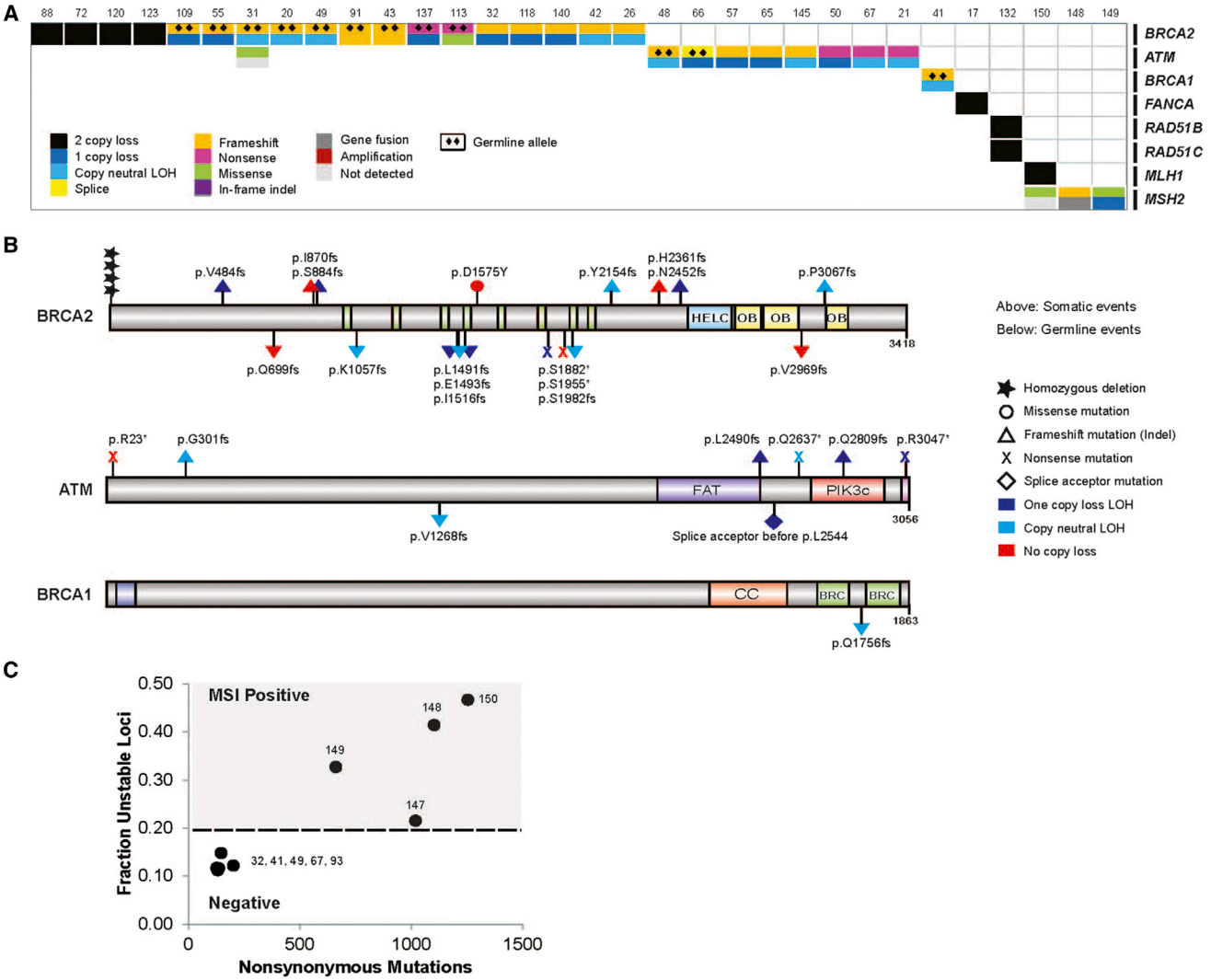

Figure 7. Aberrations in the DNA Repair Pathway Found in mCRPC

(A) Cases with aberrations in the DNA repair pathway. Case numbering as in Figure 2.

(B) Aberrations identified in BRCA2, ATM, and BRCA1. Amino acids altered are indicated. HELC, helical domain. OB, oligonucleotide binding fold. FAT, FRAP-ATM-TRRAP domain. PIK3c, PI3 kinase domain. CC, coiled coil. BRC, Brca repeat.

(C) Microsatellite instability analysis of representative hypermutated CRPC cases and non-hypermutated cases.

Kaufman et al., 2015; Weston et al., 2010) or platinum-based chemotherapy, and prior reports have implicated the presence of germline *BRCA2* alterations in primary prostate cancer with poor survival outcomes (Castro et al., 2013). Given the incidence of pathogenic germline *BRCA2* mutations in this cohort with subsequent somatic events (5%), along with enrichment for somatic *BRCA2* alterations in mCRPC (13%), germline genetic testing in mCRPC affected individuals warrants clinical consideration.

The ability to molecularly characterize mCRPC biopsy samples from affected individuals actively receiving therapy will also enable focused studies of resistance to secondary ADT therapies, including neuroendocrine-like phenotypes. This will require iterative sampling of pre-treatment and resistant tumors from matching affected individuals and may warrant multiregional biopsies from affected individuals (if feasible) given heterogeneity in mCRPC (Carreira et al., 2014; Gundem et al., 2015). Toward that end, in some affected individuals, we observed multiple *AR* mutations emerging in the same biopsy, which may indicate clonal heterogeneity within these mCRPC tumor samples. Additional genomic alterations discovered in this cohort (e.g., *ZBTB16*) warrant exploration in prostate cancer model systems, including organoid cultures (Gao et al., 2014).

Broadly, our effort demonstrates the utility of applying comprehensive genomic principles developed for primary malignancies (e.g., TCGA) to a clinically relevant metastatic tumor cohort. Our effort may also catalyze multi-institutional efforts to profile tumors from cohorts of affected individuals with metastatic, treated tumors in other clinical contexts because our results

demonstrate multiple discoveries within this advanced disease stage that have not been observed in primary tumor profiling. Moreover, this study sets the stage for epigenetic and other profiling efforts in mCRPC not taken in this study, which may enable biological discovery and have immediate therapeutic relevance in mCRPC (Asangani et al., 2014). Overall, our efforts demonstrate the feasibility of comprehensive and integrative genomics on prospective biopsies from individual mCRPC affected individuals to enable precision cancer medicine activities in this large affected individual population.

EXPERIMENTAL PROCEDURES

Affected Individual Enrollment

Affected individuals with clinical evidence of mCRPC who were being considered for abiraterone acetate or enzalutamide as standard of care, or as part of a clinical trial, were considered for enrollment. Affected individuals with metastatic disease accessible by image-guided biopsy were eligible for inclusion. All affected individuals provided written informed consent to obtain fresh tumor biopsies and to perform comprehensive molecular profiling of tumor and germline samples.

Biopsies and Pathology Review

Biopsies of soft tissue or bone metastases were obtained under radiographic guidance. Digital images of biopsy slides were centrally reviewed using schema established to distinguish usual adenocarcinoma from neuroendocrine prostate cancer (Epstein et al., 2014). All images were reviewed by genitourinary oncology pathologists (M.R., J.M.M., L.P.K., S.A.T., R.M., V.R., A.G., M.L., R.L., and M.B.).

Sequencing and Analysis

Normal DNAs from buccal swabs, buffy coats, or whole blood were isolated using the QIAGEN DNeasy Blood & Tissue Kit. Flash-frozen needle biopsies with highest tumor content for each case, as determined by pathology review, were extracted for nucleic acids. Tumor genomic DNA and total RNA were purified from the same sample using the AllPrep DNA/RNA/miRNA kit (QIAGEN) with disruption on a Tissuelyser II (QIAGEN). RNA integrity was verified on an Agilent 2100 Bioanalyzer using RNA Nano reagents (Agilent Technologies).

Whole-exome capture libraries were constructed from 100 ng to 1 μg of DNA from tumor and normal tissue after sample shearing, end repair, and phosphorylation and ligation to barcoded sequencing adaptors. Ligated DNA was size selected for lengths between 200 and 350 bp and subjected to hybrid capture using SureSelect Exome v4 baits (Agilent). Exome sequence data processing and analysis were performed using pipelines at the Broad Institute and the University of Michigan. A BAM file aligned to the hg19 human genome build was produced using Illumina sequencing reads for the tumor and normal sample and the Picard pipeline. Somatic mutation analysis was performed as described previously (Cibulskis et al., 2013; Van Allen et al., 2014c) and reviewed with Integrated Genomics Viewer (IGV) (Robinson et al., 2011).

Copy number aberrations were quantified and reported for each gene as the segmented normalized log2-transformed exon coverage ratios between each tumor sample and matched normal sample (Lonigro et al., 2011). To account for observed associations between coverage ratios and GC content across the genome, lowess normalization was used to correct per-exon coverage ratios prior to segmentation analysis. Mean GC percentage was computed for each targeted region, and a lowess curve was fit to the scatterplot of log2-coverage ratios versus mean GC content across the targeted exome using the lowess function in R (version 2.13.1) with smoothing parameter f = 0.05. The resulting copy ratios were segmented using the circular binary segmentation algorithm (Olshen et al., 2004).

Statistical analysis of recurrently mutated genes was performed using MutSig (Lawrence et al., 2013). Selective enrichment analysis (Van Allen et al., 2014b) of mutations observed in mCRPC compared to primary prostate cancer was performed by tabulating the frequency of affected-individual-normalized mutations observed in either CRPC or primary prostate cancer and performing a two-sided Fisher's exact test using allelic fraction cut off of 0.1 or greater and a set of biologically relevant cancer genes (n = 550 genes) (Futreal et al., 2004). Multiple hypothesis test correction was performed using Benjamini-Hochberg method.

Transcriptome libraries were prepared using 200–1,000 ng of total RNA. PolyA+ RNA isolation, cDNA synthesis, end-repair, A-base addition, and ligation of the Illumina indexed adapters were performed according to the TruSeq RNA protocol (Illumina). Libraries were size selected for 250–300 bp cDNA fragments on a 3% Nusieve 3:1 (Lonza) gel, recovered using QIAEX II reagents (QIAGEN), and PCR amplified using Phusion DNA polymerase (New England Biolabs). Total transcriptome libraries were prepared as above, omitting the poly A selection step and captured using Agilent SureSelect Human All Exon V4 reagents and protocols. Library quality was measured on an Agilent 2100 Bioanalyzer for product size and concentration. Paired-end libraries were sequenced with the Illumina HiSeq 2500, (2×100 nucleotide read length) with sequence coverage to 50 M paired reads and 100 M total reads.

Paired-end transcriptome sequencing reads were aligned to the human reference genome (GRCh37/hg19) using a RNA-seq spliced read mapper Tophat2 (Kim and Salzberg, 2011) (Tophat 2.0.4), with "–fusion-search" option turned on to detect potential gene fusion transcripts. Potential false-positive fusion candidates were filtered out using "Tophat-Post-Fusion" module. Further, the fusion candidates were manually examined for annotation and ligation artifacts. Gene expression, as fragments per kilobase of exon per million fragments mapped (FPKM; normalized measure of gene expression), was calculated using Cufflinks (Trapnell et al., 2012).

ACCESSION NUMBERS

The accession number for the data reported in this paper is dbGap: phs000915.v1.p1.

SUPPLEMENTAL INFORMATION

Supplemental Information includes four figures and eight tables and can be found with this article online at http://dx.doi.org/10.1016/j.cell.2015.05.001.

AUTHOR CONTRIBUTIONS

Y-M.W., N.S., R.J.L., J.-M.M., R.M., M.E.T., C.C.P., G.A., H.B., and W.A. made equal contributions. D.R., E.M.V.A., and R.J.L. coordinated overall sequencing and bioinformatics analysis. Y.M.W., D.R., E.M.V.A., R.J.L., W.A., and J.V. coordinated figures and tables. N.S. developed the SU2C-PCF IDT cBio portal. R.J.L. coordinated copy number analyses. J.-M.M. coordinated central pathology review, and L.P.K coordinated UM pathology analysis. C.C.P. coordinated hypermutation analysis and clinical germline interpretations. R.M., M.E.T, G.A., H.B., M.H., H.I.S., and E.I.H. coordinated clinical enrollment at their specific sites. R.K.B., S.P., and H.D. carried out AR splice variant analysis. J.V. managed the clinical data portal. X.C., J.S., P.F., S.M., and C.S. were involved in project management. R.M., S.A.T., V.E.R., A.G., M.L., S.P.B., R.T.L., M.B., B.D.R., J.-M.M, M.R., and L.D.T. were involved in pathology review. C.B., P.V., J.G., M.G., F.D., O.E., A. Sboner, A. Sigaras, and K.W.E. contributed to bioinformatics analysis. K.A.C., D.C.S., F.Y.F., H.I.S., D.R., S.B.S., M.J.M., R.F., Z.Z., N.T., G.G., J.C.D., J.M., D.M.N., S.T.T., E.Y.Y., Y.C., E.A.M., H.H.C., M.A.S., and K.J.P. are clinical contributors. E.M.V.A., D.R., C.L.S. and A.M.C. wrote the manuscript, which all authors reviewed. P.K., J.S.d.B., M.A.R., P.S.N., and L.A.G. are SU2C-PCF Dream Team Principals, and C.L.S. and A.M.C. are Dream Team co-Leaders.

ACKNOWLEDGMENTS

We thank the affected individuals who participated in this study to better understand the feasibility and utility of precision medicine approaches for advanced prostate cancer. Individuals at our respective institutions who helped with this study are listed by institution. University of Michigan: Karen Giles, Lynda Hodges, Erica Rabban, Ning Yu, Fengyun Su, Rui Wang, Brendan Veeneman, and Moshe Talpaz. MSKCC: Brett Carver, Kristen Curtis, and Julie

Filipenko. DFCI/Broad: Zhenwei Zhang, Daniele Depalo, and Joseph Kramkowski. University of Washington: Jina Taub, Hiep Nguyen, Colm Morrissey, and Robert Vessella. ICR/Royal Marsden: Suzanne Carreira, Ines Figueiredo, and Daniel Nava Rodrigues. This work was supported by a Stand Up To Cancer-Prostate Cancer Foundation Prostate Dream Team Translational Cancer Research Grant. Stand Up To Cancer is a program of the Entertainment Industry Foundation administered by the American Association for Cancer Research (SU2C-AACR-DT0712). The project was also supported by the following NIH awards: Clinical Sequencing Exploratory Research (CSER) UM1HG006508 (A.M.C.), Early Detection Research Network grant UO1 CA111275(A.M.C.), Prostate SPORE grants P50 CA186786 (A.M.C.), P50 CA092629 (H.I.S., C.L.S., and Y.C.), P50 CA90381 (P.K.),and P50 CA097186 (P.S.N., B.M., E.A.M., and L.D.T.), P01 CA163227 (P.S.N., S.P., R.K.B., H.D.), R01 CA116337 (M.A.R., H.B., F.D.), R01 CA155169 (C.L.S.), R01 CA092629, P50 CA092629 (H.I.S., C.L.S., and Y.C.), and R01 CA155169 (C.L.S.). This work was supported by the following DoD awards: W81XWH-09-1-0147 (PCCTC) and DOD PC121341 (H.B.). This work was also supported by the Starr Cancer Consortium (N.S., M.R., C.S., Y.C., L.A.G.). A.M.C. is an A. Alfred Taubman Scholar and an American Cancer Society Professor. H.B. is supported by Damon Runyon Cancer Research Foundation CI-67-13. C.P. is supported by a PCF Young Investigator Award and DoD PC131820. E.M.V. is supported by a NIH 1K08CA188615. E.M.V., N.S., and F.Y.F. are supported by Prostate Cancer Foundation Young Investigator Awards. The RM and ICR team is supported by the Movember Foundation and Prostate Cancer UK, PCF, the ECMC network from Cancer Research UK, the Department of Health in the UK, and BRC grant funding.

Received: March 9, 2015
Revised: April 6, 2015
Accepted: April 27, 2015
Published: May 21, 2015

REFERENCES

American Cancer Society (2015). Cancer Facts and Figures 2015. http://www.cancer.org/acs/groups/content/@editorial/documents/document/acspc-044552.pdf.

Antonarakis, E.S., Lu, C., Wang, H., Luber, B., Nakazawa, M., Roeser, J.C., Chen, Y., Mohammad, T.A., Chen, Y., Fedor, H.L., et al. (2014). AR-V7 and resistance to enzalutamide and abiraterone in prostate cancer. N. Engl. J. Med. *371*, 1028–1038.

Asangani, I.A., Dommeti, V.L., Wang, X., Malik, R., Cieslik, M., Yang, R., Escara-Wilke, J., Wilder-Romans, K., Dhanireddy, S., Engelke, C., et al. (2014). Therapeutic targeting of BET bromodomain proteins in castration-resistant prostate cancer. Nature *510*, 278–282.

Assié, G., Letouzé, E., Fassnacht, M., Jouinot, A., Luscap, W., Barreau, O., Omeiri, H., Rodriguez, S., Perlemoine, K., René-Corail, F., et al. (2014). Integrated genomic characterization of adrenocortical carcinoma. Nat. Genet. *46*, 607–612.

Baca, S.C., Prandi, D., Lawrence, M.S., Mosquera, J.M., Romanel, A., Drier, Y., Park, K., Kitabayashi, N., MacDonald, T.Y., Ghandi, M., et al. (2013). Punctuated evolution of prostate cancer genomes. Cell *153*, 666–677.

Barbieri, C.E., Baca, S.C., Lawrence, M.S., Demichelis, F., Blattner, M., Theurillat, J.P., White, T.A., Stojanov, P., Van Allen, E., Stransky, N., et al. (2012). Exome sequencing identifies recurrent SPOP, FOXA1 and MED12 mutations in prostate cancer. Nat. Genet. *44*, 685–689.

Beer, T.M., Armstrong, A.J., Rathkopf, D.E., Loriot, Y., Sternberg, C.N., Higano, C.S., Iversen, P., Bhattacharya, S., Carles, J., Chowdhury, S., et al.; PREVAIL Investigators (2014). Enzalutamide in metastatic prostate cancer before chemotherapy. N. Engl. J. Med. *371*, 424–433.

Beltran, H., Yelensky, R., Frampton, G.M., Park, K., Downing, S.R., MacDonald, T.Y., Jarosz, M., Lipson, D., Tagawa, S.T., Nanus, D.M., et al. (2013). Targeted next-generation sequencing of advanced prostate cancer identifies potential therapeutic targets and disease heterogeneity. Eur. Urol. *63*, 920–926.

Berger, M.F., Lawrence, M.S., Demichelis, F., Drier, Y., Cibulskis, K., Sivachenko, A.Y., Sboner, A., Esgueva, R., Pflueger, D., Sougnez, C., et al. (2011). The genomic complexity of primary human prostate cancer. Nature *470*, 214–220.

Cao, J., Zhu, S., Zhou, W., Li, J., Liu, C., Xuan, H., Yan, J., Zheng, L., Zhou, L., Yu, J., et al. (2013). PLZF mediates the PTEN/AKT/FOXO3a signaling in suppression of prostate tumorigenesis. PLoS ONE *8*, e77922.

Carreira, S., Romanel, A., Goodall, J., Grist, E., Ferraldeschi, R., Miranda, S., Prandi, D., Lorente, D., Frenel, J.S., Pezaro, C., et al. (2014). Tumor clone dynamics in lethal prostate cancer. Sci. Transl. Med. *6*, 254ra125.

Castro, E., Goh, C., Olmos, D., Saunders, E., Leongamornlert, D., Tymrakiewicz, M., Mahmud, N., Dadaev, T., Govindasami, K., Guy, M., et al. (2013). Germline BRCA mutations are associated with higher risk of nodal involvement, distant metastasis, and poor survival outcomes in prostate cancer. J. Clin. Oncol. *31*, 1748–1757.

Cerami, E., Gao, J., Dogrusoz, U., Gross, B.E., Sumer, S.O., Aksoy, B.A., Jacobsen, A., Byrne, C.J., Heuer, M.L., Larsson, E., et al. (2012). The cBio cancer genomics portal: an open platform for exploring multidimensional cancer genomics data. Cancer Discov. *2*, 401–404.

Cibulskis, K., Lawrence, M.S., Carter, S.L., Sivachenko, A., Jaffe, D., Sougnez, C., Gabriel, S., Meyerson, M., Lander, E.S., and Getz, G. (2013). Sensitive detection of somatic point mutations in impure and heterogeneous cancer samples. Nat. Biotechnol. *31*, 213–219.

Comstock, C.E., Augello, M.A., Goodwin, J.F., de Leeuw, R., Schiewer, M.J., Ostrander, W.F., Jr., Burkhart, R.A., McClendon, A.K., McCue, P.A., Trabulsi, E.J., et al. (2013). Targeting cell cycle and hormone receptor pathways in cancer. Oncogene *32*, 5481–5491.

Cooper, C.S., Eeles, R., Wedge, D.C., Van Loo, P., Gundem, G., Alexandrov, L.B., Kremeyer, B., Butler, A., Lynch, A.G., Camacho, N., et al.; ICGC Prostate Group (2015). Analysis of the genetic phylogeny of multifocal prostate cancer identifies multiple independent clonal expansions in neoplastic and morphologically normal prostate tissue. Nat. Genet. *47*, 367–372.

de Bono, J.S., Logothetis, C.J., Molina, A., Fizazi, K., North, S., Chu, L., Chi, K.N., Jones, R.J., Goodman, O.B., Jr., Saad, F., et al.; COU-AA-301 Investigators (2011). Abiraterone and increased survival in metastatic prostate cancer. N. Engl. J. Med. *364*, 1995–2005.

Epstein, J.I., Amin, M.B., Beltran, H., Lotan, T.L., Mosquera, J.M., Reuter, V.E., Robinson, B.D., Troncoso, P., and Rubin, M.A. (2014). Proposed morphologic classification of prostate cancer with neuroendocrine differentiation. Am. J. Surg. Pathol. *38*, 756–767.

Finn, R.S., Crown, J.P., Lang, I., Boer, K., Bondarenko, I.M., Kulyk, S.O., Ettl, J., Patel, R., Pinter, T., Schmidt, M., et al. (2015). The cyclin-dependent kinase 4/6 inhibitor palbociclib in combination with letrozole versus letrozole alone as first-line treatment of oestrogen receptor-positive, HER2-negative, advanced breast cancer (PALOMA-1/TRIO-18): a randomised phase 2 study. Lancet Oncol. *16*, 25–35.

Fong, P.C., Boss, D.S., Yap, T.A., Tutt, A., Wu, P., Mergui-Roelvink, M., Mortimer, P., Swaisland, H., Lau, A., O'Connor, M.J., et al. (2009). Inhibition of poly(ADP-ribose) polymerase in tumors from BRCA mutation carriers. N. Engl. J. Med. *361*, 123–134.

Futreal, P.A., Coin, L., Marshall, M., Down, T., Hubbard, T., Wooster, R., Rahman, N., and Stratton, M.R. (2004). A census of human cancer genes. Nat. Rev. Cancer *4*, 177–183.

Gao, J., Aksoy, B.A., Dogrusoz, U., Dresdner, G., Gross, B., Sumer, S.O., Sun, Y., Jacobsen, A., Sinha, R., Larsson, E., et al. (2013). Integrative analysis of complex cancer genomics and clinical profiles using the cBioPortal. Sci. Signal. *6*, pl1.

Gao, D., Vela, I., Sboner, A., Iaquinta, P.J., Karthaus, W.R., Gopalan, A., Dowling, C., Wanjala, J.N., Undvall, E.A., Arora, V.K., et al. (2014). Organoid cultures derived from patients with advanced prostate cancer. Cell *159*, 176–187.

Geng, C., He, B., Xu, L., Barbieri, C.E., Eedunuri, V.K., Chew, S.A., Zimmermann, M., Bond, R., Shou, J., Li, C., et al. (2013). Prostate cancer-associated

mutations in speckle-type POZ protein (SPOP) regulate steroid receptor coactivator 3 protein turnover. Proc. Natl. Acad. Sci. USA *110*, 6997–7002.

Giannakis, M., Hodis, E., Jasmine Mu, X., Yamauchi, M., Rosenbluh, J., Cibulskis, K., Saksena, G., Lawrence, M.S., Qian, Z.R., Nishihara, R., et al. (2014). RNF43 is frequently mutated in colorectal and endometrial cancers. Nat. Genet. *46*, 1264–1266.

Grasso, C.S., Wu, Y.M., Robinson, D.R., Cao, X., Dhanasekaran, S.M., Khan, A.P., Quist, M.J., Jing, X., Lonigro, R.J., Brenner, J.C., et al. (2012). The mutational landscape of lethal castration-resistant prostate cancer. Nature *487*, 239–243.

Gundem, G., Van Loo, P., Kremeyer, B., Alexandrov, L.B., Tubio, J.M., Papaemmanuil, E., Brewer, D.S., Kallio, H.M., Högnäs, G., Annala, M., et al.; ICGC Prostate UK Group (2015). The evolutionary history of lethal metastatic prostate cancer. Nature *520*, 353–357.

Hieronymus, H., Schultz, N., Gopalan, A., Carver, B.S., Chang, M.T., Xiao, Y., Heguy, A., Huberman, K., Bernstein, M., Assel, M., et al. (2014). Copy number alteration burden predicts prostate cancer relapse. Proc. Natl. Acad. Sci. USA *111*, 11139–11144.

Hong, M.K., Macintyre, G., Wedge, D.C., Van Loo, P., Patel, K., Lunke, S., Alexandrov, L.B., Sloggett, C., Cmero, M., Marass, F., et al. (2015). Tracking the origins and drivers of subclonal metastatic expansion in prostate cancer. Nat. Commun. *6*, 6605.

Hsieh, C.L., Botta, G., Gao, S., Li, T., Van Allen, E.M., Treacy, D.J., Cai, C., He, H.H., Sweeney, C.J., Brown, M., et al. (2015). PLZF, a tumor suppressor genetically lost in metastatic castration-resistant prostate cancer, is a mediator of resistance to androgen deprivation therapy. Cancer Res. Published online March 25, 2015. http://dx.doi.org/10.1158/0008-5472.CAN-14-3602.

Kaufman, B., Shapira-Frommer, R., Schmutzler, R.K., Audeh, M.W., Friedlander, M., Balmaña, J., Mitchell, G., Fried, G., Stemmer, S.M., Hubert, A., et al. (2015). Olaparib monotherapy in patients with advanced cancer and a germline BRCA1/2 mutation. J. Clin. Oncol. *33*, 244–250.

Kikugawa, T., Kinugasa, Y., Shiraishi, K., Nanba, D., Nakashiro, K., Tanji, N., Yokoyama, M., and Higashiyama, S. (2006). PLZF regulates Pbx1 transcription and Pbx1-HoxC8 complex leads to androgen-independent prostate cancer proliferation. Prostate *66*, 1092–1099.

Kim, D., and Salzberg, S.L. (2011). TopHat-Fusion: an algorithm for discovery of novel fusion transcripts. Genome Biol. *12*, R72.

Lalonde, E., Ishkanian, A.S., Sykes, J., Fraser, M., Ross-Adams, H., Erho, N., Dunning, M.J., Halim, S., Lamb, A.D., Moon, N.C., et al. (2014). Tumour genomic and microenvironmental heterogeneity for integrated prediction of 5-year biochemical recurrence of prostate cancer: a retrospective cohort study. Lancet Oncol. *15*, 1521–1532.

Lawrence, M.S., Stojanov, P., Polak, P., Kryukov, G.V., Cibulskis, K., Sivachenko, A., Carter, S.L., Stewart, C., Mermel, C.H., Roberts, S.A., et al. (2013). Mutational heterogeneity in cancer and the search for new cancer-associated genes. Nature *499*, 214–218.

Lawrence, M.S., Stojanov, P., Mermel, C.H., Robinson, J.T., Garraway, L.A., Golub, T.R., Meyerson, M., Gabriel, S.B., Lander, E.S., and Getz, G. (2014). Discovery and saturation analysis of cancer genes across 21 tumour types. Nature *505*, 495–501.

Liu, J., Pan, S., Hsieh, M.H., Ng, N., Sun, F., Wang, T., Kasibhatla, S., Schuller, A.G., Li, A.G., Cheng, D., et al. (2013). Targeting Wnt-driven cancer through the inhibition of Porcupine by LGK974. Proc. Natl. Acad. Sci. USA *110*, 20224–20229.

Lonigro, R.J., Grasso, C.S., Robinson, D.R., Jing, X., Wu, Y.M., Cao, X., Quist, M.J., Tomlins, S.A., Pienta, K.J., and Chinnaiyan, A.M. (2011). Detection of somatic copy number alterations in cancer using targeted exome capture sequencing. Neoplasia *13*, 1019–1025.

Mateo, J., Hall, E., Sandhu, S., Omlin, A., Miranda, S., Carreira, S., Goodall, J., Gillman, A., Mossop, H., Ralph, C., et al. (2014). Antitumour activity of the PARP inhibitor olaparib in unselected sporadic castration-resistant prostate cancer (CRPC) in the TOPARP trial. Annals Oncol. *25*, 1–41.

Mehra, R., Kumar-Sinha, C., Shankar, S., Lonigro, R.J., Jing, X., Philips, N.E., Siddiqui, J., Han, B., Cao, X., Smith, D.C., et al. (2011). Characterization of bone metastases from rapid autopsies of prostate cancer patients. Clin. Cancer Res. *17*, 3924–3932.

Olshen, A.B., Venkatraman, E.S., Lucito, R., and Wigler, M. (2004). Circular binary segmentation for the analysis of array-based DNA copy number data. Biostatistics *5*, 557–572.

Palanisamy, N., Ateeq, B., Kalyana-Sundaram, S., Pflueger, D., Ramnarayanan, K., Shankar, S., Han, B., Cao, Q., Cao, X., Suleman, K., et al. (2010). Rearrangements of the RAF kinase pathway in prostate cancer, gastric cancer and melanoma. Nat. Med. *16*, 793–798.

Pflueger, D., Terry, S., Sboner, A., Habegger, L., Esgueva, R., Lin, P.C., Svensson, M.A., Kitabayashi, N., Moss, B.J., MacDonald, T.Y., et al. (2011). Discovery of non-ETS gene fusions in human prostate cancer using next-generation RNA sequencing. Genome Res. *21*, 56–67.

Pritchard, C.C., Morrissey, C., Kumar, A., Zhang, X., Smith, C., Coleman, I., Salipante, S.J., Milbank, J., Yu, M., Grady, W.M., et al. (2014). Complex MSH2 and MSH6 mutations in hypermutated microsatellite unstable advanced prostate cancer. Nat. Commun. *5*, 4988.

Robinson, J.T., Thorvaldsdóttir, H., Winckler, W., Guttman, M., Lander, E.S., Getz, G., and Mesirov, J.P. (2011). Integrative genomics viewer. Nat. Biotechnol. *29*, 24–26.

Roychowdhury, S., Iyer, M.K., Robinson, D.R., Lonigro, R.J., Wu, Y.M., Cao, X., Kalyana-Sundaram, S., Sam, L., Balbin, O.A., Quist, M.J., et al. (2011). Personalized oncology through integrative high-throughput sequencing: a pilot study. Sci. Transl. Med. *3*, 111ra121.

Ryan, C.J., Smith, M.R., de Bono, J.S., Molina, A., Logothetis, C.J., de Souza, P., Fizazi, K., Mainwaring, P., Piulats, J.M., Ng, S., et al.; COU-AA-302 Investigators (2013). Abiraterone in metastatic prostate cancer without previous chemotherapy. N. Engl. J. Med. *368*, 138–148.

Scher, H.I., Fizazi, K., Saad, F., Taplin, M.E., Sternberg, C.N., Miller, K., de Wit, R., Mulders, P., Chi, K.N., Shore, N.D., et al.; AFFIRM Investigators (2012). Increased survival with enzalutamide in prostate cancer after chemotherapy. N. Engl. J. Med. *367*, 1187–1197.

Schwartz, S., Wongvipat, J., Trigwell, C.B., Hancox, U., Carver, B.S., Rodrik-Outmezguine, V., Will, M., Yellen, P., de Stanchina, E., Baselga, J., et al. (2015). Feedback suppression of PI3Kα signaling in PTEN-mutated tumors is relieved by selective inhibition of PI3Kβ. Cancer Cell *27*, 109–122.

Seshagiri, S., Stawiski, E.W., Durinck, S., Modrusan, Z., Storm, E.E., Conboy, C.B., Chaudhuri, S., Guan, Y., Janakiraman, V., Jaiswal, B.S., et al. (2012). Recurrent R-spondin fusions in colon cancer. Nature *488*, 660–664.

Taplin, M.E., Bubley, G.J., Shuster, T.D., Frantz, M.E., Spooner, A.E., Ogata, G.K., Keer, H.N., and Balk, S.P. (1995). Mutation of the androgen-receptor gene in metastatic androgen-independent prostate cancer. N. Engl. J. Med. *332*, 1393–1398.

Taylor, B.S., Schultz, N., Hieronymus, H., Gopalan, A., Xiao, Y., Carver, B.S., Arora, V.K., Kaushik, P., Cerami, E., Reva, B., et al. (2010). Integrative genomic profiling of human prostate cancer. Cancer Cell *18*, 11–22.

The Cancer Genome Atlas. (2015). The molecular taxonomy of primary prostate cancer. http://www.cbioportal.org/study.do?cancer_study_id=prad_tcga_pub.

Thorvaldsdóttir, H., Robinson, J.T., and Mesirov, J.P. (2013). Integrative Genomics Viewer (IGV): high-performance genomics data visualization and exploration. Brief. Bioinform. *14*, 178–192.

Tomlins, S.A., Rhodes, D.R., Perner, S., Dhanasekaran, S.M., Mehra, R., Sun, X.W., Varambally, S., Cao, X., Tchinda, J., Kuefer, R., et al. (2005). Recurrent fusion of TMPRSS2 and ETS transcription factor genes in prostate cancer. Science *310*, 644–648.

Tomlins, S.A., Laxman, B., Dhanasekaran, S.M., Helgeson, B.E., Cao, X., Morris, D.S., Menon, A., Jing, X., Cao, Q., Han, B., et al. (2007). Distinct classes of chromosomal rearrangements create oncogenic ETS gene fusions in prostate cancer. Nature *448*, 595–599.

Trapnell, C., Roberts, A., Goff, L., Pertea, G., Kim, D., Kelley, D.R., Pimentel, H., Salzberg, S.L., Rinn, J.L., and Pachter, L. (2012). Differential gene and

transcript expression analysis of RNA-seq experiments with TopHat and Cufflinks. Nat. Protoc. *7*, 562–578.

Van Allen, E.M., Foye, A., Wagle, N., Kim, W., Carter, S.L., McKenna, A., Simko, J.P., Garraway, L.A., and Febbo, P.G. (2014a). Successful whole-exome sequencing from a prostate cancer bone metastasis biopsy. Prostate Cancer Prostatic Dis. *17*, 23–27.

Van Allen, E.M., Mouw, K.W., Kim, P., Iyer, G., Wagle, N., Al-Ahmadie, H., Zhu, C., Ostrovnaya, I., Kryukov, G.V., O'Connor, K.W., et al. (2014b). Somatic ERCC2 mutations correlate with cisplatin sensitivity in muscle-invasive urothelial carcinoma. Cancer Discov. *4*, 1140–1153.

Van Allen, E.M., Wagle, N., Stojanov, P., Perrin, D.L., Cibulskis, K., Marlow, S., Jane-Valbuena, J., Friedrich, D.C., Kryukov, G., Carter, S.L., et al. (2014c). Whole-exome sequencing and clinical interpretation of formalin-fixed, paraffin-embedded tumor samples to guide precision cancer medicine. Nat. Med. *20*, 682–688.

Voeller, H.J., Truica, C.I., and Gelmann, E.P. (1998). Beta-catenin mutations in human prostate cancer. Cancer Res. *58*, 2520–2523.

Wang, X.S., Shankar, S., Dhanasekaran, S.M., Ateeq, B., Sasaki, A.T., Jing, X., Robinson, D., Cao, Q., Prensner, J.R., Yocum, A.K., et al. (2011). Characterization of KRAS rearrangements in metastatic prostate cancer. Cancer Discov. *1*, 35–43.

Wee, S., Wiederschain, D., Maira, S.M., Loo, A., Miller, C., deBeaumont, R., Stegmeier, F., Yao, Y.M., and Lengauer, C. (2008). PTEN-deficient cancers depend on PIK3CB. Proc. Natl. Acad. Sci. USA *105*, 13057–13062.

Weston, V.J., Oldreive, C.E., Skowronska, A., Oscier, D.G., Pratt, G., Dyer, M.J., Smith, G., Powell, J.E., Rudzki, Z., Kearns, P., et al. (2010). The PARP inhibitor olaparib induces significant killing of ATM-deficient lymphoid tumor cells in vitro and in vivo. Blood *116*, 4578–4587.

The Journal of Molecular Diagnostics, Vol. 17, No. 6, November 2015

the Journal of Molecular Diagnostics
jmd.amjpathol.org

MSIplus

Integrated Colorectal Cancer Molecular Testing by Next-Generation Sequencing

Q21 Jennifer A. Hempelmann, Sheena M. Scroggins, Colin C. Pritchard, and Stephen J. Salipante

From the Department of Laboratory Medicine, University of Washington, Seattle, Washington

Accepted for publication May 26, 2015.

Address correspondence to Stephen J. Salipante, M.D., Ph.D., University of Washington, 1959 NE Pacific St, Room NW120, Box 357110, Seattle, WA 98195-7110. E-mail: stevesal@uw.edu.

Molecular analysis of colon cancers currently requires multiphasic testing that uses various assays with different performance characteristics, adding cost and time to patient care. We have developed a single, next-generation sequencing assay to simultaneously evaluate colorectal cancers for mutations in relevant cancer genes (*KRAS*, *NRAS*, and *BRAF*) and for tumor microsatellite instability (MSI). In a sample set of 61 cases, the assay demonstrated overall sensitivity of 100% and specificity of 100% for identifying cancer-associated mutations, with a practical limit of detection at 2% mutant allele fraction. MSIplus was 97% sensitive (34 of 35 MSI-positive cases) and 100% specific (42 of 42 MSI-negative cases) for ascertaining MSI phenotype in a cohort of 78 tumor specimens. These performance characteristics were slightly better than for conventional multiplex PCR MSI testing (97% sensitivity and 95% specificity), which is based on comparison of microsatellite loci amplified from tumor and matched normal material, applied to the same specimen cohort. Because the assay uses an amplicon sequencing approach, it is rapid and appropriate for specimens with limited available material or fragmented DNA. This integrated testing strategy offers several advantages over existing methods, including a lack of need for matched normal material, sensitive and unbiased detection of variants in target genes, and an automated analysis pipeline enabling principled and reproducible identification of cancer-associated mutations and MSI status simultaneously. (*J Mol Diagn 2015, 17: 1–10; http://dx.doi.org/10.1016/j.jmoldx.2015.05.008*)

Q5 After initial diagnosis, the molecular characterization of colorectal cancers may require several separate clinical tests. Evaluation of microsatellite instability (MSI) status is recommended testing on all primary colon cancers from patients 50 years or younger (and in older patients if specific pathological features are present[1]) to serve as a screening test for Lynch syndrome, a disease of hereditary cancer predisposition.[2,3] Moreover, MSI status provides diagnostic information about disease prognosis and predicted treatment response to fluorouracil,[3–6] and can, therefore, directly inform patient care. In the case of metastatic disease, additional molecular testing beyond MSI status is indicated. Recently updated guidelines from the National Comprehensive Cancer Network recommend that extended *NRAS* and *KRAS* testing is performed on all stage IV cancers[7] to identify mutations conferring resistance to epidermal growth factor receptor inhibitors.[8–10] If *RAS* gene mutational status is negative, testing for *BRAF* mutations is then also advised, given the poor response of *BRAF*-mutated tumors to cetuximab plus irinotecan, fluorouracil, and leucovorin combination therapy,[11] and also to epidermal growth factor receptor inhibitors used beyond first-line treatment.[12,13]

Independent molecular assays are currently used to test tumor specimens for MSI status and gene mutations. Molecular diagnosis of MSI is implemented using multiplexed PCR-based MSI testing (MSI-PCR), wherein a limited number of informative microsatellite markers[14,15] are PCR amplified from tumor and matched normal material, products are

Supported by Congressionally Directed Medical Research Programs award PC131820 (C.C.P.) and a Prostate Cancer Foundation 2013 Young Investigator Award (C.C.P.).

Q2 Q3 Disclosures: None declared.

http://dx.doi.org/10.1016/j.jmoldx.2015.05.008

resolved using capillary gel electrophoresis, and the presence of additional alleles, which are the hallmark of the MSI phenotype, is qualitatively ascertained.[5,6,16] In some cases, immunohistochemical (IHC) detection of mismatch repair-pathway protein loss may additionally or alternatively be performed,[17–19] although some studies suggest that IHC does not sensitively identify all MSI-positive tumors.[17,20] In contrast, clinical testing for *NRAS*, *KRAS*, and *BRAF* gene mutations is commonly achieved using single-gene assays using melting curve analysis,[21,22] real-time PCR,[23,24] or conventional Sanger sequencing.[24] Peptide nucleic acid clamping[25] or selective amplification of mutant alleles is sometimes used to improve sensitivity.[26–28]

Next-generation sequencing (NGS) is becoming increasingly used by clinical laboratories as a cost-effective and scalable method to interrogate multiple genetic targets in parallel,[29–32] and could be adapted for the focused purpose of characterizing colorectal cancers for molecular workup. Although integrating colorectal cancer testing into an NGS diagnostic would offer practical advantages in eliminating the need for multiple, separate diagnostic tests, the unique analytic properties of NGS could also translate to performance advantages over existing testing methods. Such benefits include the following: i) The ability of the technology to detect low-prevalence, cancer-associated mutations is greater than that of conventional methods,[31–34] because each DNA molecule is examined independently by NGS, potentially providing increased sensitivity for detecting relevant cancer-associated mutations. ii) Our group[35] and others[36–38] have developed methods to computationally infer MSI status from NGS data on the basis of the quantification and distribution of observed allele lengths at microsatellite loci. This offers a standardized, statistical approach for interpreting MSI testing results, in contrast to the current practice of subjective interpretation of MSI-PCR electropherogram traces.[35] iii) Owing to the digital nature of NGS data, primary analysis can be readily automated,[31,35,39] ensuring consistency in test interpretation.

Herein, we describe the clinical validation of a novel NGS assay, MSIplus, for simultaneously evaluating tumor MSI status and mutational hotspots in *KRAS*, *NRAS*, and *BRAF* genes, and provide interpretive guidelines for its diagnostic use. In contrast to earlier research work, which has used NGS to evaluate MSI status from exome and targeted gene capture designs, our assay uses an amplicon sequencing approach, which enables effective targeting and high depth of coverage for the loci of interest. The assay is suitable for molecular characterization of colorectal cancers, does not require matched normal material for inference of MSI status, and is rapid, cost-effective, sensitive, and specific.

Materials and Methods

Selection of Target Sequences and Primer Design

For the purpose of inferring MSI status, we selected a panel of 11 microsatellite markers from our earlier analysis of colorectal cancer exome data[35] that were empirically found to be both most discriminatory for MSI and most frequently unstable in MSI-positive tumors (Table 1). We also incorporated the mononucleotide A/T tract of HSPH1,[40] the instability of which predicts sensitivity to particular anticancer agents, and the five microsatellite markers (MONO-27, BAT-25, BAT-26, NR-21, and NR-24) that compose a performance-enhanced derivative of the Bethesda panel[15] used in current clinical MSI-PCR assays.[16] Separate primers were designed to span exons containing relevant mutational hotspots in *KRAS* (exons 2, 3, and 4; codons 12, 13, 61, 117, and 147), *NRAS* (exons 2, 3, and 4; codons 12, 13, 61, 117, and 147), and *BRAF* (exon 15; codons 599, 600, and 601). [T1]

Multiplexed primer design was performed using MPprimer version 1.4[41] (*https://code.google.com/p/mpprimer*, last accessed October 15, 2013) with some manual curation. Genomic coordinates for each locus (human genome hg19/GRCh37) and PCR primer sequences are provided in Table 1. Primers were concatenated at the 5′ end to partial Illumina sequencing adaptors, which were extended in downstream steps. All oligonucleotides were synthesized by Integrated DNA Technologies (Coralville, IA). Q6

Tumor Specimens and Clinical Testing

DNA from tumor specimens, which were predominantly colorectal cancers, but included a small subset of endometrial cancers, lung cancers, ovarian cancers, melanoma, and additional tumor types, was extracted from fresh-frozen tissue or formalin-fixed, paraffin-embedded tissue blocks. All tumors had >10% neoplastic cellularity, as estimated by review of hematoxylin and eosin–stained slides. Clinical specimens were obtained in accordance with the Declaration of Helsinki and the ethics guidelines of the human subjects division of the University of Washington (Seattle, WA).

Our study design is summarized in Figure 1. Clinical testing for mutations in *BRAF*, *KRAS*, and *NRAS* was performed in 61 specimens by the University of Washington Clinical Molecular Genetics Laboratory. Variants were identified using either the UW-OncoPlex NGS oncology assay[31] (*http://tests.labmed.washington.edu/UW-OncoPlex*, last accessed June 4, 2014) or PCR-amplification and melting curve analysis assays for each individual gene target.[21,22,26] [F1] Q7

Clinical MSI-PCR testing of 81 colorectal tumor specimens was performed by the University of Washington Clinical Molecular Genetics Laboratory using the MSI analysis kit (Promega, Fitchburg, WI). Samples demonstrating instability at two or more of the five mononucleotide markers included in this panel were considered MSI positive [MSI high (MSI-H); diagnosis, 44 specimens]. All other specimens analyzed in this study did not demonstrate any unstable loci by MSI-PCR, and were considered MSI negative (microsatellite stable; diagnosis, 37 specimens). IHC staining for MLH1, MSH2, MSH6, and PMS2 was performed using standard diagnostic techniques.

FLA 5.4.0 DTD ■ JMDI435_proof ■ 12 September 2015 ■ 8:25 pm ■ EO: JMD15_0081

Table 1 Loci and Primer Sequences Q20

Assay stage	Target locus	Primer coordinates	Repeat type	Forward primer sequence	Reverse primer sequence
Stage 1 PCR	Bat-25	Chr4: 55598177-55598271	(A)22	5′-ACACTCTTTCCCTACACGACGCTCTTCCG-ATCTGGAGGATGACGAGTTGGCCCTAGAC-3′	5′-CGGTCTCGGCATTCCTGCTGAACCGCTCTTGTG-TTTCCCAAAGAGACAGCAGTTGGAACATGA-3′
Stage 1 PCR	Bat-26	Chr2: 47641524-47641622	(T)19	5′-ACACTCTTTCCCTACACGACGCTCTTCCG ATCTAGTGGAGTGGAGGAGGGGAGAGAAA-3′	5′-CGGTCTCGGCATTCCTGCTGAACCGCTCTTGTG-TTTCTTGCAGTTTCATCACTGTCTGCGGT-3′
Stage 1 PCR	MONO-27	Chr2: 39564859-39564957	(T)28	5′-ACACTCTTTCCCTACACGACGCTCTTCCG-ATCTCTACTGTCCTACTGTGCCTGGCTCC-3′	5′-CGGTCTCGGCATTCCTGCTGAACCGCTCTTGTG-TTTCCAGCCTGGGCAAGATAATGAGACCC-3′
Stage 1 PCR	NR-21	Chr14: 23652311-23652403	(A)22	5′-ACACTCTTTCCCTACACGACGCTCTTCCG-ATCTCTGGTGCACAGAGCAGAACCATCCT-3′	5′-CGGTCTCGGCATTCCTGCTGAACCGCTCTTGTG-TTTCGCAACCTCAAAAGCTGCCTCCCTTT-3′
Stage 1 PCR	NR-24	Chr2: 95849327-95849419	(T)24	5′-ACACTCTTTCCCTACACGACGCTCTTCCG-ATCTCTGTAGTCCCAGCTATTCGGGAGGC-3′	5′-CGGTCTCGGCATTCCTGCTGAACCGCTCTTGTG-TTTCAAATGACCCCTTCCTGCCCATCACT-3′
Stage 1 PCR	MSI-01	Chr1: 201754376-201754446	(T)17	5′-ACACTCTTTCCCTACACGACGCTCTTCCG-ATCTTTGATGTCCTGCGTCTAGGGTCTGC-3′	5′-CGGTCTCGGCATTCCTGCTGAACCGCTCTTGTG-TTTCGACTGGAGCCTTGGACAGGTTGAGA-3′
Stage 1 PCR	MSI-03	Chr2: 62063059-62063129	(A)17	5′-ACACTCTTTCCCTACACGACGCTCTTCCG-ATCTGCCACTGCTATTTGAAAGAGTTGCTC-3′	5′-CGGTCTCGGCATTCCTGCTGAACCGCTCTTGTG-TTTCGCCACTGCTATTTGAAAGAGTTGCTC-3′
Stage 1 PCR	MSI-04	Chr2: 108479588-108479658	(T)18	5′-ACACTCTTTCCCTACACGACGCTCTTCCG-ATCTTCCAAGATTCCTTCCCTGGCCACTC-3′	5′-CGGTCTCGGCATTCCTGCTGAACCGCTCTTGTG-TTTCACTGTCTGTAGTCCTGGCTTCGTGG-3′
Stage 1 PCR	MSI-06	Chr5: 172421726-172421796	(T)15	5′-ACACTCTTTCCCTACACGACGCTCTTCCG-ATCTAGCAGCAAACTGAACAGGTCACCAAC-3′	5′-CGGTCTCGGCATTCCTGCTGAACCGCTCTTGTG-TTTCAGCAGCAAACTGAACAGGTCACCAAC-3′
Stage 1 PCR	MSI-07	Chr6: 142691916-142691986	(T)17	5′-ACACTCTTTCCCTACACGACGCTCTTCCG-ATCTGCTGAAAGCAACCTAAGCTGTGGTGA-3′	5′-CGGTCTCGGCATTCCTGCTGAACCGCTCTTGTG-TTTCTGCTATAAGAGCTGAGCAGACGACA-3′
Stage 1 PCR	MSI-08	Chr7: 1787485-1787555	(A)17	5′-ACACTCTTTCCCTACACGACGCTCTTCCG-ATCTCCAGCCCCCATGTACACTGTAGTCG-3′	5′-CGGTCTCGGCATTCCTGCTGAACCGCTCTTGTG-TTTCCCCACCCCAAGGCCAAAATCAGTAA-3′
Stage 1 PCR	MSI-09	Chr7: 74608706-74608776	(T)13	5′-ACACTCTTTCCCTACACGACGCTCTTCCG-ATCTGTCTCGGCTACTTGGGAGGCTTAGG-3′	5′-CGGTCTCGGCATTCCTGCTGAACCGCTCTTGTG-TTTCCCGACTAAAGAGGTCATTCACTTGT-3′
Stage 1 PCR	MSI-11	Chr11: 106695477-106695550	(T)12	5′-ACACTCTTTCCCTACACGACGCTCTTCCG-ATCTAGCATGTTTGCAGCCTTCTTCTGGA-3′	5′-CGGTCTCGGCATTCCTGCTGAACCGCTCTTGTG-TTTCAGCATGTTTGCAGCCTTCTTCTGGA-3′
Stage 1 PCR	MSI-12	Chr15: 45897737-45897807	(T)14	5′-ACACTCTTTCCCTACACGACGCTCTTCCG-ATCTGCTGAGGCTAAACACTATCATGCCA-3′	5′-CGGTCTCGGCATTCCTGCTGAACCGCTCTTGTG-TTTCCAGAGGTTGCAGTGAGCCGAGATTG-3′
Stage 1 PCR	MSI-13	Chr16: 18882625-18882695	(A)15	5′-ACACTCTTTCCCTACACGACGCTCTTCCG-ATCTACATCTTCAGGTCAGGAAAACAGCTCG-3′	5′-CGGTCTCGGCATTCCTGCTGAACCGCTCTTGTG-TTTCTAATGACTTGGGCTTTGGAAGCAGC-3′
Stage 1 PCR	MSI-14	Chr17: 19314883-19314953	(T)18	5′-ACACTCTTTCCCTACACGACGCTCTTCCG-ATCTCATTTCAACTGACCTGCCTGGCCTC-3′	5′-CGGTCTCGGCATTCCTGCTGAACCGCTCTTGTG-TTTCCTTGGCAAACGGGCAAGTCTTCAGT-3′
Stage 1 PCR	*HSPH1*-T17	Chr13: 31722570-31722746	(A)17	5′-ACACTCTTTCCCTACACGACGCTCTTCCG-ATCTTGGAAAAGGAACTGCATCTGTGACGG-3′	5′-CGGTCTCGGCATTCCTGCTGAACCGCTCTTGTG-TTTCTTTTCCTAATCCCCTGTGAAACCTGT-3′
Stage 1 PCR	*BRAF* exon 15	Chr7: 140453095-140453431	NA	5′-ACACTCTTTCCCTACACGACGCTCTTCCG-ATCTACAACTGTTCAAACTGATGGGACC-3′	5′-CGGTCTCGGCATTCCTGCTGAACCGCTCTTGTG-TTTCCCTCATCCTAACACATTTCAAGCCCCA-3′
Stage 1 PCR	*KRAS* exon 4	Chr12: 25378395-25378686	NA	5′-ACACTCTTTCCCTACACGACGCTCTTCCG-ATCTTTTCAGTGTTACTTACCTGTCTTGTC-3′	5′-CGGTCTCGGCATTCCTGCTGAACCGCTCTTGTG-TTTCTGACAAAAGTTGTGGACAGGT-3′
Stage 1 PCR	*KRAS* exon 3	Chr12: 25380233-25380491	NA	5′-ACACTCTTTCCCTACACGACGCTCTTCCG-ATCTCCCAGTCCTCATGTACTGGTCCCT-3′	5′-CGGTCTCGGCATTCCTGCTGAACCGCTCTTGTG-TTTCCCGTCATCTTTGGAGCAGGAACA-3′
Stage 1 PCR	*KRAS* exon 2	Chr12: 25398245-25398504	NA	5′-ACACTCTTTCCCTACACGACGCTCTTCCG-ATCTTGAATTAGCTGTATCGTCAAGGCACTC-3′	5′-CGGTCTCGGCATTCCTGCTGAACCGCTCTTGTG-TTTCACACGTCTGCAGTCAACTGGAATTT-3′
Stage 1 PCR	*NRAS* exon 4	Chr1: 115252168-115252401	NA	5′-ACACTCTTTCCCTACACGACGCTCTTCCG-ATCTAATGCTGAAAGCTGTACCATACC-3′	5′-CGGTCTCGGCATTCCTGCTGAACCGCTCTTGTG-TTTCCCCAGCCTAATCTTGTTTTTCTT-3′
Stage 1 PCR	*NRAS* exon 3	Chr1: 115258629-115258838	NA	5′-ACACTCTTTCCCTACACGACGCTCTTCCG-ATCTTGTGGCTCGCCAATTAACCCTG-3′	5′-CGGTCTCGGCATTCCTGCTGAACCGCTCTTGTG-TTTCTGAGAGACAGGATCAGGTCAGCGG-3′
Stage 1 PCR	*NRAS* exon 2	Chr1: 115256475-115256731	NA	5′-ACACTCTTTCCCTACACGACGCTCTTCCG-ATCTAGGAAGCCTTCGCCTGTCCTCA-3′	5′-CGGTCTCGGCATTCCTGCTGAACCGCTCTTGTG-TTTCACCAGATAGGCAGAAATGGGCTTGA-3′
Stage 2 PCR	NA	NA	NA	5′-AATGATACGGCGACCACCGAGATCTAC-ACTCTTTCCCTACACGACGC-3′	5′-CAAGCAGAAGACGGCATACGAGATXXXXXXXXCG-GTCTCGGCATTCCTGCTGAACCG-3′*
Index read	NA	NA	NA	5′-AGATCGGAAGAGCGGTTCAGCAGGA-ATGCCGCGCCCG-3′	NA

*X indicates the presence of an 8-bp sample-specific index sequence.
NA, not applicable.

Determination of mSINGS Baseline Reference Values

Determining MSI status by mSINGS analysis of NGS data[35] entails comparing experimental results against baseline reference values at each microsatellite locus to assess its instability. Because amplifying microsatellite loci by PCR generates a distribution of alternate fragments (stutter artifact) that results from template slippage during cycling,[42,43] it is necessary to establish assay-specific baseline values for each locus. To establish baseline reference values, we extracted DNA from 42 peripheral blood specimens and analyzed them using the MSIplus assay. Q8

FLA 5.4.0 DTD ■ JMDI435_proof ■ 12 September 2015 ■ 8:25 pm ■ EO: JMD15_0081

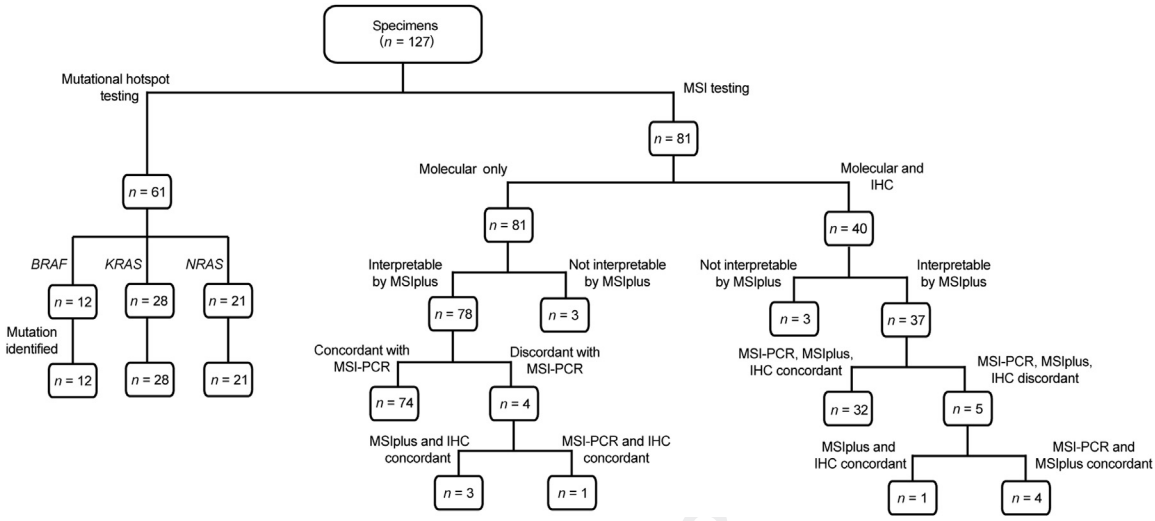

Figure 1 Study design and summary of results. Diagnostic testing algorithm and results are depicted. The number of specimens at each stage is indicated numerically at corresponding nodes. Fifteen specimens were tested for both microsatellite instability (MSI) status and mutational hotspots; thus, inclusion in these categories is not mutually exclusive. IHC, immunohistochemistry.

Library Preparation and Sequencing

Sequencing libraries were generated by PCR amplification in two separate stages. The purpose of the first stage was to simultaneously amplify the loci of interest from the genome and to incorporate partial Illumina sequencing adaptors into the amplification product. The second stage of PCR fully extended the sequencing adaptors and incorporated unique 8-bp, sample-specific index sequences (Table 1), which enabled the multiplexing of multiple specimens together onto the same sequencing run. In addition to the tumor samples, control DNA from HapMap individual NA12878 (Coriell Institute, Camden, NJ) was included with each library preparation and sequencing run, and served as a negative control for both MSI status and *RAS* and *BRAF* mutations, as was a nontemplate amplification control.

The first stage of PCR was performed in two separate reactions, one using an equimolar pool of the microsatellite primers, and the other using primers targeting mutational hotspots. In the latter primer pool, primers were combined in equimolar amounts, except for the primer pairs amplifying *NRAS* exon 2 (included at 0.5× concentration) and *NRAS* exon 4 (included at 1.5× concentration). Both first-stage PCRs were performed in a 25-μL volume using the Qiagen Multiplex PCR Kit (Qiagen, Valencia, CA), and incorporating 50-ng template DNA, 0.25 μmol/L of the appropriate primer pool, and 1× Qiagen Q-solution. PCR cycling for both primer pools was as follows: 5 minutes' incubation at 95°C; 30 cycles of 94°C for 30 seconds, 60°C for 90 seconds, and 72°C for 60 seconds; and a final extension at 72°C for 10 minutes. Before the second stage of PCR, amplification products were purified using a 0.8× volume of Agencourt AMPure XP magnetic beads (Beckman-Coulter, Indianapolis, IN), according to the manufacturer's instructions.

The second stage of PCR was performed using 5 ng of amplification products from the first stage of PCR as template. PCR was performed in a 25-μL volume using KAPA HiFi HotStart ReadyMix PCR Kit (KAPABiosystems, Wilmington, MA), and 0.3 μmol/L of each of the second-stage primers (Table 1). This phase incorporated a reverse primer carrying a sample-specific index sequence; however, the same reverse primer was used in separately amplifying the microsatellite and mutational hotspot amplicons derived from the same specimen. PCR cycling conditions were as follows: 3 minutes' incubation at 95°C; five cycles of 98°C for 20 seconds, 65°C for 15 seconds, and 72°C for 60 seconds; and a final extension at 72°C for 5 minutes. PCRs were purified using a 1.8× volume of Agencourt AMPure XP magnetic beads.

Amplicons derived from the same specimen were pooled in an 8:1 volumetric ratio of microsatellite PCR product/mutational hotspot PCR product before sequencing. Sequencing was performed on an Illumina MiSeq (San Diego, CA) using 200-bp, single-ended reads and an 8-bp index read, with the addition of a custom index read primer (Supplemental Table S1). A 5% concentration of PhiX Control version 3 (Illumina) was included in each sequencing run. Sequencing used a Micro or Nano MiSeq Reagent version 2 300-cycle kit (Illumina), depending on the number of samples pooled for sequencing (up to 32 samples and up to 9 samples, respectively).

Data Analysis

Single-ended sequence reads were initially aligned to the human genome (hg19/GRCh37) using bwa version 0.6.1-r104[44] (*http://sourceforge.net/projects/bio-bwa*, last accessed October 28, 2013) and SAMtools version 0.1.18 (*http://sourceforge.net/projects/samtools*, last accessed October 28, 2013).[45] Sample-level, fully local indel realignment was then

FLA 5.4.0 DTD ■ JMDI435_proof ■ 12 September 2015 ■ 8:25 pm ■ EO: JMD15_0081

performed using Genome Analysis Toolkit version 3.2 (*https://www.broadinstitute.org/gatk*, last accessed May 28, 2014),[39,46] followed by quality score recalibration, to generate a final, realigned, and recalibrated alignment, which was used for subsequent analyses.

Identification of single-nucleotide variants, insertions, and deletions in *KRAS*, *NRAS*, and *BRAF* was performed using VarScan version 2.3.7 (*http://varscan.sourceforge.net*, last accessed May 16, 2014),[47] with the minimum variant frequency set to 0.005 reads, the minimum number of variant reads set to 2, and strand filtering disabled. In addition to primary variant calls, we also tabulated the absolute number of sequence reads matching specific variants of clinical actionability (Supplemental Table S2) using the VarScan readcounts function.

MSI status was determined using the mSINGS package (*https://bitbucket.org/uwlabmed/msings*, last accessed April 27, 2015)[35] with multiplier set to 1.75, msi_min_threshold set to 0.27, and msi_max_threshold set to 0.54.

Results

Sensitivity and Specificity for *KRAS*, *NRAS*, and *BRAF* Mutations

We evaluated the ability of MSIplus to detect mutations in *KRAS*, *NRAS*, and *BRAF* for a panel of 61 formalin-fixed, paraffin-embedded tumor specimens known to be positive for mutations in these genes on the basis of prior clinical testing (Table 2). We first estimated the frequency of false-positive sequence reads at each clinically significant site in *KRAS*, *NRAS*, and *BRAF* by tallying mutant reads (Supplemental Table S1) at known wild-type sites, on the basis of prior clinical testing. Of a total of 517,062 sequence reads examined from a subset of 27 specimens, 2127 sequence reads (0.4%) carried a false-positive mutation. Regardless, multiple reads must carry the same artifact mutation for a variant to be called; thus, this analysis overestimates false-positivity rate. We, therefore, considered each of the mutant calls independently, which yielded an average allele fraction of 0.07% (SD, 0.17%) for false-positive calls of any particular mutation. We set a minimum threshold of 2% allele fraction for calling mutations using MSIplus, a threshold that should exclude virtually all false-positive variant calls (z-score $= 1.5 \times 10^{-25}$) and that defines the practical limit of detection for this assay.

We next evaluated the assay's ability to detect clinically relevant mutations within the three target genes for each of 61 positive control specimens (Figure 1 and Table 2). Average read depth across the seven separate amplicons covering mutational hotspots was 1652 reads (interquartile range, 225 to 2306 reads). We achieved 100% sensitivity [61 of 61 expected variants recovered; 95% CI, 94.1%–100% by the Clopper-Pearson (exact binomial) method].

No specimen demonstrated a false-positive variant call occurring at or above a 2% allele fraction for any of the 44 possible nucleotide sequence variants encoding a clinically relevant mutation (Supplemental Table S1). These results equate to a specificity of 100% (2684 of 2684 true-negative variant calls; 95% CI, >99.3% to 100%). In addition, we observed a high degree of correlation ($R^2 = 0.84$) between the allele fraction of mutations detected by MSIplus and the estimated mutant allele fraction from previous clinical testing using targeted gene-capture NGS methods[31] (subset of 55 specimens) (Figure 2 and Supplemental Table S2). Approximate linearity between these estimates was observed over a range of 2.0% to 59.2% estimated variant allele fraction. This finding suggests that the amplification bias or other artifacts potentially affecting the calculated allele fraction are not pronounced in the MSIplus assay. Furthermore, variants in two specimens with 2.0% mutant allele frequencies were successfully identified, supporting the assay's theoretical limit of detection.

Table 2 Detection of *KRAS*, *NRAS*, and *BRAF* Mutations

Mutation	No. of samples	No. detected
KRAS p.G12S	1	1
KRAS p.G12D	5	5
KRAS p.G12C	2	2
KRAS p.G12V	6	6
KRAS p.G13C	1	1
KRAS p.G13D	8	8
KRAS p.Q61H	3	3
KRAS p.K117N	1	1
KRAS p.A146V	1	1
NRAS p.G13V	1	1
NRAS p.G13R	1	1
NRAS p.G12S	1	1
NRAS p.G12D	6	6
NRAS p.Q61R	8	8
NRAS p.Q61L	2	2
NRAS p.Q61K	1	1
NRAS p.Q61H	1	1
BRAF p.V600K	1	1
BRAF p.V600E	11	11
Total	61	61

To evaluate the reproducibility of mutation detection, we examined a subset of eight control specimens across three or more independent batches of library preparation and sequencing (Supplemental Table S3). The expected mutations were recovered in all 36 independent technical replicates. The CV for the estimated allele fraction was 0.06 (range, 0.03 to 0.15).

Determination of MSI Status

We separately assessed the assay's ability to detect the MSI-positive phenotype on the basis of mSINGS analysis of targeted microsatellite loci.[35] By using MSIplus, we typed a collection of 81 specimens (Figure 1) previously subjected to MSI-PCR testing in our laboratory (44 microsatellite unstable, or MSI-H, results and 37 microsatellite stable results). We first evaluated the reproducibility of mSINGS score determination (corresponding to the total

FLA 5.4.0 DTD ■ JMDI435_proof ■ 12 September 2015 ■ 8:25 pm ■ EO: JMD15_0081

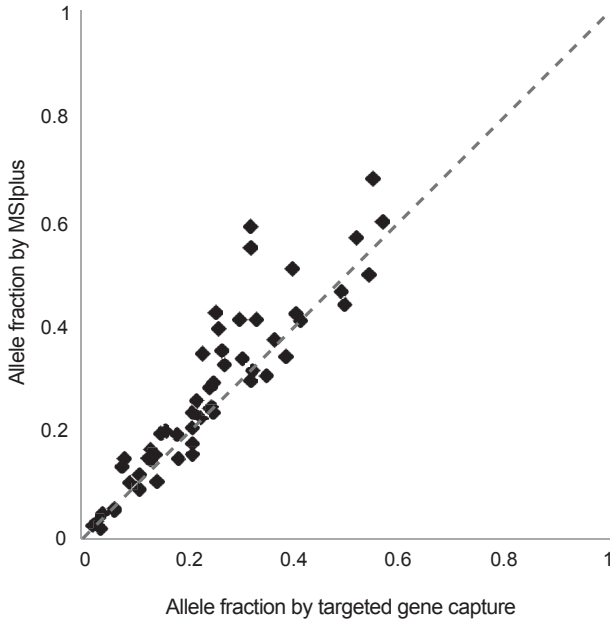

Figure 2 Correlation of allele fraction by MSIplus and targeted gene-capture next-generation sequencing. Allele fractions are estimated by either the MSIplus assay or the UW-OncoPlex targeted gene-capture sequencing panel. The subset of 55 specimens for which data from both assays were available is shown. Dashed gray line indicates a theoretical perfect correlation between the two estimations.

fraction of typed microsatellite loci that are unstable) by examining at least two separately prepared and sequenced technical replicates each for a subset of 48 specimens (Supplemental Table S4). Because several specimens had mSINGS scores of 0, calculating the CV was not meaningful. On average, the SD observed among technical replicates was 0.07 mSINGS units, and the SD of values around this mean was 0.03.

On the basis of the qualitative separation of microsatellite stable from MSI-H groups[35] (Figure 3), we initially set an empirical threshold of a 0.40 mSINGS score for differentiating MSI-positive from MSI-negative tumors. However, in light of mSINGS score variability, specimens with scores falling close to this threshold could be assigned the wrong MSI status by chance alone. To prevent improper MSI classifications resulting from assay variability, specimens with mSINGS values falling between 0.27 and 0.54 [threshold ± (average mSINGS variability + standard deviation of mSINGS variability × 2)] were consequently considered uninterpretable. In contrast, specimens with mSINGS scores lower or higher than those values could be confidently classified as MSI negative or MSI positive, respectively. Seventy-seven specimens had interpretable mSINGS scores, and we repeated library preparation for the remaining four samples that did not. On retyping, mSINGS scores for one of the four specimens became interpretable, whereas the remaining three results remained ambiguous. Thus, the MSI status of 95% of all specimens was initially interpretable, and on repeat typing, this proportion increased only modestly, to 96%.

Most MSI-negative specimens were readily distinguished from MSI-positive specimens on the basis of mSINGS score, and mSINGS interpretations were fully concordant with MSI-PCR interpretations in most cases (Figure 3 and Supplemental Table S5). However, four samples had discordant results between the two methods, which warranted further investigation.

One specimen was classified as MSI negative by MSI-PCR, but had a high mSINGS score (0.63) and was, therefore, interpreted as MSI positive by the MSIplus assay. Review of laboratory records indicated that, on subsequent workup, the tumor was found to have deficient MHS6 expression by IHC and that gene sequencing identified a germline MSH6 mutation in the patient, establishing a diagnosis of Lynch syndrome. We conclude that this instance represents a false-negative MSI-PCR result, and that the correct diagnosis was achieved by MSIplus. The other three discrepancies corresponded to specimens typed as MSI positive by MSI-PCR but classified as MSI negative using MSIplus. In two cases, clinical IHC testing was performed and did not reveal loss of expression in any mismatch repair proteins. Although MSI positivity has been observed in a background of normal MMR protein expression in approximately 5% of cases,[16] these cases are most consistent with false-positive MSI-PCR results. Conversely, the remaining discrepant case likely represents a false negative by MSIplus because loss of MSH2 and MSH6 expression was seen by IHC and a germline *MSH6* mutation was identified by genetic testing.

Accounting for these additional clinical data, and assuming that all specimens receiving a concordant

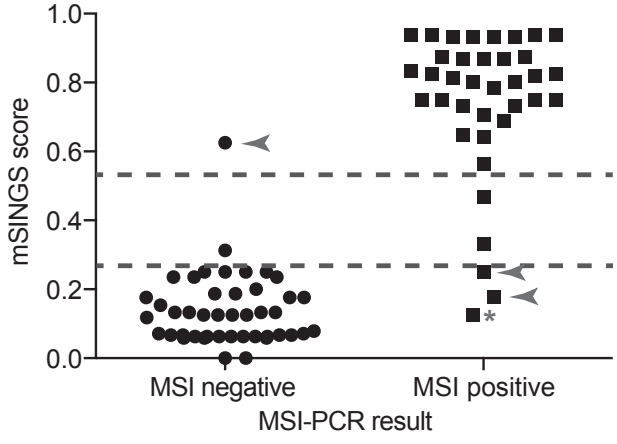

Figure 3 Inferring microsatellite instability (MSI) status by MSIplus. Data are stratified according to testing results by MSI-PCR. The mSINGS score (the fraction of interrogated microsatellite loci that are unstable) is plotted for each specimen. The dashed lines at mSINGS scores of 0.27 and 0.54 indicate the cutoffs for delineating MSI-positive and MSI-negative specimens by MSIplus: mSINGS scores falling below these values were interpreted as negative, scores above those values were interpreted as positive, and scores falling between the values could not be reliably interpreted. **Arrowheads** indicate specimens misclassified by MSI-PCR; **asterisk** indicates specimen misclassified by MSIplus, as resolved by alternative clinical testing results (immunohistochemical and/or genetic testing). For specimens that were typed multiple times, one representative mSINGS score is displayed.

FLA 5.4.0 DTD ■ JMDI435_proof ■ 12 September 2015 ■ 8:25 pm ■ EO: JMD15_0081

diagnosis by MSI-PCR and MSIplus were correctly assigned an MSI status, we conclude that the validation set used in our study comprised a total of 36 MSI-positive cases and 42 MSI-negative cases. We calculate that MSIplus has an overall sensitivity of 97.1% (34 of 35 MSI-positive cases identified; 95% CI, 85.1%–99.9%) and a specificity of 100% (42 of 42 MSI-negative cases identified; 95% CI, 91.6%–100%) for determining tumor MSI status. The positive predictive value and negative predictive value for MSIplus were 97.1% and 97.7%, respectively. For the same panel of test specimens, MSI-PCR demonstrated a sensitivity of 97.1% (34 of 35 MSI-positive cases identified; 95% CI, 85.1%–99.9%), a specificity of 95.2% (40 of 42 MSI-negative cases identified; 95% CI, 83.8%–99.4%), a positive predictive value of 94.6%, and a negative predictive value of 95.6% for the same set of validation specimens.

Correlation of MSIplus, MSI-PCR, and IHC

Although our primary objective was to compare the results of molecular MSI testing by MSI-PCR and MSIplus, we additionally correlated our findings with IHC for 40 cases where this information was available (Figure 1 and Supplemental Table S5). The diagnosis rendered by each of the three approaches (IHC, MSI-PCR, and MSIplus) was fully concordant in 32 of 37 cases where MSIplus was interpretable. One discrepant case, discussed above, evidenced isolated loss of MSH6 by IHC, and was negative by MSI-PCR but positive by MSIplus, suggesting that MSIplus and IHC obtained the proper diagnosis. Three additional cases receiving a MSI-positive diagnosis by both MSI-PCR and MSIplus showed no loss of MMR protein expression by IHC, suggesting a MSI-positive status without loss of MMR protein expression.[20] One specimen was negative by MSI-PCR and MSIplus, but demonstrated reduction of MLH1 and PMS2 expression by IHC: it is possible that this latter case represents either a false-negative molecular result or a false-positive result by IHC.[20]

Quantitative Correlation of MSIplus and Conventional MSI-PCR

Last, we examined whether there was a correlation between the fraction of unstable markers characterized by MSIplus (ie, the mSINGS score) and the fraction of unstable microsatellite loci detected by MSI-PCR (Figure 4). We excluded from analysis specimens with discordant results between the two assays and those three having non-interpretable mSINGS scores.

Overall, the two measurements of MSI demonstrated a strong, positive correlation ($R^2 = 0.89$). Of 42 specimens with no unstable loci detectable by MSI-PCR, 20 demonstrated nonzero mSINGS scores; nevertheless, a trend of mSINGS overestimating the fraction of unstable loci was not consistent across all specimens deemed MSI positive by MSI-PCR. We noted that if MSI-negative MSI-PCR results were removed from consideration, the correlation of mSINGS score and the fraction of unstable loci observed for MSI-H specimens was not statistically meaningful ($R^2 = 9.1 \times 10^{-3}$). This finding suggests that, above the threshold for delineating an MSI-positive phenotype, the fraction of unstable markers identified by MSI-PCR cannot be generalized to infer the degree of overall genomic instability.

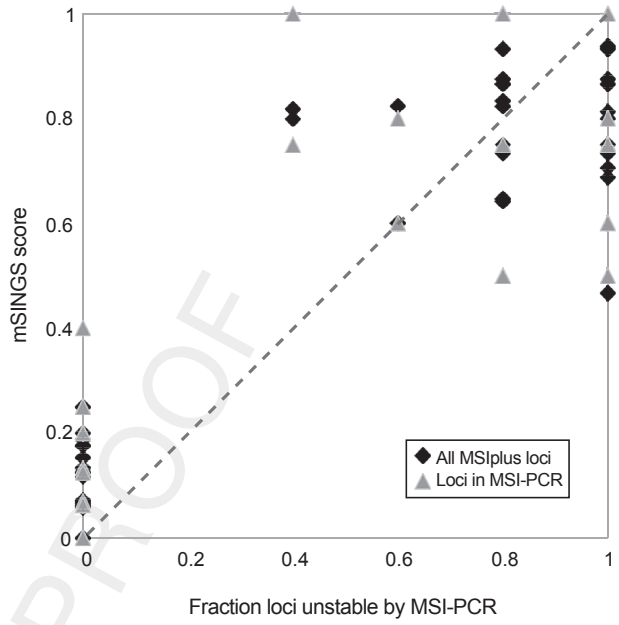

Figure 4 Correlation of locus instability measured by microsatellite instability (MSI)-PCR and MSIplus. The mSINGS score (the fraction of interrogated microsatellite loci that are unstable) is plotted against the fraction of unstable loci determined by MSI-PCR. Overall mSINGS score for the MSIplus assay is shown separately from mSINGS score calculated for the five loci in common with MSI-PCR. Dashed gray line indicates a theoretical perfect correlation between the two measures of instability.

We separately evaluated correlation between the fraction of unstable loci identified by either MSI-PCR or MSIplus for the subset of five loci that are represented in both assays. Again, a strong positive correlation was observed between these two metrics ($R^2 = 0.80$), although the lack of identity between them indicates subtle differences in individual loci being scored as stable or unstable between the two assays.

Discussion

Because the number of single-gene molecular tests needed to adequately characterize tumors continues to increase, the practical consequences of increased health care costs, increased test turnaround times, and the potential to deplete available tissue material during the course of testing become an increasing concern.[31] The use of highly scalable NGS technologies has proved a means to overcome this challenge, in many cases improving the quality and capabilities

FLA 5.4.0 DTD ■ JMDI435_proof ■ 12 September 2015 ■ 8:25 pm ■ EO: JMD15_0081

of molecular testing.[30–33] In light of these considerations, we developed MSIplus, an NGS assay for characterizing colorectal tumor specimens that integrates extended *RAS* and *BRAF* gene testing with MSI analysis and, therefore, encompasses recommended molecular testing guidelines in a single assay.[7]

MSIplus had an overall sensitivity of 100% and a specificity of 100% for identifying cancer-associated mutations in *BRAF*, *KRAS,* and *NRAS* genes, as calculated from a panel of 61 specimens carrying a spectrum of known mutations (Table 2). The ability of a molecular assay to detect mutations present in a tumor specimen is dependent, in part, on the proportion of neoplastic cells in the sample and the fraction of total tumor cells that carry the mutation of interest.[31] The limit of detection for MSIplus is a 2% mutant allele fraction, lower than other prevalent clinical diagnostic methods.[21,22] Because the limit of detection in this assay partially reflects the rate of false-positive sequence reads, the sensitivity of MSIplus for low-prevalence mutations could potentially be improved in future iterations through practices such as incorporating molecular tagging-mediated sequencing error correction.[34,48,49] However, such methods present technical challenges and could negatively affect other aspects of the assay's performance.

Because it is a sequencing-based approach, MSIplus should be able to identify most single-nucleotide polymorphisms or small insertions or deletions occurring within the selected target regions. Compared with real-time PCR or melt-curve assays, which are designed to detect only a specific subset of actionable mutations,[23,24] MSIplus is capable of identifying variants without prior knowledge or expectation of the underlying genetic change. This property greatly improves the ability of MSIplus to identify rare or unusual clinically significant nucleotide alterations.

MSIplus had 97.1% sensitivity and 100% specificity for characterizing the MSI phenotype in a test set of 78 tumors, performance characteristics that were similar to those reported for MSI-PCR in other studies[5,16] and slightly better than the performance of MSI-PCR for the same set of specimens. Although MSIplus does not substantially improve sensitivity or specificity compared with MSI-PCR, it has important advantages over existing assays. Evaluation of MSI by mSINGS analysis eliminates the need for matched normal patient material,[35] which is typically required for conventional MSI-PCR, thereby expanding the scope of available patient specimens that can be successfully typed using MSIplus. The interpretation of MSIplus uses an automated analysis pipeline that is based on quantitative, descriptive statistics. This feature may improve the consistency of MSI diagnosis and reduce interlaboratory and intralaboratory variation.

We were unable to confidently call MSI status using MSIplus for a small subset of specimens (95% of specimens were interpretable with the first round of testing, whereas only 5% were not). Three of the four specimens with indeterminate mSINGS scores again yielded uninterpretable results after repeated testing, suggesting that the assay cannot confidently type MSI status for a small fraction of samples. Although the biological significance of these persistently indeterminate mSINGS scores, if any, is unclear,[50,51] studies examining larger numbers of microsatellite markers have suggested that such cases do not represent a distinct disease category of subtype of MSI.[35,38] These indeterminate specimens could potentially be resolved by increasing the number of microsatellite loci examined in the assay to enable more accurate assessment of the mSINGS score.[35]

Our study identified several cases where IHC and molecular testing were discordant, as expected.[17,20] It is known that isolated MSH6 deficiencies may result in false-negative MSI-PCR results,[52] and our sample cohort contained one such case. Unlike MSI-PCR, MSIplus identified this MSH6-deficient specimen as MSI positive, rendering a proper molecular diagnosis. Moreover, all indeterminate MSIplus results occurred in cases where IHC indicated reduced MMR protein expression, including two testing negative by MSI-PCR. Although anecdotal, these findings suggest an improved ability of MSIplus to identify MSH6-mutated specimens and improved sensitivity for detecting MMR pathway deficiencies compared with MSI-PCR. With further refinement, the MSIplus assay may offer significant performance advantages over MSI-PCR for such cases.

We anticipate that MSIplus will prove useful in characterizing colorectal cancers while potentially reducing operating costs and standardizing the interpretation of testing results. The assay is rapid, and compatible with a 2- or 3-day turnaround time: library preparation, approximately 8 hours; sequencer setup, approximately 1 hour; sequencing, approximately 8 hours; data analysis, approximately 2 hours per specimen on a four-processor machine, but scalable on larger computing systems to process multiple specimens simultaneously. Because the assay uses PCR-mediated library preparation, it requires minimal input DNA (50 ng) and should function even for partially degraded specimens. The modular nature of the multiplexed primer design will enable relatively straightforward expansion of the assay to additional molecular targets, as necessary, in response to future diagnostic requirements. The approach of focused, integrated NGS testing, tailored to a specific tumor type or diagnostic workflow, is a powerful paradigm that can be adapted to other clinical scenarios, and will become more common as NGS technologies are increasingly integrated into clinical laboratories.

Acknowledgments

We thank the Molecular Diagnostics laboratory staff for their help in identifying and obtaining specimens and Tina Lockwood (Seattle, WA) for helpful conversations.

Supplemental Data

Supplemental material for this article can be found at *http://dx.doi.org/10.1016/j.jmoldx.2015.05.008*.

References

1. Jenkins MA, Hayashi S, O'Shea AM, Burgart LJ, Smyrk TC, Shimizu D, Waring PM, Ruszkiewicz AR, Pollett AF, Redston M, Barker MA, Baron JA, Casey GR, Dowty JG, Giles GG, Limburg P, Newcomb P, Young JP, Walsh MD, Thibodeau SN, Lindor NM, Lemarchand L, Gallinger S, Haile RW, Potter JD, Hopper JL, Jass JR; Colon Cancer Family Registry: Pathology features in Bethesda guidelines predict colorectal cancer microsatellite instability: a population-based study. Gastroenterology 2007, 133:48–56
2. Beamer LC, Grant ML, Espenschied CR, Blazer KR, Hampel HL, Weitzel JN, MacDonald DJ: Reflex immunohistochemistry and microsatellite instability testing of colorectal tumors for Lynch syndrome among US cancer programs and follow-up of abnormal results. J Clin Oncol 2012, 30:1058–1063
3. Vilar E, Gruber SB: Microsatellite instability in colorectal cancer: the stable evidence. Nat Rev Clin Oncol 2010, 7:153–162
4. Ribic CM, Sargent DJ, Moore MJ, Thibodeau SN, French AJ, Goldberg RM, Hamilton SR, Laurent-Puig P, Gryfe R, Shepherd LE, Tu D, Redston M, Gallinger S: Tumor microsatellite-instability status as a predictor of benefit from fluorouracil-based adjuvant chemotherapy for colon cancer. N Engl J Med 2003, 349:247–257
5. Goel A, Nagasaka T, Hamelin R, Boland CR: An optimized pentaplex PCR for detecting DNA mismatch repair-deficient colorectal cancers. PLoS One 2010, 5:e9393
6. de la Chapelle A, Hampel H: Clinical relevance of microsatellite instability in colorectal cancer. J Clin Oncol 2010, 28:3380–3387
7. NCCN Guidelines(R) Updates. J Natl Compr Canc Netw 2013, 11: xxxii–xxxvi
8. Plesec TP, Hunt JL: KRAS mutation testing in colorectal cancer. Adv Anat Pathol 2009, 16:196–203
9. De Roock W, Claes B, Bernasconi D, De Schutter J, Biesmans B, Fountzilas G, et al: Effects of KRAS, BRAF, NRAS, and PIK3CA mutations on the efficacy of cetuximab plus chemotherapy in chemotherapy-refractory metastatic colorectal cancer: a retrospective consortium analysis. Lancet Oncol 2010, 11:753–762
10. Douillard JY, Oliner KS, Siena S, Tabernero J, Burkes R, Barugel M, Humblet Y, Bodoky G, Cunningham D, Jassem J, Rivera F, Kocakova I, Ruff P, Blasinska-Morawiec M, Smakal M, Canon JL, Rother M, Williams R, Rong A, Wiezorek J, Sidhu R, Patterson SD: Panitumumab-FOLFOX4 treatment and RAS mutations in colorectal cancer. N Engl J Med 2013, 369:1023–1034
11. Van Cutsem E, Kohne CH, Lang I, Folprecht G, Nowacki MP, Cascinu S, Shchepotin I, Maurel J, Cunningham D, Tejpar S, Schlichting M, Zubel A, Celik I, Rougier P, Ciardiello F: Cetuximab plus irinotecan, fluorouracil, and leucovorin as first-line treatment for metastatic colorectal cancer: updated analysis of overall survival according to tumor KRAS and BRAF mutation status. J Clin Oncol 2011, 29:2011–2019
12. Di Nicolantonio F, Martini M, Molinari F, Sartore-Bianchi A, Arena S, Saletti P, De Dosso S, Mazzucchelli L, Frattini M, Siena S, Bardelli A: Wild-type BRAF is required for response to panitumumab or cetuximab in metastatic colorectal cancer. J Clin Oncol 2008, 26: 5705–5712
13. Bokemeyer C, Van Cutsem E, Rougier P, Ciardiello F, Heeger S, Schlichting M, Celik I, Kohne CH: Addition of cetuximab to chemotherapy as first-line treatment for KRAS wild-type metastatic colorectal cancer: pooled analysis of the CRYSTAL and OPUS randomised clinical trials. Eur J Cancer 2012, 48:1466–1475
14. Boland CR, Thibodeau SN, Hamilton SR, Sidransky D, Eshleman JR, Burt RW, Meltzer SJ, Rodriguez-Bigas MA, Fodde R, Ranzani GN, Srivastava S: A National Cancer Institute Workshop on Microsatellite Instability for cancer detection and familial predisposition: development of international criteria for the determination of microsatellite instability in colorectal cancer. Cancer Res 1998, 58:5248–5257
15. Umar A, Boland CR, Terdiman JP, Syngal S, de la Chapelle A, Ruschoff J, Fishel R, Lindor NM, Burgart LJ, Hamelin R, Hamilton SR, Hiatt RA, Jass J, Lindblom A, Lynch HT, Peltomaki P, Ramsey SD, Rodriguez-Bigas MA, Vasen HF, Hawk ET, Barrett JC, Freedman AN, Srivastava S: Revised Bethesda Guidelines for hereditary nonpolyposis colorectal cancer (Lynch syndrome) and microsatellite instability. J Natl Cancer Inst 2004, 96:261–268
16. Bacher JW, Flanagan LA, Smalley RL, Nassif NA, Burgart LJ, Halberg RB, Megid WM, Thibodeau SN: Development of a fluorescent multiplex assay for detection of MSI-High tumors. Dis Markers 2004, 20:237–250
17. Lindor NM, Burgart LJ, Leontovich O, Goldberg RM, Cunningham JM, Sargent DJ, Walsh-Vockley C, Petersen GM, Walsh MD, Leggett BA, Young JP, Barker MA, Jass JR, Hopper J, Gallinger S, Bapat B, Redston M, Thibodeau SN: Immunohistochemistry versus microsatellite instability testing in phenotyping colorectal tumors. J Clin Oncol 2002, 20:1043–1048
18. Shia J: Immunohistochemistry versus microsatellite instability testing for screening colorectal cancer patients at risk for hereditary nonpolyposis colorectal cancer syndrome, part I: the utility of immunohistochemistry. J Mol Diagn 2008, 10:293–300
19. Zhang L: Immunohistochemistry versus microsatellite instability testing for screening colorectal cancer patients at risk for hereditary nonpolyposis colorectal cancer syndrome, part II: the utility of microsatellite instability testing. J Mol Diagn 2008, 10:301–307
20. Müller A, Giuffre G, Edmonston TB, Mathiak M, Roggendorf B, Heinmöller E, Brodegger T, Tuccari G, Mangold E, Buettner R, Rüschoff J; German HNPCC Consortium German Cancer Aid (Deutsche Krebshife): Challenges and pitfalls in HNPCC screening by microsatellite analysis and immunohistochemistry. J Mol Diagn 2004, 6:308–315
21. Ikenoue T, Hikiba Y, Kanai F, Ijichi H, Togo G, Ohta M, Watabe H, Yamaji Y, Okamoto M, Aragaki J, Matsumura M, Kawabe T, Omata M: Rapid detection of mutations in the BRAF gene using real-time polymerase chain reaction and melting curve analysis. Cancer Genet Cytogenet 2004, 149:68–71
22. Nikiforova MN, Lynch RA, Biddinger PW, Alexander EK, Dorn GW 2nd, Tallini G, Kroll TG, Nikiforov YE: RAS point mutations and PAX8-PPAR gamma rearrangement in thyroid tumors: evidence for distinct molecular pathways in thyroid follicular carcinoma. J Clin Endocrinol Metab 2003, 88:2318–2326
23. Sakai K, Yoneshige A, Ito A, Ueda Y, Kondo S, Nobumasa H, Fujita Y, Togashi Y, Terashima M, De Velasco MA, Tomida S, Nishio K: Performance of a novel KRAS mutation assay for formalin-fixed paraffin embedded tissues of colorectal cancer. Springerplus 2015, 4:7
24. Qu K, Pan Q, Zhang X, Rodriguez L, Zhang K, Li H, Ho A, Sanders H, Sferruzza A, Cheng SM, Nguyen D, Jones D, Waldman F: Detection of BRAF V600 mutations in metastatic melanoma: comparison of the Cobas 4800 and Sanger sequencing assays. J Mol Diagn 2013, 15:790–795
25. Oh JE, Lim HS, An CH, Jeong EG, Han JY, Lee SH, Yoo NJ: Detection of low-level KRAS mutations using PNA-mediated asymmetric PCR clamping and melting curve analysis with unlabeled probes. J Mol Diagn 2010, 12:418–424
26. Pritchard CC, Akagi L, Reddy PL, Joseph L, Tait JF: COLD-PCR enhanced melting curve analysis improves diagnostic accuracy for KRAS mutations in colorectal carcinoma. BMC Clin Pathol 2010, 10:6
27. Li J, Wang L, Mamon H, Kulke MH, Berbeco R, Makrigiorgos GM: Replacing PCR with COLD-PCR enriches variant DNA sequences and redefines the sensitivity of genetic testing. Nat Med 2008, 14: 579–584

FLA 5.4.0 DTD ■ JMDI435_proof ■ 12 September 2015 ■ 8:25 pm ■ EO: JMD15_0081

28. Westwood M, van Asselt T, Ramaekers B, Whiting P, Joore M, Armstrong N, Noake C, Ross J, Severens J, Kleijnen J: KRAS mutation testing of tumours in adults with metastatic colorectal cancer: a systematic review and cost-effectiveness analysis. Health Technol Assess 2014, 18:1−132
29. Pritchard CC, Smith C, Salipante SJ, Lee MK, Thornton AM, Nord AS, Gulden C, Kupfer SS, Swisher EM, Bennett RL, Novetsky AP, Jarvik GP, Olopade OI, Goodfellow PJ, King MC, Tait JF, Walsh T: ColoSeq provides comprehensive lynch and polyposis syndrome mutational analysis using massively parallel sequencing. J Mol Diagn 2012, 14:357−366
30. Frampton GM, Fichtenholtz A, Otto GA, Wang K, Downing SR, He J, et al: Development and validation of a clinical cancer genomic profiling test based on massively parallel DNA sequencing. Nat Biotechnol 2013, 31:1023−1031
31. Pritchard CC, Salipante SJ, Koehler K, Smith C, Scroggins S, Wood B, Wu D, Lee MK, Dintzis S, Adey A, Liu Y, Eaton KD, Martins R, Stricker K, Margolin KA, Hoffman N, Churpek JE, Tait JF, King MC, Walsh T: Validation and implementation of targeted capture and sequencing for the detection of actionable mutation, copy number variation, and gene rearrangement in clinical cancer specimens. J Mol Diagn 2014, 16:56−67
32. Cottrell CE, Al-Kateb H, Bredemeyer AJ, Duncavage EJ, Spencer DH, Abel HJ, Lockwood CM, Hagemann IS, O'Guin SM, Burcea LC, Sawyer CS, Oschwald DM, Stratman JL, Sher DA, Johnson MR, Brown JT, Cliften PF, George B, McIntosh LD, Shrivastava S, Nguyen TT, Payton JE, Watson MA, Crosby SD, Head RD, Mitra RD, Nagarajan R, Kulkarni S, Seibert K, Virgin HW 4th, Milbrandt J, Pfeifer JD: Validation of a next-generation sequencing assay for clinical molecular oncology. J Mol Diagn 2014, 16:89−105
33. Harismendy O, Schwab RB, Bao L, Olson J, Rozenzhak S, Kotsopoulos SK, Pond S, Crain B, Chee MS, Messer K, Link DR, Frazer KA: Detection of low prevalence somatic mutations in solid tumors with ultra-deep targeted sequencing. Genome Biol 2011, 12:R124
34. Hiatt JB, Pritchard CC, Salipante SJ, O'Roak BJ, Shendure J: Single molecule molecular inversion probes for targeted, high-accuracy detection of low-frequency variation. Genome Res 2013, 23:843−854
35. Salipante SJ, Scroggins SM, Hampel HL, Turner EH, Pritchard CC: Microsatellite instability detection by next generation sequencing. Clin Chem 2014, 60:1192−1199
36. Lu Y, Soong TD, Elemento O: A novel approach for characterizing microsatellite instability in cancer cells. PLoS One 2013, 8:e63056
37. Niu B, Ye K, Zhang Q, Lu C, Xie M, McLellan MD, Wendl MC, Ding L: MSIsensor: microsatellite instability detection using paired tumor-normal sequence data. Bioinformatics 2014, 30:1015−1016
38. Kim TM, Laird PW, Park PJ: The landscape of microsatellite instability in colorectal and endometrial cancer genomes. Cell 2013, 155:858−868
39. McKenna A, Hanna M, Banks E, Sivachenko A, Cibulskis K, Kernytsky A, Garimella K, Altshuler D, Gabriel S, Daly M, DePristo MA: The Genome Analysis Toolkit: a MapReduce framework for analyzing next-generation DNA sequencing data. Genome Res 2010, 20:1297−1303
40. Dorard C, de Thonel A, Collura A, Marisa L, Svrcek M, Lagrange A, Jego G, Wanherdrick K, Joly AL, Buhard O, Gobbo J, Penard-Lacronique V, Zouali H, Tubacher E, Kirzin S, Selves J, Milano G, Etienne-Grimaldi MC, Bengrine-Lefevre L, Louvet C, Tournigand C, Lefevre JH, Parc Y, Tiret E, Flejou JF, Gaub MP, Garrido C, Duval A: Expression of a mutant HSP110 sensitizes colorectal cancer cells to chemotherapy and improves disease prognosis. Nat Med 2011, 17:1283−1289
41. Shen Z, Qu W, Wang W, Lu Y, Wu Y, Li Z, Hang X, Wang X, Zhao D, Zhang C: MPprimer: a program for reliable multiplex PCR primer design. BMC Bioinformatics 2010, 11:143
42. Clarke LA, Rebelo CS, Goncalves J, Boavida MG, Jordan P: PCR amplification introduces errors into mononucleotide and dinucleotide repeat sequences. Mol Pathol 2001, 54:351−353
43. Salipante SJ, Horwitz MS: Phylogenetic fate mapping. Proc Natl Acad Sci U S A 2006, 103:5448−5453
44. Li H, Durbin R: Fast and accurate short read alignment with Burrows-Wheeler transform. Bioinformatics 2009, 25:1754−1760
45. Li H, Handsaker B, Wysoker A, Fennell T, Ruan J, Homer N, Marth G, Abecasis G, Durbin R; 1000 Genomes Project Data Processing Subgroup: The Sequence Alignment/Map format and SAMtools. Bioinformatics 2009, 25:2078−2079
46. DePristo MA, Banks E, Poplin R, Garimella KV, Maguire JR, Hartl C, Philippakis AA, del Angel G, Rivas MA, Hanna M, McKenna A, Fennell TJ, Kernytsky AM, Sivachenko AY, Cibulskis K, Gabriel SB, Altshuler D, Daly MJ: A framework for variation discovery and genotyping using next-generation DNA sequencing data. Nat Genet 2011, 43:491−498
47. Koboldt DC, Zhang Q, Larson DE, Shen D, McLellan MD, Lin L, Miller CA, Mardis ER, Ding L, Wilson RK: VarScan 2: somatic mutation and copy number alteration discovery in cancer by exome sequencing. Genome Res 2012, 22:568−576
48. Kinde I, Wu J, Papadopoulos N, Kinzler KW, Vogelstein B: Detection and quantification of rare mutations with massively parallel sequencing. Proc Natl Acad Sci U S A 2011, 108:9530−9535
49. Schmitt MW, Kennedy SR, Salk JJ, Fox EJ, Hiatt JB, Loeb LA: Detection of ultra-rare mutations by next-generation sequencing. Proc Natl Acad Sci U S A 2012, 109:14508−14513
50. Pawlik TM, Raut CP, Rodriguez-Bigas MA: Colorectal carcinogenesis: MSI-H versus MSI-L. Dis Markers 2004, 20:199−206
51. Tomlinson I, Halford S, Aaltonen L, Hawkins N, Ward R: Does MSI-low exist? J Pathol 2002, 197:6−13
52. Hampel H, Frankel W, Panescu J, Lockman J, Sotamaa K, Fix D, Comeras I, La Jeunesse J, Nakagawa H, Westman JA, Prior TW, Clendenning M, Penzone P, Lombardi J, Dunn P, Cohn DE, Copeland L, Eaton L, Fowler J, Lewandowski G, Vaccarello L, Bell J, Reid G, de la Chapelle A: Screening for Lynch syndrome (hereditary nonpolyposis colorectal cancer) among endometrial cancer patients. Cancer Res 2006, 66:7810−7817